DEVELOPING ALTERNATIVE SOURCES OF FEEDSTOCKS FOR INDUSTRIAL HYDROCARBONS: OPTIMISATION OF BIOMASS AND STRESS-INDUCED LIPID PRODUCTION IN Synechocystis SR

DIANA FABIOLA ALARCON-GUTIERREZ

DEVELOPING ALTERNATIVE SOURCES OF FEEDSTOCKS FOR INDUSTRIAL HYDROCARBONS: OPTIMISATION OF BIOMASS AND STRESS-INDUCED LIPID PRODUCTION IN *Synechocystis SR*

Diana Fabiola Alarcón-Gutiérrez

Thesis Submitted for the Degree of
Master of Science by Research in Biological Sciences

Dr. Steve Chivasa
Supervisor

Department of Biosciences

Durham University

September 2020

Diana Fabiola Alarcón-Gutiérrez

DEVELOPING ALTERNATIVE SOURCES OF FEEDSTOCKS FOR INDUSTRIAL HYDROCARBONS: OPTIMISATION OF BIOMASS AND STRESS-INDUCED LIPID PRODUCTION IN *Synechocystis SR*

Abstract

Hydrocarbons from fossil fuels play a key role in supporting diverse socio-economic activities and growth of the global economy. Principally, hydrocarbons are used as fuels for energy generation and as raw materials for manufacturing products of high economic value, such as lubricants, packaging material, and agrochemicals. Due to greenhouse gas emissions associated with use of fossil fuel products, alternative sources of feedstocks to manufacture industrial hydrocarbons are highly sought after. This project explored the utility of a newly discovered cyanobacterial strain (*Synechocystis SR*) as a source of lipids for industrial applications. In experiments to optimise biomass production, a two-stage system sequencing 5 days of high light (150 $\mu mol.m^{-2}.s^{-1}$) followed by 2 days of low light (75 $\mu mol.m^{-2}.s^{-1}$) incubation of cyanobacterial cultures produced the best growth results. Because lipid production in cyanobacteria is activated by stress, the impact of NaCl and the mycotoxin fumonisin B1 (FB1) on growth was evaluated. FB1 exhibited no growth inhibitory activity against neither *Synechocystis SR* nor the control strain *Synechocystis PCC 6803*. However, salinity stress imposed by NaCl had a disproportionately higher impact on the growth of *Synechocystis PCC 6803* than *Synechocystis SR*. The effects of salinity on cyanobacterial growth were dependent on light, with high light totally inhibiting growth while low light incubation followed by high light enabled the cultures to acclimate and survive the stress. Salinity stress activated expression of all the fatty acid biosynthetic pathway genes, with *Synechocystis SR* showing higher gene expression than *Synechocystis PCC 6803*. The activation in gene expression led to a two-fold increase in total lipid accumulation in *Synechocystis SR*. Even though there was an increase in the amount of total lipid, the profile of fatty acid methyl esters (FAMEs) remained unchanged. FAMEs extracted from *Synechocystis SR* could be used as an industrial feedstock for production of diverse industrial hydrocarbon products.

Table of Contents

List of Figures

List of Tables

List of Abbreviations

2DE	two-dimensional gel electrophoresis
AccA	subunit A of the protein complex acetyl-CoA carboxylase
AccB	subunit B of the protein complex acetyl-CoA carboxylase
AccC	subunit C of the protein complex acetyl-CoA carboxylase
AccD	subunit D of the protein complex acetyl-CoA carboxylase
ACN	acetonitrile
ACP	Acyl Carrier Protein
AD	Anaerobic Digestion
ATP	Adenosine triphosphate
BG-11	Blue-Green 11
BLAST	Basic Local Alignment Search Tool
BSA	Bovine Serum Albumin
cDNA	complementary DNA
CHAPS	3-((3-cholamidopropyl) dimethylammonio)-1-propanesulfonate
CI	chloroform:isoamylacohol
CID	collision-induced dissociation
cps	counts per second
DH	dehydratase
DMSO	Dimethyl Sulfoxide
DNA	deoxyribonucleic acid
DTT	dithiothreitol
E	expected/score value
EDTA	ethylenediaminetetraacetic acid
$EDTANa_2$	ethylenediaminetetraacetic acid disodium salt dihydrate
FA	formic acid
FabA	β-hydroxy-acyl-ACP dehydratase
FabB	β-keto-acyl-ACP synthase I
FabD	malonyl-coa:ACP transacylase
FabF	β-keto-acyl-ACP synthase II
FabG	β-keto-acyl-ACP reductase
FabH	β-keto-acyl-ACP synthase III
FabI	enoyl-ACP reductase
FabZ	β-hydroxy-acyl-ACP dehydratase
FAMEs	Fatty Acid Methyl Esters
FAS	Fatty Acid Synthase
FB1	Fumonisin B1
FOG	Fat, Oil and Grease
GC-MS	Gas Chromatography-Mass Spectrometry
GDP	Gross Domestic Product
GHG	Greenhouse Gases
h	hour
HILIC	Hydrophilic Interaction Liquid Chromatography

HTL	hydrothermal liquefaction
IEF	isoelectric focusing
iTRAQ	Isobaric Tags for Relative and Absolute Quantification
LB	Lysis Buffer
LC-MS	Liquid Chromatography-Mass Spectrometry
M	molar
m/z	mass/charge
MeOH:DCM	methanol:dichloromethane
min	minute
mL	millilitre
mM	millimolar
mm	millimetre
MMTS	methyl methanethiosulfonate
MOPS	3-(n-morpholino)propanesulfonic acid
MPa	megapascal
ms	millisecond
MS-MS	tandem mass spectrometry
MTT	3-(4,5-dimethylthiazol-2-yl)-2,5-diphenyltetrazolium bromide
N	normal
NADPH	nicotinamide adenine dinucleotide phosphate
NCBI	National Centre for Biotechnology Information
nM	nanomolar
NPQ	Non-Photochemical Quenching
NS	no significant difference
PBRs	photobioreactors
PCI	Phenol:Chloroform:Isoamylalcohol
PCR	Polymerase Chain Reaction
PDH	pyruvate dehydrogenase
PSI	photosystem I
PSII	photosystem II
qPCR	Quantitative Polymerase Chain Reaction
RNA	ribonucleic acid
rpm	revolutions per minute
rRNA	ribosomal ribonucleic acid
RT-PCR	Reverse Transcription Polymerase Chain Reaction
SD	standard deviation
SDS	Sodium Dodecyl Sulphate
SDS-PAGE	Sodium Dodecyl Sulphate–Polyacrylamide Gel Electrophoresis
sec	second
SPE	solid phase extraction
TAE	tris-acetate-EDTA
TAGs	triglycerides
tcep	tris(2-carboxyethyl)phosphine
TE	thioesterase

TEM	Transmission Electron Microscopy
TEMED	tetramethylethylenediamine
TesA	thioesterase A
TesB	thioesterase B
Tris	tris(hydroxymethyl)aminomethane
Tris-HCl	tris(hydroxymethyl)aminomethane hydrochloride
UV	ultraviolet radiation
V	volt
v/v	volume/volume ratio
VFAs	volatile fatty acids
vs	volatile solid
W	watt
w/v	weight/volume ratio

Declaration

I declare that the material contained in this thesis has not been previously submitted, in whole or in part, for a degree in Durham University or any other institution. Except where states otherwise by reference or acknowledgment, the work presented is entirely my own and supervisor’s which has been generated by us as the result of original research.

Statement of Copyright

Acknowledgements

I would like to thank God and my parents, Fabiola and Humberto for allowing me to get where I am now, for their unconditional love and support, and for being the fundamental pillars of my life; los amo:)

I would like to express my gratitude to Dr. Steve Chivasa, my admired supervisor who became my mentor, for sharing his endless enthusiasm related to constant work and science, for his absolute guidance and for the complete training provided.

Thanks to my sister Ana Lucía, for its singular support, for always encourage me to try and always support me even from distance; to my siblings M-M-R-L for all the fun and happiness.

Many thanks to Colleen Turnbull, a valuable friend who contributed a lot, not only to my learning and the development of this research project, but mainly as support in my daily life abroad.

Thanks to Dr. Ian Cummins, Dr. Adrian Brown, Dr. Rachael Dack and MSc. Christine Richardson for collaborating in this project.

Thanks to Itzel Romero, the best roommate I can ever asked and for living this great adventure together; te quiero, tonta :)

Thanks to Balder Nieto, for his love and comprehension, for giving me the opportunity to live such wonderful experiences and always be with me; ta♥

Thanks to Diego, David, Martha, Ana Cristina, Karen, Jeroen & Alexandra, for the small family we created in Durham and for the good times shared.

Thanks to Graciela, Estefany, Itzayana, Vicky, Luis Angel & Castro for maintaining friendship despite the distance.

Many thanks to all my maternal and paternal family for their support, love and for believing in me even when I don't.

I would like to express my gratitude to Prof Teresa Alonso and MC. Marcial Arrambí for offering the opportunity and their full support to carry out my postgraduate studies abroad.

Finally, thanks to CONACyT-SENER for financing my studies at Durham University, a great school for its human resources and facilities.

¡Gracias Totales!

1 Literature Review

1.1 Introduction

The hydrocarbons sector has been critical for global economic growth and creation of breakthrough technologies that have impacted human life and the environment. For example, hydrocarbons are exploited for energy generation, in the manufacture of beauty products such as creams and cosmetics, in the pharmaceutical industry, and as important resources in the chemical sector to produce lubricants, cleaning products, and agrochemicals. The predominant hydrocarbons in use are fossil fuels.

Oil, coal, and natural gas are the most abundant hydrocarbons harnessed as feedstocks for industrial processes and for energy production. Natural gas is composed of a high percentage of methane, together with ethane, propane and other alkanes and alkenes (Schobert, 2013). In 2017, the global consumption of natural gas was 3,757 billion cubic meters, which represents a 3.2% growth on the 2016 total consumption (IEA, 2017). Projections from 2018 to 2023 of natural gas production estimate that 14.3% will be destined for transportation, 16.90% will be used in residential and commercial sectors, 25.48% for power (electricity) generation, and 43.49% will be destined for use by the manufacturing industries (IEA, 2018). These estimates show that industry will utilise a far greater proportion of natural gas, which has better environmental impact since it is the least carbon dioxide emitter of all the fossil fuels.

During 2017, 34.2% primary energy consumption was derived from oil, 27.6% came from coal, and natural gas accounted for 23.4% (BP, 2018). Renewable sources contributed 3.6%, which includes wind, geothermal, solar, biomass and waste (BP, 2018). These data indicate that fossil fuels are the main source of global energy, contributing an estimated total of ~85.2%. Because fossil fuels have a fundamental role in many sectors, a report in 2017 predicted increased future consumption by 1.7% per year (BP, 2018). If this trend continues, the outlook suggests that the remaining reserves of oil, natural gas and coal will only last for the next 50, 53 and 134 years, respectively (BP, 2018).

The dependence on fossil fuels is associated with environmental pollution arising from emissions of greenhouse gases (GHG). Carbon dioxide (CO_2) is the main greenhouse gas that is released to the atmosphere as a result of anthropogenic activities. The main driver of CO_2 emissions is combustion of fossil fuels. Over the 2007 – 2017 decade, there was a ~1% annual growth in carbon dioxide emissions, starting off at 30,078.7 million tonnes and closing the decade at 33,444 million tonnes (BP, 2018). Of this 2017 total, 89% arose from fossil fuels, 40% of which came from coal combustion, 31% from oil and 18% from natural gas (Olivier & Peters, 2018). In light of the inevitable, depletion of fossil fuel resources and the current GHG emissions forecast to exacerbate the rise in global warming, developing cleaner alternative sources of energy has become imperative. While total replacement of fossil fuels will take time to implement, diversification of primary energy supplies by including alternative renewable energy resources will address environmental concerns and secure future energy supply chains.

Mexico is one of the most important oil and liquid petroleum-producing countries, with the hydrocarbon sector being important for its economy (González-López & Giampietro, 2018). The energy sector represents an essential operational base to develop the primary, secondary and tertiary activities which form the Gross Domestic Product (GDP) of the nation. Although in 2015 oil and gas accounted for only 5% GDP, it contributes 33% revenue to the public sector as the major company in oil production is state-owned (González-López & Giampietro, 2018). In 2018, the GDP contribution of agriculture and manufacturing sectors were 3.39% and 30.94%, respectively (World-Bank, 2019). Both sectors are entirely supported by oil and gas as energy resources, illustrating the importance of the sector to the broader economy. However, production of hydrocarbons in Mexico decreased steadily since 2004 due to a low yield of Cantarell oil fields, one of the principal reserves of oil in the world (González-López & Giampietro, 2018).

Because of the relevance of energy to the global economy (including México), investments to develop alternatives to fossil fuels is a key consideration to ensure future economic growth. Interest in renewable energy as alternatives to fossil fuels has been on the increase in the last few decades. Renewable energy refers

to resources that cannot be depleted (Panwar et al., 2011), for example solar, wind, and biomass. These are clean sources of energy that promote a sustainable use of the supplies producing minimal waste and decreasing adverse environmental consequences (Panwar et al., 2011).

The alternative renewable energy sources, such as solar and wind, require photovoltaic cells or a turbine and generator, respectively, for conversion to electricity. Even though the use of these clean energy resources represents an environmentally friendly alternative to fossil fuels, implementation and exploitation requires additional investments for installation of wind and solar power infrastructure. Furthermore, efficiency could be intermittent as power production is highly dependent on weather conditions, season, location and time of the day (Paolini & Paolini, 2010).

Harnessing sunlight as a source of energy represents an affordable, abundant, and sustainable resource with minimal or no negative impact on the environment or human health (Crabtree & Lewis, 2007). Sunlight energy is used by photosynthetic organisms to fix atmospheric CO_2 for production of biomass, which provides an easy route for exploitation of solar energy (Crabtree & Lewis, 2007). The biomass can then be converted to usable energy via anaerobic digestion (AD) to produce biogas (Panwar et al., 2011). A possible source of biomass for use in biofuel production are food crops. However, this is not desirable since it threatens food security (Rittmann, 2008). Instead of using food crops, a readily available biomass resource could be bio-solids from municipal and industrial waste collected by waste treatment companies in major urban centres. The biosolids are fed into industrial anaerobic digestion tanks that produce substantial amounts of biogas, which creates a viable revenue stream for the companies.

1.2 Photosynthetic systems as sources of industrial feedstock

Photosynthesis is a process that harnesses sunlight energy to drive a set of complex chemical reactions utilizing CO_2 and water to make organic compounds, with oxygen as a by-product. Through photosynthesis, plants, algae and some bacteria synthesise key molecules used as building blocks for growth and high

energy compounds for fuelling metabolic reactions. Thus, photosynthesis is solely responsible for production of biomass in photosynthetic organisms. Because sunlight energy is freely available, photosynthetic organisms are thus a promising resource for exploitation in making industrial feedstocks for various applications. Biomass produced by photoautotrophic organisms is predicted to become the main future resource for generating biofuels (Tsuzuki et al., 2019). Therefore, plants, microalgae and cyanobacteria are being explored as possible resources for making alternative renewable energy and numerous industrial products.

Large-scale cultivation of photosynthetic organisms presents challenges, such as poor productivity, high labour demand and huge energy consumption from seeding to harvest, with various specialist requirements along the production chain (Sydney et al., 2011; Abomohra et al., 2013; Nascimento et al., 2013; Tsuzuki et al., 2019). The requirement for arable land, fresh water supplies, use of agrochemicals and sometimes deforestation are just some of the hurdles that need to be considered in crop-based systems (Nascimento et al., 2013). Furthermore, the ethical debate about diverting prime agricultural land to energy crop farming continues to rage, and has again come into sharp focus given the threats on food security posed by climate change.

Microalgae and cyanobacteria have super-efficient metabolism supported by a very high capacity to fix carbon dioxide (Sydney et al., 2011). Their ability to rapidly grow on wastewater with no competition for arable land and freshwater resources makes them an attractive production system for industrial applications. Growing and harvesting microalgae could provide an alternative renewable resource for use across a wide range of applications, including agriculture, hygiene and beauty products, food, and energy. For example in the agriculture sector, Uysal et al. (2015) developed a fertilizer from *Chlorella vulgaris* (a microalga) that improved growth of wheat and maize, while Silva-Neto et al. (2012) made a fish feed additive from *Spirulina platensis* (a cyanobacterium) that serves as an attractant to juvenile fish of the species *Litopenaeus vannamei* when mixed with fishmeal. In the food sector, Soselisa et al. (2019) fortified shark liver oil supplements with *Spirulina platensis* powder, thereby improving the nutritional

value by the added essential amino acids and minerals. Also, in the food sector, Fradique et al. (2010) produced fresh spaghetti made with semolina flour and fortified with microalgal biomass of *Chlorella vulgaris and Spirulina maxima.* Analysis indicated that the formulations resulted with a higher content of protein, fat and ash than pasta without fortification.

In the case of the beauty industry, a company called ALGENIST® manufactures skincare products derived from diverse species of microalgae such as *Dunaliella salina*. Their products include concealers, moisturizers, serums, face oils and different types of skin treatments (Joshi et al., 2018). In the energy sector, algal biomass is being exploited as a feedstock to produce substitutes for some petroleum derivatives, with the added advantage of reduced attendant GHG emissions. Biofuel production is one of the industrial processes that could benefit most from the use of biomass of photosynthetic organisms.

It is very important to consider the economic aspects of proposed industrial processes to ensure both technical feasibility and profitability. Researchers have explored lowering production costs by use of domestic/industrial wastewater to grow microalgae for generating massive amounts of biomass, which is then converted to biofuels (Sydney et al., 2011). The wastewater effluent is abundant and microalgal growth converts the waste into an attractive resource. Furthermore, adoption of this approach has positive impacts on the environment, such as removal of nutrients from the effluent to prevent pollution of fresh water sources and reduction of GHG emissions by way of generating cleaner biofuels (Sydney et al., 2011).

1.3 Microalgae and cyanobacteria biomass conversion to hydrocarbons

Several methods have been developed for the conversion of biomass to liquid and gaseous biofuels. In an elaborate workflow proposed to maximise output from cyanobacteria and microalgae, the living cells are first used to produce hydrogen gas, followed by lipid extraction for bioconversion to biodiesel, with the residual biomass finally being converted to ethanol, biogas, or bio-oil via fermentation, anaerobic digestion, or hydrothermal liquefaction, respectively (Figure 1.1) (Pawlita-Posmyk et al., 2018).

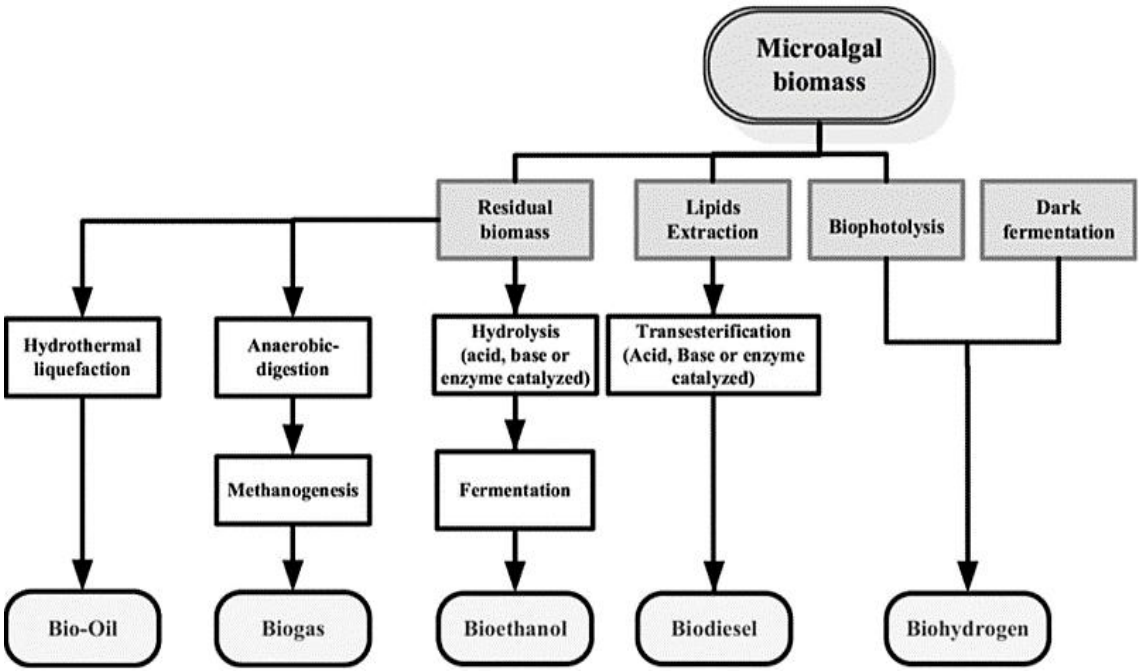

Figure 1.1 Schematic diagram showing how microalgal biomass can be converted into bioenergy.
Three processes can be used in production of bioenergy from algae. The first is production of biohydrogen via photolysis or dark fermentation using the live organisms. The second requires lipid extraction and transesterification to produce biodiesel. The residual biomass can be turned into (i) bioethanol after hydrolysis followed by fermentation, (ii) biogas via anaerobic digestion, or (iii) bio-oil via hydrothermal liquefaction. Image taken from Pawlita-Posmyk et al. (2018).

1.3.1 Biohydrogen production

Biohydrogen production is achieved via biophotolysis (direct and indirect), photofermentation, or dark fermentation (Ferreira et al., 2012). In direct biophotolysis, the supracomplex consisting of the oxygen-evolving complex and photosystem II complex utilises solar energy to dissociate water molecules into oxygen gas and protons plus electrons (Manish & Banerjee, 2008), with the latter two being used by ferredoxin and hydrogenase enzymes in a reaction that yields hydrogen gas. Indirect photolysis uses cellular organic compounds, such as carbohydrates originally produced via photosynthesis, as substrates for H_2 production (Nagarajan et al., 2017; Abedi et al., 2019a). While photofermentation similarly uses organic compounds for production of H_2, it differs from indirect photolysis in using exogenously supplied organic compounds (Oey et al., 2016).

Dark fermentation is a H_2-producing process, in which anaerobic bacteria use organic compounds in biomass as substrates in reactions not requiring light (Manish & Banerjee, 2008). In addition to hydrogen, dark fermentation also produces CO_2 and volatile fatty acids (VFAs), such as butyric and acetic acids (Liu et al., 2013). Batista et al. (2015) used biomass of *Chlorella vulgaris*, *Scenedesmus obliquus* and a naturally occurring algal *Consortium C* to produce biohydrogen through dark fermentation with *Enterobacter aerogenes*. The highest production rate was 56.8 mL H_2/g volatile solid (VS) obtained using *S. obliquus* biomass.

1.3.2 Biodiesel production

Biodiesel is generally synthesised through a chemical transesterification process. Oil extracted from various sources is subjected to chemical transesterification, which transforms the triglycerides (TAGs) into biodiesel components - long linear chains of fatty acid methyl esters (FAMEs) (Shah et al., 2018). Key requirements for this process are: (i) an alcohol (methanol or ethanol are often used) and (ii) a homogenous acid or base, or (iii) heterogenous carbonates or metal oxides functioning as a catalyst (Johnson & Wen, 2009; Shah et al., 2018). Oils derived from seeds, animals, vegetables, residues and plants are extensively used as

feedstock, since they contain free fatty acids, but mainly TAGs are the easiest compounds to transform to biofuel (Nascimento et al., 2013; Shah et al., 2018). However, oils originating from organisms such as algae and cyanobacteria have a favourable fatty acid profile with abundant C16 and C18 fatty acids, hence they are an important resource for biodiesel production (Ihsanullah et al., 2015). For example, Johnson & Wen (2009) produced biodisel using biomass of a heterotrophic microalga *Schizochytrium limacinum* as feedstock. They evaluated two techniques, two-stage transesterification and direct one-stage transesterification, and investigated the impact of using fresh or freeze-dried biomass and different types of reagents. Chloroform proved to be the ideal solvent for use in transesterification, yielding high FAMEs content, while freeze-dried biomass had a better yield performance than fresh biomass (Johnson & Wen, 2009). Application of the two-stage method or one-stage processing methods gave rise to 66.37% and 63.47% FAMEs, respectively, demonstrating that biodiesel yield from *S. limacinum* biomass remains high regardless of the technique used (Johnson & Wen, 2009).

1.3.3 Bio-oil production

Bio-oil can be obtained through hydrothermal liquefaction (HTL) from residual microalgae biomass (Figure 1.1) HTL is based on subjecting biomass to high temperature and pressure (250-350 °C, 5-15 MPa) for conversion to oil (Vardon et al., 2012). This process works ideally in the transformation of algal “waste” residues to oil, since these importantly have considerable water content required to act as an optimal medium for the reactions breaking down organic molecules into low molecular weight compounds from which bio-oil is obtained (Shuping et al., 2010; Vardon et al., 2012). Because algal biomass grows in liquid medium, it is usable in its natural condition without the need for drying/rewetting cycles necessary for other types of biomass – this reduces energy costs. Shuping et al. (2010) reported the use of residues from the microalga *Dunaliella tertiolecta* as substrate for bio-oil production through HTL. They also found that a temperature of 360 °C held for 50 min with addition of 5% reaction catalyst were optimal conditions for maximal bio-oil production. However, other forms of biomass from

diverse sources, such as swine manure (Vardon et al., 2011), cyanobacteria (Huang et al., 2016), wood residue (Pedersen et al., 2016) and coffee (Yang et al., 2016), have been processed via HTL for bio-oil production.

1.3.4 Bioethanol production

Bioethanol is a distinct biofuel which is generated mainly from starch and lignocellulosic sources. However, exploitation of starch and lignocellulose as feedstocks is associated with several environmental and processing disadvantages (Ho et al., 2013). For example, the main feedstocks for bioethanol production in the USA and Brazil are corn and sugarcane, respectively, crops that require prime arable land, fresh water for irrigation, fertilizers and crop protection agrochemicals. For this reason, there is much interest in using algal biomass as an alternative substrate since some strains have high content of carbohydrates, which can be transformed into bioethanol (Kim et al., 2014). A distinct advantage of using microalgal biomass is that the carbohydrate content mainly consist of starch and cellulose, without the hard-to-digest lignin, making fermentation much simpler (Ho et al., 2013).

Chemical (acid and alkali) or enzymatic hydrolysis followed by fermentation, are the main processes required to generate bioethanol from algal biomass (Ho et al., 2013; Tan & Lee, 2015). Several pre-treatment processes before hydrolysis are required for full release of fermentable sugars and increased bioethanol production (Kim et al., 2014). Regardless of whether pre-treatment was applied or not, hydrolysis of the feedstock is necessary to fragment carbohydrates into simple sugars to make them more accessible to the fermentation process.

Bioethanol production via fermentation was reported by Kim et al. (2014), who used *Chlorella vulgaris* biomass. In this study, the microalga was grown under stress conditions (nitrogen-limitation), which raised carbohydrate composition from 16% to 22.4% on dry weight basis. Diverse pre-treatments and enzymes were tested to facilitate conversion during subsequent stages, and bead-beating pre-treatment enhanced hydrolysis by 25% in comparison with no process applied and 79% saccharification yield was achieved by using *Aspergillus*

aculeatus pectinase. For the fermentation phase, *Saccharomyces cerevisiae* was applied to the pre-treated biomass, producing a final yield of 89% bioethanol.

1.3.5 Biogas production

Anaerobic digestion (AD) is a process that is carried out by a consortium of specific microorganisms in the absence of oxygen. This decomposes organic matter into simpler compounds and the main commercially valuable product is methane. The AD process has four distinct phases which are carried out by different microbial consortia (González-Fernández et al., 2012; Molino et al., 2013; González-Fernández et al., 2015; Zaidi et al., 2018; Anto et al., 2019):

1. Hydrolysis: This is the first set of AD reactions, where degradation of macromolecules such as lipids, proteins, and carbohydrates are broken down into fatty acids, amino acids, and simple sugars, respectively. Major groups of hydrolytic enzymes (lipases, proteases, carbohydrases) are released into the biomass and digest target macromolecules for absorption by the microbes. This is a fundamental stage required to breakdown complex macromolecules into simpler molecules that can be used in the next phase. The final biogas yield depends on the extent to which hydrolysis has been effective in breaking down available macromolecules.

2. Acidogenesis: The monomers obtained during the previous hydrolysis phase are converted by acidogenic bacteria (acidogens) into volatile fatty acids (VFAs), such as acetic, butyric, lactic and propionic acids.

3. Acetogenesis: In this phase, the acids formed in the acidogenesis stage are used by acetogenic bacteria (acetogens) to produce acetate, carbon dioxide and hydrogen.

4. Methanogenesis: The last stage of AD is where methanogenic microorganisms (methanogens) complete the final step of biogas production. Acetate, carbon dioxide and hydrogen are used as substrates by methanogens to produce methane as the main product. This phase is critical and often rate-limiting, particularly because of the slow growth rate of

methanogens. This causes overproduction of VFAs synthesised in previous phases, which leads to inhibition of methanogenic bacterial activity, thereby reducing methane production.

Mendez et al. (2016) cultivated in wastewater two cyanobacterial species, *Aphanizomenon ovalisporum* and *Anabaena planctonica*, and the microalga *Chorella vulgaris*. The biomass was used as AD substrate for the production of methane, and higher methane yield was recorded for the cyanobacteria than the microalga, presumably due to better digestibility of the former.

Co-digestion of different types of substrates has been reported to enhance methane production from AD systems. For example, Ehimen et al. (2011) explored the effects of glycerol co-digestion with biomass residues of the microalga *Chlorella sp*. on biogas production. They observed enhanced methane production with co-digestion, presumably due to improved balance of the microbial consortium across the four AD phases. Inclusion of fat, oil and grease (FOG) in a regular anaerobic digestion system for co-digestion is reported to massively enhance methane production (Kurade et al., 2019). The benefits of co-digestion with FOGs are thought to be derived from the positive effects of altering the bacterial consortia in the AD system (Amha et al., 2017). Caporgno et al. (2015) also evaluated biogas production from co-digestion of sewage sludge with biomass from microalgae species *Isochrysis galbana* and *Selenastrum capricornutum.* In this case, co-digestion did not improve methane yields, perhaps suggesting that only specific substrate combinations in co-digestion result in enhancement of methane yields.

1.4 Bacterial fatty acids as hydrocarbon precursors

Fatty acid biosynthesis represents a highly conserved process through evolution and across different life domains. It is one of the most important pathways in prokaryotic and eukaryotic organisms that contributes to the formation and development of essential cell structures and biological functions (Janssen & Steinbuchel, 2014). Because of this conservation, here it is considered the fatty

acid biosynthetic pathway of *Escherichia coli* (Figure 1.2) as a prokaryotic model that could be used to identify homologous genes in cyanobacteria.

E. coli lipid biosynthesis begins with the carboxylation of acetyl-CoA to malonyl-CoA in a reaction catalysed by acetyl-CoA carboxylase, which is a protein complex consisting of four subunits AccA, AccB, AccC and AccD. Malonyl-CoA is converted to malonyl-acyl carrier protein (malonyl-ACP) by malonyl-CoA:ACP transacylase (FabD). The malonyl-ACP is then processed reiteratively through several elongation cycles, which progressively add more carbons to the growing fatty acid chain until the necessary chain length is achieved (Figure 1.2). First, Claisen condensation of acetyl-CoA and malonyl-ACP is carried out by β-keto-acyl-ACP synthase III (FabH), which produces β-keto-acyl-ACP. The product is in turn reduced consecutively twice, and then dehydrated once to generate acyl-ACP. Acyl-ACP is used as a substrate for fatty acid chain elongation via condensation reactions with malonyl-ACP catalysed by β-keto-acyl-ACP synthase I (FabB) and β-keto-acyl-ACP synthase II (FabF). During elongation, β-hydroxy-acyl-ACP is produced by β-keto-acyl-ACP reductase (FabG) and transformed to trans-Δ^2-enoyl-acyl-ACP by β-hydroxy-acyl-ACP dehydratase (FabA) and β-hydroxy-acyl-ACP dehydratase (FabZ) (Lennen et al., 2010; Tao et al., 2016). After six additional cycles, the final stage of fatty acid biosynthesis is catalysed by enoyl-ACP reductase (FabI) where palmitoyl-ACP is produced and acyl-ACP thioesterases TesA and TesB dissolve acyl-ACPs to release free fatty acids from ACP which, with the action of β-oxidation enzymes, can be transformed to acetyl-CoA and start the process again (Lennen et al., 2010; Janssen & Steinbuchel, 2014). All the enzymes involved in fatty acid biosynthesis in *E. coli* are part of type-II fatty acid synthase (FAS), which is a multi-protein complex that is mainly present in prokaryotic organisms and plants (plastids). FAS is responsible for elongation of fatty acid chains that have already entered the chain elongation phase, but cannot start performing chain elongation from scratch (Blatti et al., 2013).

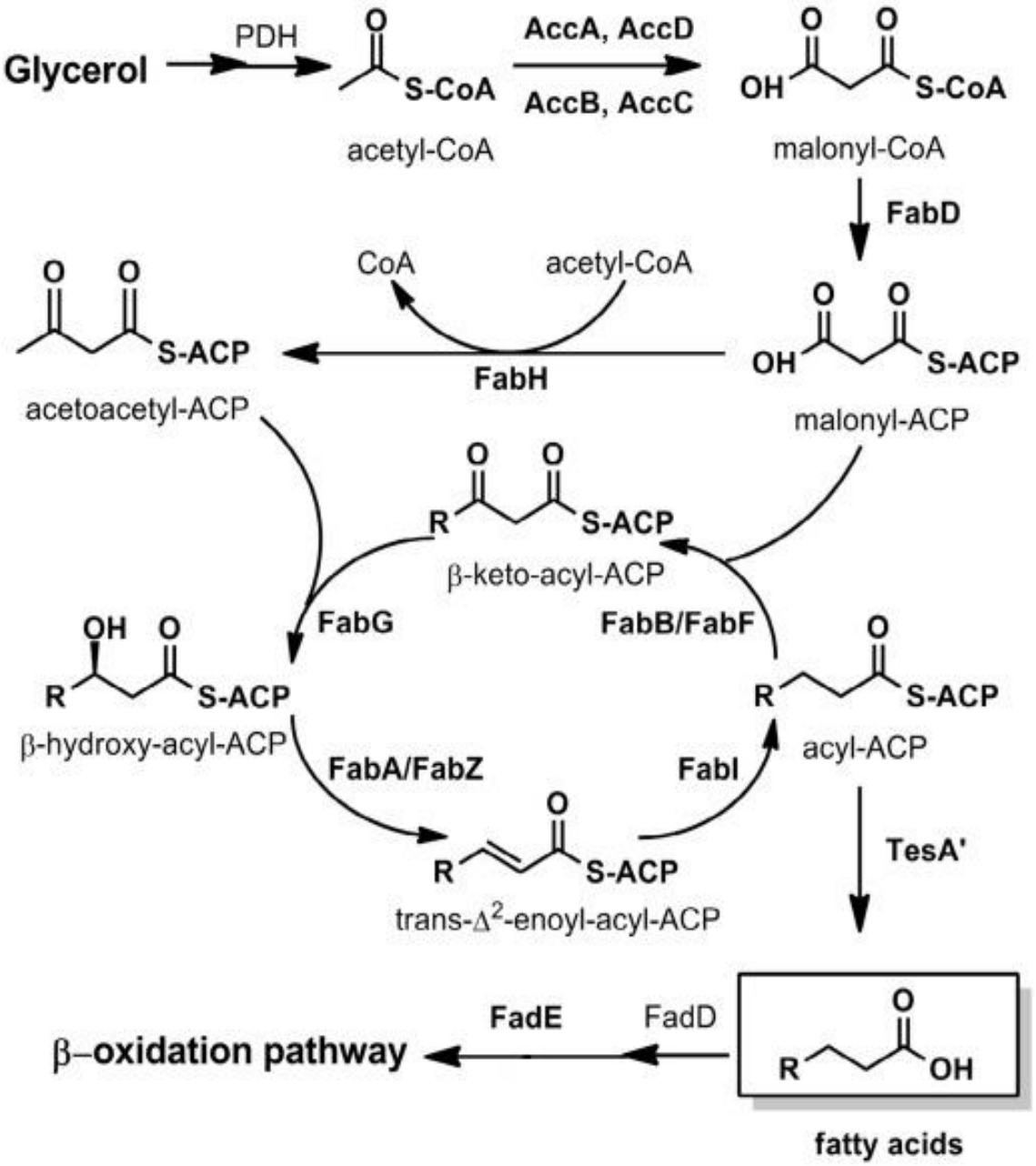

Figure 1.2 Schematic diagram of fatty acid biosynthesis in *Escherichia coli*.

(Full explanation in text). PDH: pyruvate dehydrogenase; AccA: subunit A of the protein complex acetyl-CoA carboxylase; AccB: subunit B of the protein complex acetyl-CoA carboxylase; AccC: subunit C of the protein complex acetyl-CoA carboxylase; AccD: subunit D of the protein complex acetyl-CoA carboxylase; FabD: malonyl-CoA:ACP transacylase; ACP; acyl carrier protein; FabH: β-keto-acyl-ACP synthase III; FabG: β-keto-acyl-ACP reductase; FabA: β-hydroxy-acyl-ACP dehydratase; FabZ: β-hydroxy-acyl-ACP dehydratase; FabI: enoyl-ACP reductase; FaB: β-keto-acyl-ACP synthase I; TesA: thioesterase A; FabF: β-keto-acyl-ACP synthase II; FadD: acyl-CoA synthase; FadE: acyl-CoA dehydrogenase. Image taken from Tao et al. (2016)

Since the fatty acid biosynthesis pathway has been extensively studied and characterized in plants and bacteria, by following it theoretically, it is possible to deduce cyanobacterial and algal fatty acid biosynthetic pathways in which homologous genes can be identified (Blatti et al., 2013). This is shown in Figure 1.3 with a diagram developed for an algal strain.

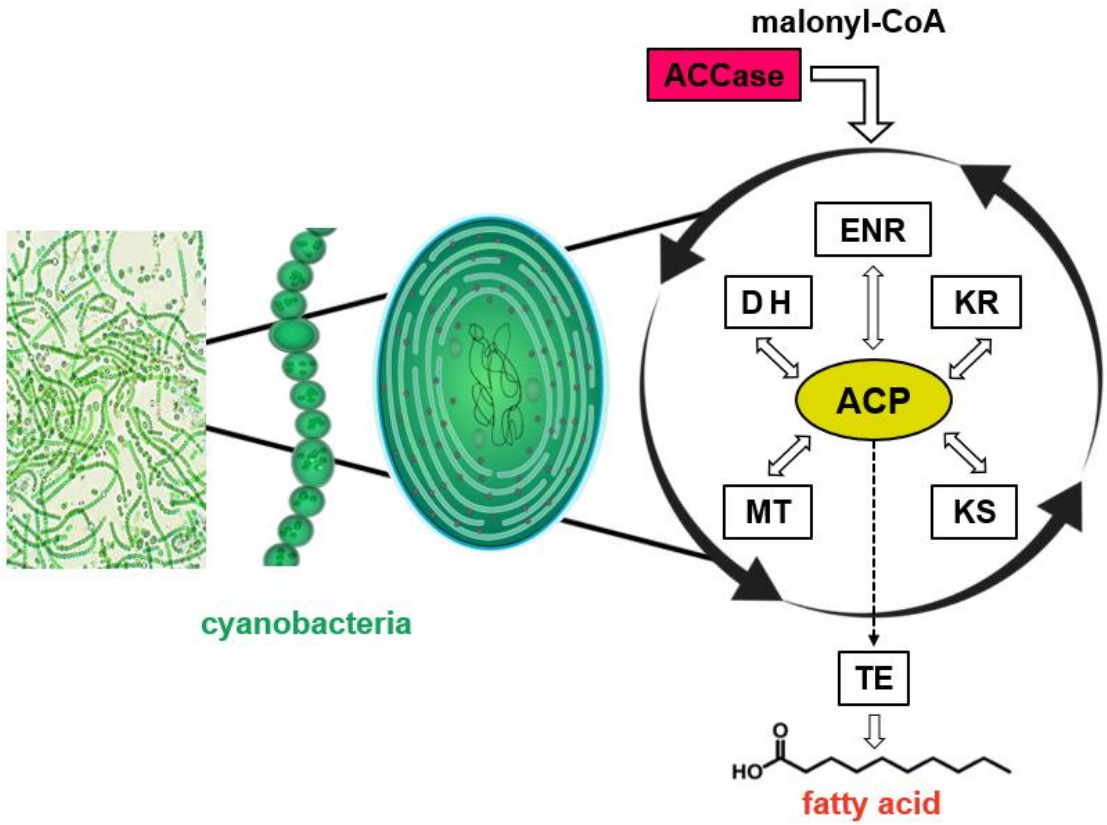

Figure 1.3 Schematic diagram of an algal strain lipid biosynthesis pathway. Fatty acid biosynthesis starts with acetyl-CoA-carboxylase (ACCase)-catalysed reaction, which carboxylates acetyl-CoA to make malonyl-CoA. The malonate is tethered to the acyl carrier protein (ACP), paving way to an iterative cycle of chain elongation initiated by ketosynthase (KS), followed by ketoreductase (KR), dehydratase (DH), and ending with enoyl reductase (ENR). Each turn leads to net addition of two carbons to the nascent fatty acid chain. On reaching the mature fatty acid length still attached to the ACP (yellow), thioesterase (TE) activity releases the fatty acid from ACP via hydrolysis. Image adapted from Blatti et al. (2013).

1.5 Stress-activation of lipid biosynthesis in cyanobacteria and microalgae

In nature, only a few cyanobacterial species in the genus *Nannochloropsis* yield high amounts of lipids. For example, lipids constitute 53% of total biomass in *Nannochloropsis oceanica* IMET1, 41% in *Nannochloropsis limnetica* CCMP505, 60% in *Nannochloropsis granulata* CCMP52, 52% in *Nannochloropsis oculata* CCMP529, and 39% in *Nannochloropsis salina* CCMP537 (Ma et al., 2014). With the exception of the so-called oleaginous *Nannochloropsis* spp. (Jinkerson et al., 2013), many cyanobacteria generate very little amounts of lipids (below 12% of biomass) under normal growth conditions. For example, *Synechocystis PCC 6803* accumulates 13% lipid, *Synechococcus PCC 7942* has 11%, *Nostoc muscorum* and *Oscillatoria* sp. have 7.5% lipid, *Anabaena cylindrica* only has 5%, *Lyngbya* sp. averages 10.5% and *Phormidium* sp. reaches only 8.5% (Patel et al., 2018).

However, it has been noted that exposure to chemical or environmental stress promotes lipid biosynthesis and accumulation. For example, the cyanobacteria *Microcoleus* sp. (SP18) recorded increases of 26.8% and 153% in lipid accumulation after exposure to nutrient limitation in nitrogen or phosphorous, respectively (Kumar et al., 2017). Takagi and Yoshida (2006) demonstrated between 67-70% increase in lipid content of *Dunaliella* cells exposed to salinity stress using NaCl. Miranda et al. (2002) analysed the response of *Euglena gracilis* to heavy metal stress (zinc and copper) and reported over 2-fold increases in lipids. Similarly, Lui et al. (2008) reported a 56.6% increase in lipid content of *Chlorella vulgaris* in response to iron metals. In addition to ionic stress, lipid content is also increased in response to temperature shifts. For example, a decrease of 8°C from the optimal 26°C growth temperature of *Chlorella sorokiniana* LS-2 enhanced lipid content from 132 $mg.g^{-1}$ to 149 $mg.g^{-1}$ (Wang et al., 2016). Finally, modest increases in lipid composition of cyanobacteria responding to light stress have also been registered. For example, increasing light intensity from 500 to 2000 lux increased the lipid composition of *Phormidium* sp. *FW01*, *Phormidium* sp. *FW02*, *Oscillatoria sp*. *FW01* and *Oscillatoria* sp. *FW02* from 6 to 7.5%, 7.8 to 9.5%, 9.5 to 12.5% and 8.5 to 10.5%, respectively (Yadav et al., (2021).

1.6 Hypothesis and objectives

Microalgal and cyanobacterial biomass represents a viable alternative resource for use in industrial applications. In designing this research project, the value of lipids as a versatile raw material that can be turned into numerous industrial products was considered. Thus, a key objective of the project was to investigate ways of boosting lipid production in *Synechocystis SR*. In addition to the potential usefulness of the cyanobacterial system as a source of lipids, unpublished preliminary data from our research group indicated that biomass of *Synechocystis SR* can potentially be used in biogas production.

Biogas is an alternative energy source currently underutilised due to low yields. Therefore, any improvements in yield could incentivise the energy sector to increase uptake of this renewable energy resource. As explained above (section 1.3.5), co-digestion of different biomass substrates can sometimes boost methane yields from anaerobic digestion systems. Unpublished results from our group show that co-digestion of sludge liquor with a very small amount of cyanobacterial biomass can enhance biogas production by nearly 500-fold. This occurs only when biomass of *Synechocystis SR* is used, but not the control strain *Synechocystis* PCC 6803. *Synechocystis SR* was recently identified by our group as a stress-resilient (*SR*) cyanobacterium, which can forge a commensal relationship with the nitrogen-fixing *Trichormus variabilis* in order to survive in a nitrogen-depleted environment (Abedi et al., 2019b). Co-digestion with fatty acids is thought to alter the AD system's microbial consortium and massively boost methane production (Caporgno et al., 2015; Amha et al., 2017; Kurade et al., 2019; Kurade et al., 2020). Thus, if the lipid content of *Synechocystis SR* is increased prior to inoculating digesters, the gas yield could be further increased, making this system economically attractive to industry.

The stress resilience of *Synechocystis SR* was demonstrated by its ability to thrive in mixed industrial wastewater, in which other cyanobacteria (such as *Trichormus variabilis*) fail to grow due to toxic compounds (Abedi et al., 2019b). Preliminary results from our laboratory also show that *Synechocystis SR* survives at high temperatures that kill other cyanobacteria, suggesting that its resilience against multiple stresses.

Therefore, this project aimed to optimise cyanobacterial biomass production and develop a system for increasing the lipid content of *Synechocystis SR* in order to (i) provide a clean alternative raw material industrial manufacturing of diverse valuable chemicals and products and (ii) and provide a raw ingredient for turbocharging methane production when the biomass is added for co-digestion in anaerobic digestion systems. Because lipid content in microalgae and cyanobacteria is enhanced by stress (Kim et al., 2014; Neag et al., 2019), the specific goal of the project was to develop a biotic or abiotic stress system, which is effective at enhancing lipid accumulation in the cyanobacterial cells. Additionally, the stress system should be cheap and adaptable for industrial scale-up to make the technology economically feasible.

1.6.1 Hypothesis

The hypothesis of this research was that salinity stress stimulates cellular lipid biosynthesis and accumulation in *Synechocystis SR*. If this hypothesis is correct, then the cyanobacterial cells can be cultivated and exposed to high salinity stress utilisation in lipid extraction or for use as a potent ingredient of a methane booster additive in anaerobic digestion. To make the production technology affordable, salinity can be achieved by using sea water, which is an abundant resource for coastal countries. Therefore, this project focused on investigating salinity-induced regulation of the fatty acid synthesis (FAS) genes in cyanobacteria.

In addition to investigating salinity stress as a potential industrial tool for cyanobacterial lipid production, the project also aimed to explore the response of cyanobacteria to biotic stress. A thorough search of the literature did not reveal any prior studies linking biotic stress to altered lipid production in cyanobacteria. Thus, a second hypothesis of the project was that sub-lethal biotic stress can equally activate lipid production. A mycotoxin derived from the fungus *Fusarium verticillioides*, which activates cell death in plants and cell suspension cultures of plants (Stone et al., 2000; Blacutt et al., 2018; Zeng et al., 2020) was used to test this hypothesis.

1.6.2 Specific objectives

1. Optimization of cyanobacterial growth with and without salinity stress.
2. Proteome and transcriptome identification of key components of the cyanobacterial fatty acid synthase (FAS) machinery and analysis of gene expression in response to salinity.
3. Metabolomic analysis of lipid profiles in response to salinity stress.
4. Explore the stress response of cyanobacteria to a fungal mycotoxin (fumonisin B1) and its impact on lipid synthesis.

2 Materials and Methods

2.1 Biological material and cultivation of cell cultures

The biological material used in this project consisted of the microalga *Chlamydomonas reinhardtii*, the cyanobacteria *Synechocystis PCC 6803* and *Synechocystis sp.* strain *SR* (Abedi et al., 2019b), and cell suspension cultures of *Arabidopsis thaliana* ecotype *Landsberg erecta* (May & Leaver, 1993).

Cyanobacterial and algal cultures were cultivated in Blue-Green 11 (BG-11) growth medium developed by Stainer et al. (1971). BG-11 contains the following final concentrations: 17.6 mM $NaNO_3$, 229.6 µM K_2HPO_4, 304.3 µM $MgSO_4 \cdot 7H_2O$, 242.9 µM $CaCl_2 \cdot 2H_2O$, 31.2 µM citric acid, 22.8 µM ferric ammonium citrate green, 2.7 µM $EDTANa_2$, 188.8 µM Na_2CO_3, 46.5 µM H_3BO_3, 9.1 µM $MnCl_2 \cdot 4H_2O$, 0.8 µM $ZnSO_4 \cdot 7H_2O$, 1.6 µM $Na_2MoO_4 \cdot 2H_2O$, 320 nM $CuSO_4 \cdot 5H_2O$ and 170 nM $Co(NO_3)_2 \cdot 6H_2O$. For long-term storage, cultured cells were kept suspended in sterile 20% glycerol, snap-frozen in liquid nitrogen and stored at -80°C. For subculturing, inoculum of between 4 - 20 mg (fresh weight) cells was added to sterile BG-11 medium in glass test tubes (3 cm diameter x 20 cm depth) with a capacity of 100 mL or in flattened glass flasks with a capacity of 750 mL (Figure 2.1). The tube or flask was capped with a foam bung perforated with a hole to accommodate a thin aerating glass tube for delivering compressed air to the culture. The bottom end of the glass tube was submerged in the medium with the orifice close to the bottom of the test tube or flask, while the top end of the aerating glass tube opened into a wider compartment filled with sterile cotton wool. Compressed air was delivered from a tank via rubber tubing with a 0.2 µm filter located just before connection of the air supply to the top end of the aerating glass tube using an airtight rubber bung (Figure 2.1). The culture flasks or tubes were incubated in temperature-controlled (30°C) water baths with continuous illumination from an external light source set at either low or high light intensity (75 or 150 $\mu mol.m^{-2}.s^{-1}$), depending on the requirements of each experiment.

Arabidopsis cell cultures were grown in Murashige and Skoog medium (Murashige & Skoog, 1962) which contains the following: 3% (w/v) sucrose, 0.44% (w/v) Murashige and Skoog with Minimal Organics (Sigma-Aldrich, Dorset,

UK), 0.05% (w/v) 1-napthaleneacetic acid and 0.05% (w/v) kinetin. The cultures were maintained by subculturing 1-week-old inoculum in 9-fold volume of fresh growth medium once per week. The cells were incubated at 23°C on a rotary shaker (120 rpm) in a 16 h light-8 h dark cycle, with the light intensity set at 150 $\mu mol.m^{-2}.s^{-1}$. The cells were used for experiments 3 days post-subculturing and after adjusting the cell density to 5% weight/volume ratio.

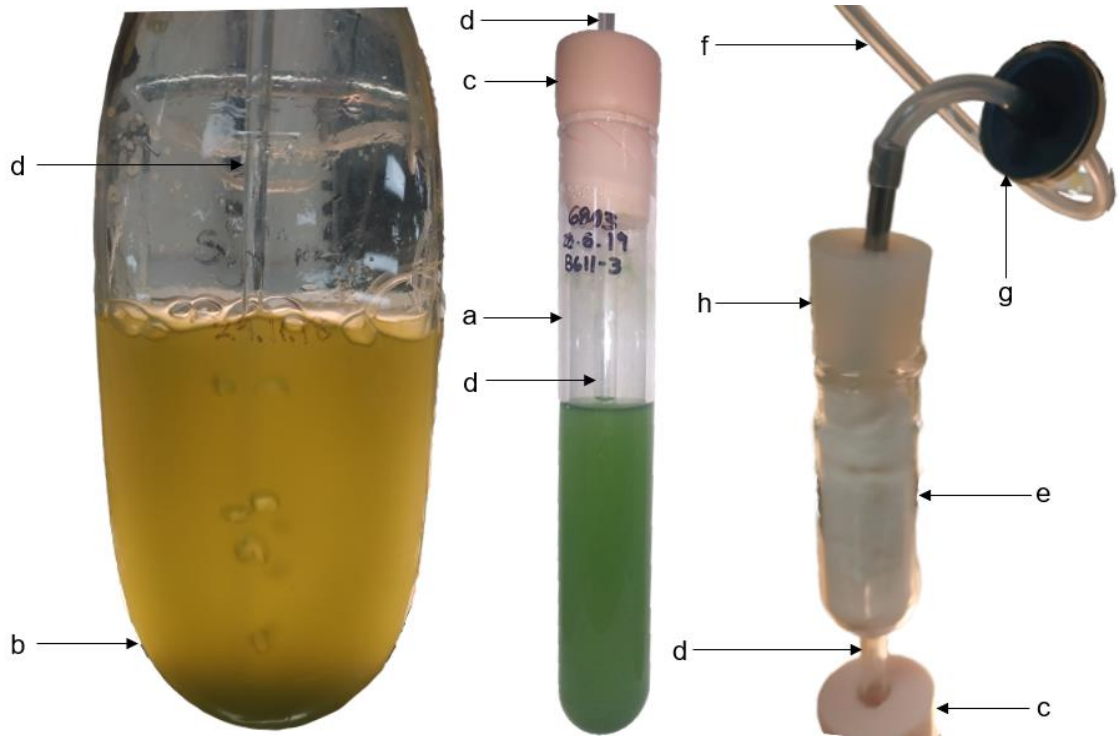

Figure 2.1 Culture vessels used to cultivate cyanobacteria and microalgae. The cell culture equipment consisted of either (**a**) a 100 mL-capacity glass test tube or (**b**) a 750 mL-capacity flattened glass flask capped with (**c**) a foam bung through which (**d**) a thin aerating glass tube passed. Compressed (**e**) sterile cotton wool in the flanged top neck of the aerating tube provided a sterile barrier. A (**f**) rubber tubing was used to deliver compressed air via (**g**) a 0.2 µm filter connected to the cotton wool-packed flange via (**h**) an airtight rubber bung with a glass tube delivering the sterile air through it.

2.1.1 Bulking algal and cyanobacterial biomass

To generate biomass for subsequent use in experiments, algal or cyanobacterial cultures were bulked in 500 mL of BG-11 medium in glass flasks (Figure 2.1). The medium was inoculated with 5 mL of culture containing 20 mg of cells and

the flask fitted with the aeration-delivery tube and connected to filtered compressed air as described above. The cultures were allowed to grow for 5 days with continuous illumination at 150 µmol.m^{-2}.s^{-1} and for a further 2 days at a lower light intensity of 75 µmol.m^{-2}.s^{-1}. After this, the aeration was switched off and the cultures stored at room temperature (21°C) until required for experiments.

2.1.2 Treatment of cell cultures with Fumonisin B1

Aliquots of 5 mL cyanobacterial, algal, or plant cell cultures were pipetted into sterile 25 mL capacity glass conical flasks. The mycotoxin fumonisin B1 (FB1) (Sigma-Aldrich, Dorset, UK) was added to a final concentration between 0-10 µM and the flasks were incubated at 23°C on a rotary shaker (130 rpm) in a 16 h-photoperiod (150 µmol.m^{-2}.s^{-1}). Each treatment had 3 replicates. The cultures were monitored for a week and photographed 7 days later.

2.1.3 Treatment of cyanobacteria with NaCl

Salinity stress was imposed on cyanobacterial cultures by application of NaCl. Two types of high salinity stress experiments were conducted as follows: (i) where fresh BG-11 growth medium was mixed with NaCl and immediately inoculated with cyanobacterial cells for monitoring cell multiplication in the presence of stress, and (ii) where dense cultures of cyanobacteria, grown in the absence of stress for 7 days, were exposed to NaCl stress and monitored over a period between 5–10 days.

In the first set of experiments to evaluate the effects of salinity stress on cyanobacteria during growth, 60 mL of fresh BG-11 growth medium were placed in 100 mL capacity glass tubes. Aliquots of sterile 5 M NaCl stock solution were added to the 60 mL of growth medium to give a final volume of 70 mL with a concentration range of 0, 200, 400, and 600 mM NaCl. Three replicate tubes at each concentration for each cyanobacterial strain (*Synechocystis PCC 6803* or *Synechocystis SR*) were inoculated with the same amount of inoculum. The culture tubes were connected to the filtered aeration system and incubated at 30°C with 75 µmol.m^{-2}.s^{-1} continuous illumination for 4 days and at the same

temperature with 150 µmol.m^{-2}.s^{-1} light for a further 3 days. The cultures were photographed after the 7 days growth period.

The second set of experiments were aimed at evaluating the effects of salinity stress on cyanobacterial cells previously grown in the absence of stress. Aliquots of 60 mL *Synechocystis PCC 6803* or *Synechocystis SR* dense cyanobacterial culture were placed in 100 mL capacity glass tubes and an appropriate amount of sterile 5 M stock solution added to give a final concentration of 0, 200, 400 or 600 mM NaCl in a final volume of 70 mL. Three biological replicates for each NaCl concentration were generated. The culture tubes were connected to the filtered aeration system and incubated for 5 days at 30°C with light intensity of 75 µmol.m^{-2}.s^{-1}.

2.1.4 Growth curve measurements

For quantitative analysis of the effects of stress on cyanobacteria, growth curves of control and stressed cultures were established using optical density or fresh weight measurements in a time-course experiment. Duplicate 1 mL aliquots were withdrawn from each of 3 biological replicates at the start of the experiment and every 24 h subsequently until the experiment was terminated. The 1 mL aliquots were transferred cuvettes and the optical density measured against a BG-11 medium blank at wavelength 600 nm in a spectrophotometer (Ultrospec 500 Pro, Amersham Biosciences, Amersham, UK). The optical density of each of the 3 biological replicates were obtained by averaging the two technical duplicate values. The optical density was plotted against time to produce the growth curves for evaluating the effects of stress on cyanobacterial growth.

For fresh weight measurements, 1 mL aliquots were withdrawn from each of the 3 biological replicate cultures and placed in 1.5 mL Eppendorf tubes. The tubes were centrifuged (Heraus Pico 17, Thermo Fisher Scientific, Cramlington, UK) at 17,000 x **g** for 5 min. When the supernatant was removed, the cell fresh weight was calculated by subtracting the net tube weight from the gross weight. The fresh weight was plotted against time to give an alternative set of growth curves.

2.1.5 Evaluation of cell viability using the MTT assay

To measure cell viability after treatments with stress, 100 µL cell aliquots were withdrawn and transferred to a 1.5 mL Eppendorf tube. The cells were vortex-mixed after addition of 200 µL of 5 mg/mL 3-(4,5-dimethylthiazol-2-yl)-2,5-diphenyltetrazolium bromide (MTT). The samples were left to stand at room temperature (21°C) for 1 h and then centrifuged at 17,000 x **g** for 5 min. The supernatant was removed and 1 mL of dimethyl sulfoxide (DMSO) was added to dissolve the cell pellet and release the purple formazan compound formed in viable cells. The tubes were again centrifuged at 17,000 x **g** for 5 min and 800 µL of the supernatant transferred to a cuvette. The samples were read in a spectrophotometer at wavelength of 570 nm against a DMSO blank. Average absorbance from 3 replicates was plotted on a bar graph and the Student's t-test used for testing statistical significance of the difference between controls and stressed cultures.

2.1.6 Cyanobacteria sample harvesting and metabolic inactivation

To preserve the metabolome, proteome, and transcriptome intact and unchanged during sample processing for lipid extraction, protein extraction, or RNA extraction, a phenol/ethanol mixture was added to stop all metabolic processes and denature proteins. To 40 mL of cyanobacterial culture was added 5 mL of ice-cold (-20°C) 5% (w/v) phenol in ethanol. After vortex-mixing, the cells were pelleted by centrifugation (Avanti 30, Beckman Coulter, High Wycombe, UK) at 4°C and 7,000 x **g** for 5 min. The supernatant was discarded and the pellet washed twice by resuspension in 10 mL of ice-cold 5% (w/v) phenol in ethanol and centrifugation (7,000 x **g**, 10 min, 4°C). The final cell pellet was resuspended in 1 mL of the phenol/ethanol solution and transferred to an Eppendorf tube. The cells were again pelleted by centrifugation (7,000 x **g**, 5 min, 4°C), the supernatant discarded and the pellet stored at -20°C until further processing for lipid extraction, protein extraction or RNA extraction.

2.2 RNA extraction

Cell pellets metabolically inactivated and harvested in Eppendorf tubes as described above were resuspended in 500 µL of extraction buffer (20 mM Tris-HCl, 5 mM EDTA and 0.5% SDS) using a plastic micro-pestle. An aliquot of 500 µL phenol (pH 4.3) was added to the slurry and vortex-mixed for 10 sec. The tubes were securely closed, fitted with plastic cap-locks and incubated in a heating block (BI-516 S, Astec-Bio, Fukuoka, Japan) at 65°C for 25 min, with vortex-mixing every 5 min for 5 sec. The samples were then centrifuged at 17,000 x **g** for 5 min and the upper aqueous phase retained and transferred to a fresh Eppendorf tube.

An equal volume (~500 µL) of phenol:chloroform:isoamylalcohol (PCI) mixture at a ratio of 25:24:1 was added to the tubes and vortex-mixed for 10 sec. The samples were centrifuged at 16,000 x **g** for 5 min and the upper aqueous phase carefully recovered and transferred to a fresh tube. PCI extraction was repeated 3 times followed by a final extraction with a 24:1 chloroform:isoamylalcohol (CI) mixture. The final upper aqueous phase was transferred to a fresh Eppendorf tube.

The total nucleic acids in the samples were precipitated by addition of a tenth volume 3 M sodium acetate (pH 4) and 2.5-fold volume of ice-cold ethanol and overnight incubation at -20°C. The precipitates were centrifuged (16,000 x **g** for 10 min at 4°C), the supernatant discarded. DNA in the samples was digested using the On-Column DNAse kit (Sigma-Aldrich). The pellet was resuspended in 70 µL of DNAse I reaction buffer and 10 µL DNAse I solution containing 10 µg of enzyme added. After DNA digestion at 37°C for 30 min, 80 µL of 5 µg/µL protease K in 0.5% SDS were added and samples incubated at 37°C for a further 30 min. The DNAse and protease K proteins were removed from the samples by one round of PCI extraction. The upper aqueous phase was transferred to a fresh Eppendorf tube.

RNA in the samples was precipitated using 3 M sodium acetate (pH 4), ice-cold ethanol, and overnight incubation at -20°C as described above. The precipitates were centrifuged (16,000 x **g** for 30 min at 4°C). The pellet was dissolved in 50

µL of sterilized deionised water and quantified using a Nanodrop (ND-1000 Spectrophotometer, Thermo Fisher Scientific). The RNA quality was checked by running the samples in RNA gels as described in Appendix II. RNA samples were kept at -20°C for long-term storage.

2.3 Reverse transcription - cDNA synthesis

The ReadyScript cDNA Synthesis kit (Sigma-Aldrich) was used for reverse transcription reactions. For each experiment, cDNA synthesis was carried out using the same amount of template RNA across all samples. In a final reaction volume of 20 µL in 500 µL microfuge tubes were 4 µL of 5X cDNA synthesis mix (with reaction buffer, the 4 deoxy-nucleotides, oligo-(dT), reverse transcriptase, and RNase inhibitor) and 2 µg sample RNA. The reaction mixtures were incubated in a thermal cycler (GS1, G-Storm, Somerton, UK) with the following settings: 25°C for 5 min, 42°C for 30 min and 85°C for 5 min. After synthesis the cDNA was diluted 25-fold in sterile deionised water and stored at -20°C.

2.4 Cyanobacteria FAS gene identification and primer design

In order to identify *Synechocystis* fatty acid synthase (FAS) genes and the constitutive reference control genes, the known FAS genes of another prokaryotic organism (*Escherichia coli*) were first identified from literature and the protein sequence retrieved from the genome database at the National Centre for Biotechnology Information (NCBI) site (https://www.ncbi.nlm.nih.gov/protein). The FASTA protein sequence of the *E. coli* protein was used to perform a BLAST-search on the CyanoBase database (http://genome.kazusa.or.jp/cyanobase), restricting the search to *Synechocystis sp. PCC 6803*. The probability-based similarity score value (E) was used to select *Synechocystis* FAS orthologues showing statistically significant similarity to the *E. coli* bait protein. The cDNA sequence was then downloaded from CyanoBase and used for primer design.

PCR primers for all genes thus identified were designed using the Primer-BLAST tool (https://www.ncbi.nlm.nih.gov/tools/primer-blast/), which interrogates the selected genome database of the target organism to ensure primer specificity for

the target gene. Primer-BLAST is linked to the NCBI genome databases found at (https://www.ncbi.nlm.nih.gov/). DNA sequences of primers designed and used in this research are listed in Appendix I. Primer sequences were sent for commercial synthesis by Integrated DNA Technologies (Leuven, Belgium).

2.5 PCR analyses

Polymerase Chain Reaction (PCR) analyses were performed using My Taq DNA Polymerase kit (Bioline, London, UK). Reactions were set up in sterile 0.2 mL PCR tubes with a flat cap. Each reaction was carried in 1X MyTaq Reaction Buffer, in a final volume of 25 µL containing 5 µL of 50-fold diluted genomic DNA or 25-fold diluted cDNA, 100 nM each of the forward and reverse primers, and 1.25 units of MyTaq DNA Polymerase. After manual mixing with a pipette tip, the tubes were placed in a thermal cycler (GS1) with the following cycling conditions: heated lid at 112°C and automatic initial heating of 95°C for 1 min, 40 cycles of denaturation at 94°C for 30 sec, annealing at 56°C for 1 min, elongation at 72°C for 1 min and a final elongation step at 72°C for 5 min. The list of primers used to amplify target genes is given in Appendix I.

2.6 Quantitative RT-PCR analyses

Quantitative RT-PCR (qPCR) analyses were conducted using cDNA generated as described in section 2.3. Three technical replicates per biological sample were set up in 100 µL Rotor-Gene Q tubes. The reaction mix was in a final volume of 20 µL containing: 5 µL of 25-fold dilution cDNA sample, 100 nM each of the forward and reverse primers and 10 µL of SensiFAST buffer (SYBR No-ROX Kit, Bioline) containing the reaction buffer, the 4 deoxy-nucleotides, DNA polymerase, and the fluorescent label. The tubes were placed in a real time PCR cycler (Rotor-Gene Q, Qiagen, Hilden, Germany). The cycling programme was: 2 min at 95°C, followed by 40 cycles of 5 sec at 95°C and 30 sec at 60°C. The list of primers used to amplify target genes is given in Appendix I. The 16S rRNA gene was used as a constitutive reference control. All data were analysed using REST 2009 Software (Qiagen).

2.7 Gel electrophoresis

2.7.1 DNA gel electrophoresis

PCR products were separated in 3.5% agarose (Bioline, London, UK) gels prepared by dissolving the appropriate amount of agarose in TAE buffer [40 mM Tris base, 20 mM glacial acetic acid, 1 mM EDTA, pH 8.3] and boiling in a microwave oven. When the temperature of the gel solution had cooled to 50°C, 5 µL of 10 mg/mL ethidium bromide were added per 100 mL of gel solution and then poured into a gel casting tray with a comb. Ten microliter aliquots of PCR samples were mixed with 1 µL DNA sample loading buffer (final concentration: 40 mM Tris base, 20 mM acetic acid, 1 mM EDTA, pH 8.3, 3% (w/v) glycerol, 0.2% (w/v) Orange G) and loaded in the wells after submerging the gel under TAE buffer. The HyperLadder V (25 to 500 base pair) DNA ladder (Bioline) was used as a size marker. Electrophoretic separation was performed using the GPS 200/400 power pack (Pharmacia LKB, Uppsala, Sweden) set at 90 volts for ~45 min. After completion, the DNA bands were visualised using a UV transilluminator.

2.7.2 RNA gel electrophoresis

To evaluate the quality of RNA samples, 1.2% agarose gels were made in MOPS buffer (20 mM MOPS, 5 mM sodium acetate, 1 mM EDTA, pH 7). The appropriate amount of agarose was added to the MOPS buffer and dissolved by heating in a microwave oven. After cooling to 50°C, the solution was carefully poured into a gel casting tray with a comb and allowed to set at room temperature. The gel was placed inside the gel tank and submerged under the running buffer (MOPS). Sample aliquots with 300 ng RNA were mixed with RNA loading buffer (final concentration: 64% (v/v) formamide, 8.2% (v/v) formaldehyde, 130 mM MOPS, 130 µg/mL ethidium bromide, 0.1% (w/v) Orange G) and incubated at 65°C for 10 min. The samples were loaded into the gel wells and run at ~80 V for ~60 min. The gel was observed using UV transilluminator.

2.8 Lipid extraction and analyses

Lipid extraction was performed according to the Bligh-Dyer method (Bligh & Dyer, 1959) using cells treated and harvested as described in section 2.1.6. For lipid extraction only glassware is used due to the presence of solvents, which damage any plasticware. Triplicate cell samples from each treatment were dried in an oven (60°C) to measure the dry weight. The dried pellets in plastic microfuge tubes were resuspended in 500 µL of sterilized deionised water using a micro-pestle. The slurry was transferred to a glass Potter-Elvehjem tissue homogenizer and 1 mL of methanol:dichloromethane 2:1 (MeOH:DCM) added. After mixing 50 times by carefully moving the pestle up and down, 20 µL of 10 mM heptadecanoic acid (C17:0) were added to serve as internal standard. Another 1 mL of MeOH:DCM was added and mixed again with the pestle 20 more times. After the mixture had been properly homogenized, it was transferred to a fresh 20 mL glass test tube with a screw cap. Aliquots of 0.67 mL of DCM and 1.2 mL of 0.9% KCl were added and vortex-mixed for 30 sec. The tubes were centrifuge at 1,000 x **g** for 5 min and the lower phase was carefully transferred to a fresh test tube with screw cap, avoiding contact with the upper solvent phase. The samples were placed in a fume hood to dry under nitrogen gas at 30°C for ~15 min. Likewise, 3 mL of 3N methanol were combined with 6 mL of dry methanol and from this solution, 500 µL were added to each dry sample, and the tubes incubated at 80°C for 1 h. Aliquots of 0.5 mL hexane and 1 mL of 0.9% KCl were transferred to each tube and vortexed for 30 sec, after which the tubes were centrifuged at 1,000 x **g** for 5 min. Finally, just the upper phase was transferred to a 1.5 mL vial avoiding any contact with the solvent. The samples were analysed by Gas Chromatography-Mass Spectrometry (GC-MS) in order to quantify fatty acid content.

GCMS analysis was performed using a single quadrupole gas chromatograph-mass spectrometer (GC-MS-QP-2010 SE, Shimadzu Scientific Instruments, Howard, USA). The samples were freeze-dried and dissolved in the same volume of hexane and 2 µL were introduced into a capillary column DB-23 (30 m x 0.25 mm x 0.15 µm, Agilent Technologies, Santa Clara, USA), with instrument settings of split injection and scan mode. Helium was used as a carrier gas, considering

a linear flow of 30 cm/sec, and the initial column was held for 2 min at 160°C, then at 200°C for 4°C/min and finally increased to 224°C for 6 °C/min. The temperature for detector and injector were set at 250°C. The total sample run time was 18 min.

2.9 Protein

2.9.1 Protein extraction and quantification

Cyanobacterial samples treated and harvested as described in section 2.1.6 were used for protein extraction. A total of 3 biological replicates for each treatment at each time-point were generated. Cells were disrupted by homogenisation of pellets in 200 µL of DMSO using a plastic micro-pestle. Protein was precipitated by addition of 5 µL of 1.5 M Tris-HCl (pH 8.8) and 800 µL of ice-cold acetone and overnight incubation at -20°C. The protein pellets were centrifuged at 17,000 x **g** for 10 min, the supernatant discarded, and the pellets washed 3 times by resuspension in 500 µL of 80% acetone and centrifugation (17,000 x **g** for 5 min). The final pellets were dissolved in 200 µL of lysis buffer (LB) [9 M urea, 2 M thiourea, 4% (w/v) CHAPS, 30 mM Tris-HCl (pH 8.8)].

Protein quantification was performed using a modification of the method developed by Bradford (Bradford, 1976). To generate a calibration curve, protein assay reactions with 0, 1, 2, 4, 8 or 10 µg/mL Bovine Serum Albumin as the protein standard were prepared in a final volume of 1 mL containing: 90 mM urea, 20 mM thiourea, 0.04% CHAPS, 0.3 mM Tris, 1 mM HCl, 900 µL of 4-fold dilution of BioRad protein assay dye (Bio-Rad Laboratories, Watford, UK). Sample aliquots of 1 µL were added to tubes with a similar reaction mixture in a final volume of 1 mL. The absorbance of the reaction mixture was measured in a spectrophotometer set at wavelength 595 nm against a reagent blank between 5-30 min after addition of the BioRad protein assay dye, when the reaction progresses linearly. The values were plotted using Microsoft Excel and the protein concentration in samples calculated using a linear regression equation obtained from the calibration curve.

2.9.2 Protein gel electrophoresis for sample quality control

Protein samples were labelled with cyanine3 NHS ester minimal dye (Cy3) or Cy5 (Lumiprobe, Hannover, Germany), which react with lysine residues in polypeptide chains. Aliquots of 50 µg protein sample were mixed with 800 picomoles of Cy3 or Cy5 in total volume of 39 µL containing a final concentration of: 9 M urea, 2 M thiourea, 4% (w/v) CHAPS, 30 mM Tris-Cl, pH 8.5. The labelling reaction was initiated by the addition of the dye and proceeded in total darkness on an ice-water bath for 30 mins. At the end of the incubation time, the reaction was stopped by the addition of 1 µL of 10 mM lysine.

Protein sample quality was checked using sodium dodecyl sulphate-polyacrylamide gel electrophoresis (SDS-PAGE) and limited visualisation of protein changes conducted using two-dimensional gel electrophoresis (2DE). For SDS-PAGE, a combined gel system with 5% polyacrylamide stacking gel on top of a 12% polyacrylamide resolving gel was used. The stock solution used to prepare the gels contained 30% (w/v) acrylamide and 1% (w/v) N, N'-bis-methylene acrylamide. To catalyse polymerisation of the resolving gel mixture [12% (w/v) acrylamide, 375 mM Tris-HCl (pH 8.8), 0.1% (w/v) SDS] or stacking gel mixture [5% (w/v) acrylamide, 125 mM Tris-HCl (pH 6.8), 0.1% (w/v) SDS] 0.05% (w/v) ammonium persulphate and 0.02% (v/v) TEMED were added.

The Mini-PROTEAN system (Bio-Rad Laboratories) was used to cast 1 mm-thick gels using 10-well Teflon combs. After fitting the gels into the gel running assembly, the inner and outer buffer chambers were filled with the protein gel running buffer (25 mM Tris-HCl, 190 mM glycine and 0.1% SDS), ready to receive the protein samples. Protein samples were prepared by adding 5 µg sample in a final 10 µL volume containing sample loading buffer [final concentration: 62.4 mM Tris-HCl (pH 6.8), 10% glycerol, 2% (w/v) SDS, 1% (w/v) dithiothreitol, 0.01% bromophenol blue] and boiled for 5 min. After loading samples into the wells, a constant voltage of 50 V was applied until the samples had left the stacking gel and entered the resolving gel, after which voltage was increased to 100 V. Electrophoresis was stopped when the bromophenol blue dye front reached the end of the resolving gel.

For fluorescently-labelled proteins, the gels were fixed by incubating in two changes of 10% acetic acid for 30 min each and then scanning with the Typhoon 9400 Variable Mode Imager (GE Healthcare, Chicago, USA).

For 2DE, isoelectric focusing (IEF) of the samples was conducted in 24 cm gels with a pH 4-7 immobilised linear gradient (GE Healthcare, Chicago, USA) and the second SDS-PAGE dimension in homogenous 12% acrylamide gels. Dehydrated IEF gels were rehydrated overnight with 450 µL rehydration solution containing: 9 M urea, 2 M thiourea, 4% (w/v) CHAPS, 2% (v/v) IPG Buffer pH 4-7 (GE Healthcare, Chicago, USA), 1% (w/v) DTT, and 0.1% (w/v) bromophenol blue. Samples were multiplexed by mixing 10 µg Cy3-labelled and 10 µg of Cy5-labelled samples (20 µg total) in a final volume of 100 µL with the same composition as the rehydration solution. Sample multiplexing combinations included: Control-Cy3 and NaCl-treated-Cy5, or Control *Synechocystis PCC 6803*-Cy3 and Control *Synechocystis SR*-Cy5.

Rehydrated IEF gels were loaded onto an IPGphor IEF system (GE Healthcare, Chicago, USA) and the samples applied to the gels through the cup-loading method, with concurrent electro-focussing for a total of 70,000 volts hours applied using a gradient programme overnight. The IEF gels were then equilibrated by incubation for 15 min in 5 mL of equilibration buffer [50 mM Tris-HCl (pH 8.8), 6 M urea, 0.002% (w/v) bromophenol blue, 2% (w/v) SDS and 30% (v/v) glycerol] containing 1% (w/v) DTT and then for another 15 min in equilibration solution containing 4.8% (w/v) iodoacetamide. The IEF gels were then transferred to 260 x 200 x 1mm gels (12% acrylamide) cast in optically clear low fluorescence glass plates. SDS-PAGE was run in a DALT12 system (GE Healthcare, Chicago, USA) by applying a constant power of 5 W per gel for 30 min and then at 17 W per gel at 25°C. Gels were scanned using the Typhoon 94000 Variable Mode Imager (GE Healthcare, Chicago, USA).

2.9.3 iTRAQ analysis

Isobaric Tags for Relative and Absolute Quantification (iTRAQ) was used for analysis of the effects of NaCl treatment on the proteome of *Synechocystis SR*

using 4 biological replicates each of controls and 200 mM NaCl treatment (section 2.1.3). Sample aliquots containing 12.5 µg protein were mixed with 100 µL of deionised water, 5 µL of 1.5 M Tris-HCl (pH 8.8) and 400 µL of acetone and incubated overnight at -20°C. The precipitated protein was pelleted by centrifugation (16,000 x **g** for 30 min) and the supernatant discarded. The protein pellets were prepared for labelling using reagents from the iTRAQ Reagent Multiplex Buffer Kit (Sigma-Aldrich). After drying for 5 min, 2 µL of 2% SDS were added to the pellet and the tubes incubated at 60°C for 1 h. An aliquot of 45 µL dissolution buffer was added to the pellet and the tube incubated on a vortex shaker for 30 min at room temperature (21 °C). The proteins were reduced by the addition of 1 µL reducing agent (TCEP) and incubated at 60°C for 1 h. The cysteine residues were blocked by addition of 0.5 µL of blocking agent (MMTS) followed by incubation at room temperature (21°C) for at least 10 min. The protein samples were mixed with 2 µL of 0.5 µg/ µL trypsin gold (Promega, Southampton, UK) and incubated at 37°C overnight.

After digestion, the samples were freeze-dried and redissolved in 25 µL of deionised water. An aliquot of 25 µL iTRAQ label in 100% isopropanol was added to the tube and the pH checked to ensure it was at pH 7.5. More dissolution buffer was added if the pH was lower. The labelling reaction was allowed to proceed at room temperature for 2 h. The 4-replicate control samples were labelled with iTRAQ labels of molecular mass 113, 114, 115, or 116, while the 4-replicate NaCl-treated samples were labelled with iTRAQ labels of molecular mass 117, 118, 119, or 121. At the end of labelling reaction, the contents of all 8 tubes were pooled and then divided into 2 equal parts (200 µL each with 50 µg protein). The two tubes with multiplexed sample were freeze-dried.

Fifty micrograms of freeze-dried sample were dissolved in 75 µL of a solution containing 0.1% formic acid (FA) and 3% acetonitrile (ACN). An aliquot of 150 µL 0.3 M ammonium formate (pH 3) was added and the pH adjusted to 3 using trifluoroacetic acid as necessary. The sample was clarified by centrifugation (10,000 x **g**, 10 min) and then mixed with 1275 µL ACN. Buffer salts and unincorporated labels were removed from the samples using HILIC SPE cartridges (PolyLC Inc., Columbia, USA) packed with 300 mg of 12 µm

polyhydroxyethyl-A. Prior to sample clean-up, the cartridges were equilibrated by washing through 4 times with 3 mL of peptide release buffer (5% ACN, 30 mM ammonium formate pH 3.0) followed by 4 washes of 3 mL binding buffer (85% ACN, 30 mM ammonium formate pH 3.0). To the SPE cartridge was added 1.5 mL of sample and the flow-through recovered for a second passage. A volume of 2 mL binding buffer was used to wash the column. After a second wash, 2 x 1 mL peptide release buffer was used to elute bound peptides. After freeze-drying the eluate, the peptide residue was dissolved in 3% ACN, 0.1% formic acid for analysis by Liquid Chromatography-Mass Spectrometry (LC-MS).

2.9.4 Protein mass spectrometric analysis

The iTRAQ-labelled samples were analysed by LC-MS using a TripleTOF 6600 mass spectrometer (AB Sciex, Warrington, UK) connected to an Eksigent 425 LC system 425 (AB Sciex) Nanospray III source. Samples were applied onto a trap column (Triart C18 column 1/32'', 5 µm, 5 x 0.5 mm) purchased from YMC (Kyoto, Japan) followed by online segregation of peptides using a Triart C18 column 1/32'', 3 µm, 150 x 0.3 mm (YMC) programmed to run a flow rate of 5 µL/min. Two buffer system were used for the program: buffer A (aqueous 0.1% FA) and buffer B (0.1% FA in ACN). Linear gradients of 3-5% buffer B for 2 minutes, 5-30% buffer B for 66 minutes, 30-35 % buffer B for 5 minutes, and 35-80% buffer B for 2 minutes were sequentially applied. The column was washed with 80% buffer B for 3 min. The column was returned to 3% buffer B over 1 min and held for equilibration over 8 mins. Gradient initiation over 85 min commenced with instrument settings: data-dependent MS-MS acquisition of the top-30 ions; collision energy set for peptides with iTRAQ label tags. Precursor-ion scans (400 to 1600 m/z) of 250 ms resulted in up to 30 multiply-charged ions (>500 cps) being selected over 50 ms for CID fragmentation and MS/MS spectrum acquisition (m/z 100-1500). To limit multiple fragmentation of the same peptide, settings of 1.8 sec cycle time and 15 sec rolling precursor exclusion were applied. Spectrometer data were acquired using Analyst TF 1.7.1 instrument control and data processing software (AB Sciex).

2.10 Protein data analysis

The raw.wiff data files were processed against an in-house *Synechocystis sp*. database downloaded from Uniprot database (https://www.uniprot.org/) in October 2019. ProteinPilot™ 5.0.1 version 4895 software, which integrates the Paragon™ Algorithm 5.0.1.0.4874 (AB Sciex) was used as the processing software. The iTRAQ 8-plex Paragon method allowing for trypsin digestion, MMTS-blocked thiol groups on cysteine residues, 1 missed cleavage, and TripleTOF 6600 spectrometer instrument, was applied. Correction for label bias was applied and the 'Run False Discovery Rate Analysis' option selected, with a 0.05 threshold for protein detection set as the "Unused ProtScore confidence".

2.11 TEM microscopy analysis

Cyanobacterial cells used for analysis using Transmission Electron Microscopy (TEM) were control samples or 600 mM NaCl-treated *Synechocystis PCC 6803* or *Synechocystis SR* cells as described in section 2.1.3. About 40 mL of cell culture from each treatment were centrifuged at 17,000 x **g** for 8 min and the supernatant discarded. The cell pellet was resuspended in a small volume of 20% BSA, which acts as filler solution and cryoprotectant. A high-pressure freezer (EM ICE, Leica Microsystems, Wetzlar, Germany) was used to cryofix the cells in 100 mm specimen carriers. Super quick freeze substitution was achieved using 1% OsO_4, 0.5% uranyl acetate and 5% H_2O in acetone, followed by embedding into epoxy (McDonald & Webb, 2011). With a diamond knife (DiATOME, Hatfield, USA) and using an ultramicrotome (UC7, Leica Microsystems, Wetzlar, Germany), ultrathin sections of 50 nm were generated, contrasted for 10 min each first in 1% uranyl acetate in ethanol and then in Reynold's lead citrate. Sections were observed with a transmission electron microscope (H-7600, Hitachi-High Technologies Science America, Chatsworth, USA) at 100 kV and images were taken with a camera (Xarosa, EMSIS GmbH, Münster, Germany) using an imaging software (Radius, EMSIS GmbH, Münster, Germany).

2.12 Statistical analysis

All the experiments in this research project were conducted using a minimum of 3 independent biological replicates as indicated in each Figure legend. Analyses of data were performed using the statistical software Minitab (version 18.1). One-way analysis of variance (ANOVA) and Tukey's Honestly Significant Difference (HSD) post-hoc test were used for comparison of sample means. The levels of significance applied were represented by * when $p \leq 0.05$, ** when $p \leq 0.01$ and *** when $p \leq 0.001$.

3 Results

3.1 Optimising cyanobacterial growth

The cyanobacteria used in this project were the novel *Synechocystis SR* strain (Abedi et al., 2019b) and the widely used *Synechocystis PCC 6803* as a reference control strain. To begin with, cultivation of both strains was optimized for maximal biomass production by modulating light intensity, which is a key parameter influencing growth. Cyanobacterial inoculum was added to BG-11 standard growth medium, which is colourless and transparent (Figure 3.1). By 4-5 days after inoculation, the medium had developed a light-green turbidity, indicating the rapid proliferation of cyanobacterial cells. As the cell density increased, very fine cell clumps perfectly floating in the medium were formed - it took several hours for the cells to sediment after the bubbled air supply was disconnected.

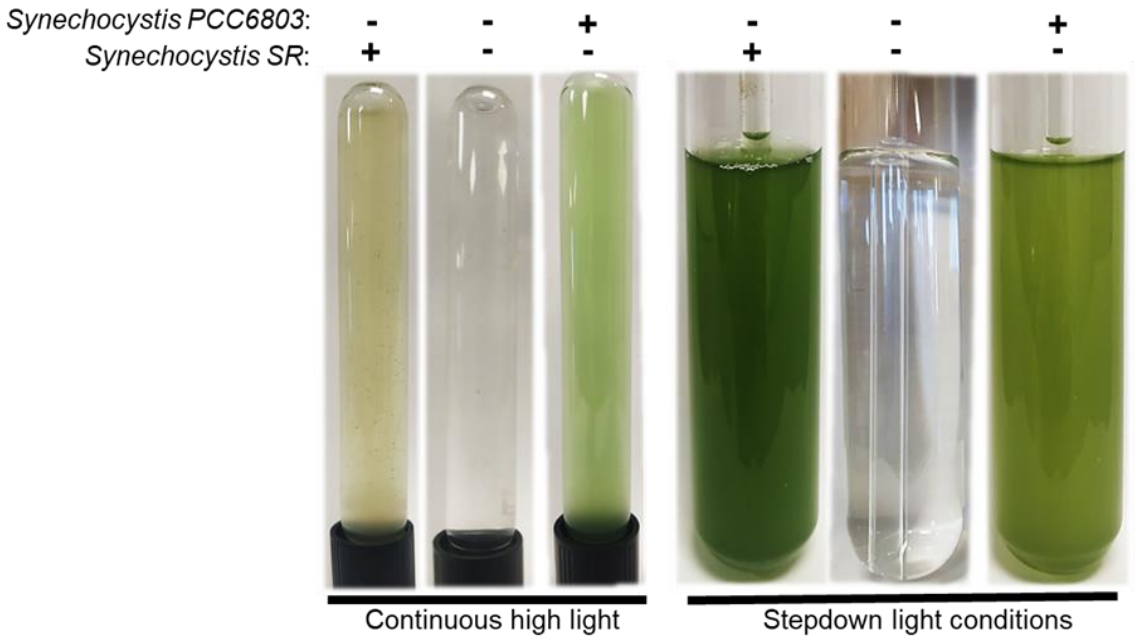

Figure 3.1 Appearance of *Synechocystis SR* and *Synechocystis PCC 6803*. *Synechocystis SR* or *Synechocystis PCC 6803* inoculum was added to BG-11 medium and grown under continuous high light intensity for 7 days or step-down light conditions (initially under high light intensity for 5 days followed by 2 days of low light). Plus sign (+) denotes inoculation with the indicated cyanobacterial strain; minus sign (-) denotes absence of the indicated strain.

In the first instance, the cyanobacterial cultures were grown for a week under continuous illumination at a high light intensity of 150 µmol.m^{-2}.s^{-1} (Figure 3.2). The growth pattern of both strains conformed to a typical sigmoidal curve with distinct lag, exponential, and stationary phases within the 12 days period of the experiment (Figure 3.3). The exponential phase, during which the bulk of biomass is generated, started at about 2 days and lasted until 6 days. The resultant cultures were characterised by a pale green colour, demonstrating that the growth conditions were not optimal for both cyanobacterial strains (Figure 3.1).

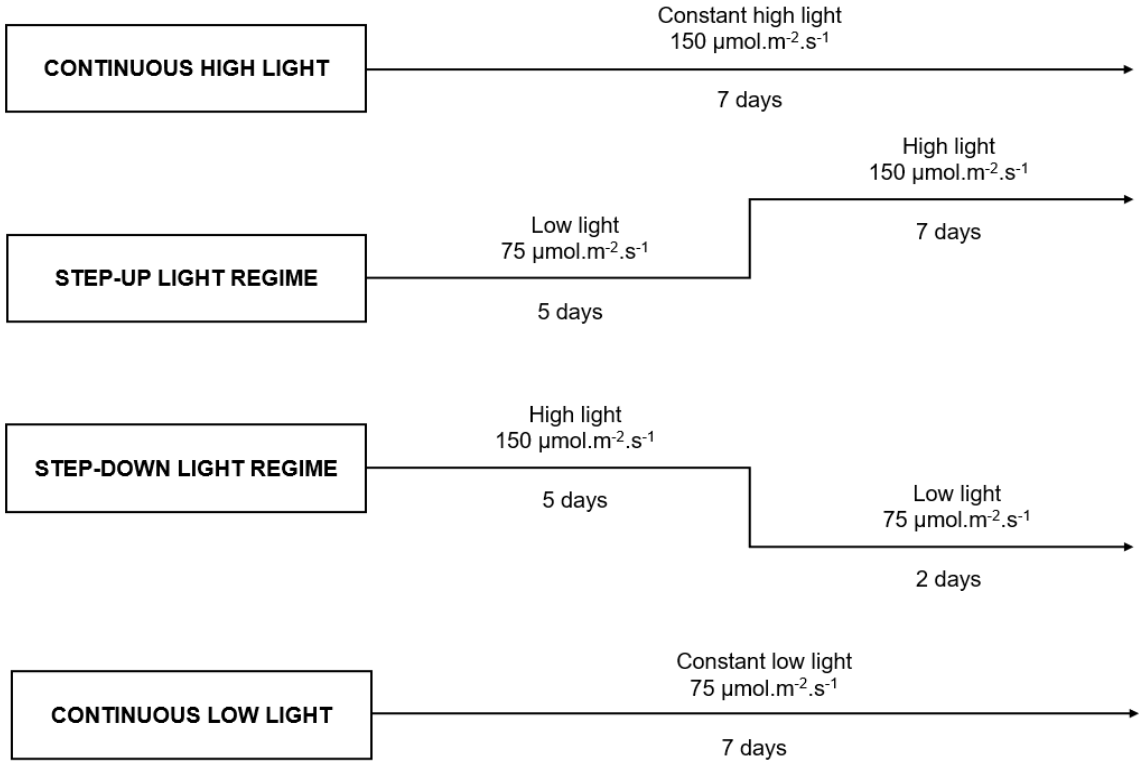

Figure 3.2 Schematic diagram of different light regimes used.
Cell cultures were incubated under 4 different light conditions according to the requirements of individual experiments. (i) Continuous high light: constant high light intensity of 150 µmol.m^{-2}.s^{-1} for 7 days; (ii) step-up light regime: low light of 75 µmol.m^{-2}.s^{-1} for 5 days and high light of 150 µmol.m^{-2}.s^{-1} for 7 days; (iii) step-down light regime: hight light of 150 µmol.m^{-2}.s^{-1} for 5 days and low light of 75 µmol.m^{-2}.s^{-1} for 2 days; and, (iv) continuous low light: constant low light intensity of 75 µmol.m^{-2}.s^{-1} for 7 days.

A different light regime was then implemented to evaluate its impact on growth. Immediately after inoculation, the cultures were incubated at a low light intensity of 75 µmol.m^{-2}.s^{-1} for the first 5 days, after which the light intensity was increased to 150 µmol.m^{-2}.s^{-1} until the end of the experiment. It was reasoned that the low light intensity could prolong the lag phase and perhaps lead to a longer exponential phase upon increasing the light intensity, thereby improving biomass yield. As expected, growth during the first 5 days was very subdued and the cells immediately entered the exponential phase after the light intensity was stepped up (Figure 3.3). For *Synechocystis SR*, the multiplication of these cells had started to overtake the equivalent cultures grown under constantly high light intensity (150 µmol.m^{-2}.s^{-1}) by 11 days (Figure 3.3a). However, in *Synechocystis PCC 6803*, the latter conditions led to inferior growth kinetics (Figure 3.3b).

In relation to *Synechocystis SR*, it was clear that alternating between low and high light intensity would lead to better growth. One could extrapolate that allowing further growth time beyond 12 days could improve biomass yield of the cultures started at low light and stepped up to higher light. However, reversing the order of light regime so as to start with high light intensity (150 µmol.m^{-2}.s^{-1}) and step-down to low light intensity (75 µmol.m^{-2}.s^{-1}) was explored. The design was to grow the cultures at high light (150 µmol.m^{-2}.s^{-1}) for 5 days and step-down to 75 µmol.m^{-2}.s^{-1} for 2 days. The rationale was that high light provides a short lag phase and the step-down implemented at the peak of the exponential phase would relieve any pressure on the photosystems that could arise from excessive light and activation of photoprotective strategies. Theoretically, this could boost cell multiplication and biomass yield.

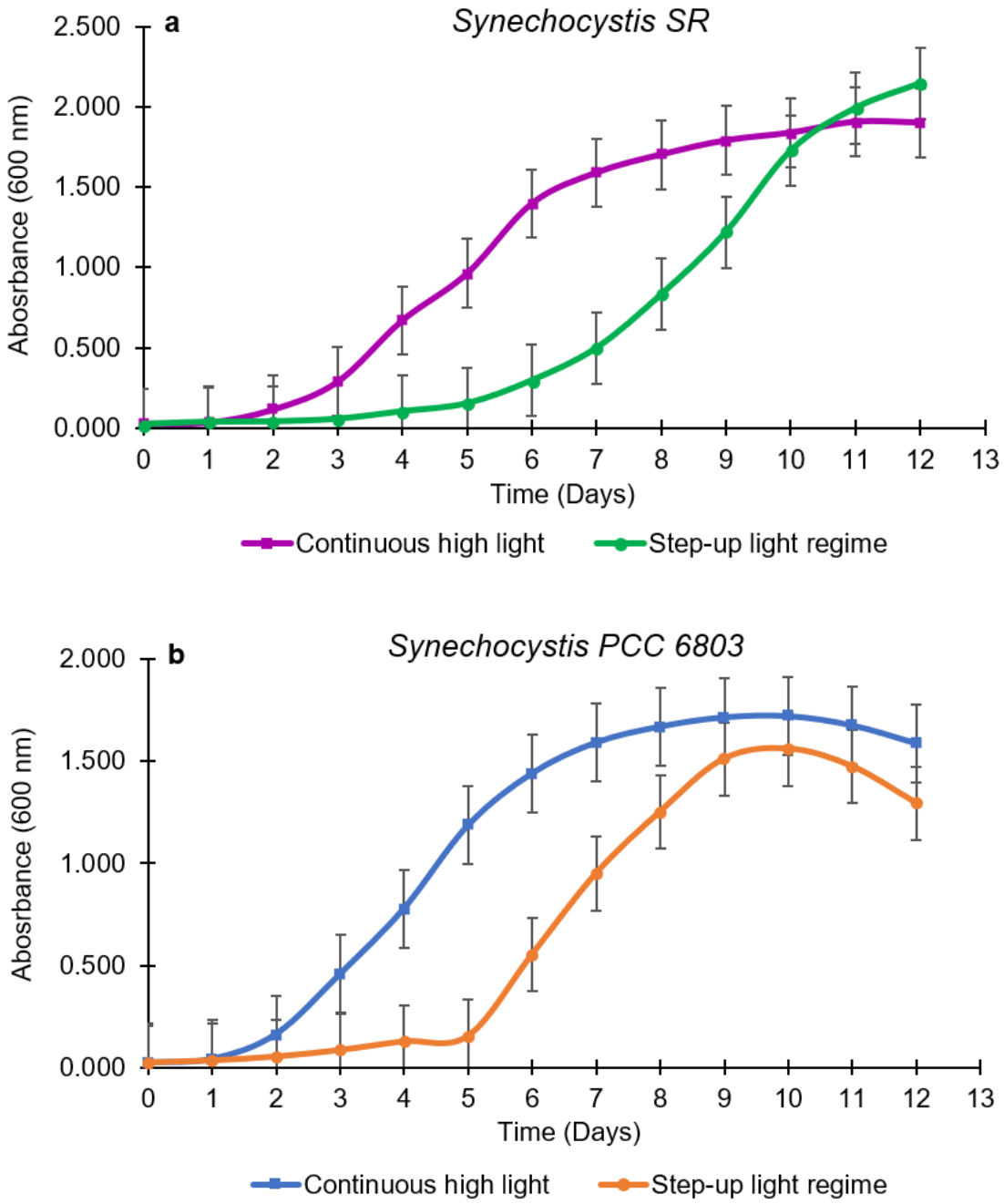

Figure 3.3 Effects of light intensity on the growth cyanobacteria.
Cyanobacterial inoculum was added to tubes with fresh growth medium and the cultures grown for 12 days either under continuous high light (continuous high light) or low light for the first 5 days followed by 7 days of high light (step-up light regime). **a)** *Synechocystis SR.* **b)** *Synechocystis PCC 6803.*
Error bars represent standard error of mean (*n* = 3).

Thus, immediately after inoculating fresh medium, cultures were incubated at the high light intensity (150 µmol.m^{-2}.s^{-1}) for 5 days and the light intensity stepped-down to 75 µmol.m^{-2}.s^{-1} for the last 2 days. This led to robust growth of both *Synechocystis SR* and *Synechocystis PCC 6803* and the cultures had a dark-green appearance (Figure 3.1) indicating high levels of chlorophyll accumulation. The step-down light regime stimulated better growth, particularly for *Synechocystis SR*. The colour and density of the cultures were far better than cultures grown under continuous high light intensity over a longer growth period (Figure 3.1). This method was adopted for bulking up biomass used in subsequent experiments.

Although light is an essential factor required for photosynthesis, it can cause cell damage when present in excess mounts (Czarnocka et al., 2021). Excess energy beyond the photosynthesis light saturation point is misdirected towards generation of cell-damaging reactive oxygen species (ROS), thereby curbing growth. The light requirements of cyanobacterial cultures growing under normal and stress conditions differ, and the range of optimal light required changes as the cell density increases during the growth cycle.

Therefore, the impact of different light regimes on growth with and without salt stress were investigated in order to identify the optimal conditions for maximal biomass production.

In order to observe the cell ultrastructure and measure cell size, cells of the 2 cyanobacterial strains were analysed by transmission electron microscopy. Both strains have isodiametric cells with clearly visible internal membranous structures (Figure 3.4). The average cell diameter of *Synechocystis SR* was ~1.81 ± 0.48 µm (n = 35), while *Synechocystis PCC* 6803 cell diameter was ~1.64 ± 0.24 µm (n = 35) (Figure 3.5). Statistical analysis revealed no significant differences between the cell diameter. The similarity in cell size and shape is not surprising given that both cyanobacterial strains belong to the same genus. However, it was noted that cell diameter had higher biological variation in *Synechocystis SR* than in *Synechocystis PCC 6803* (Figure 3.5). The basis for this difference is not clear at the moment.

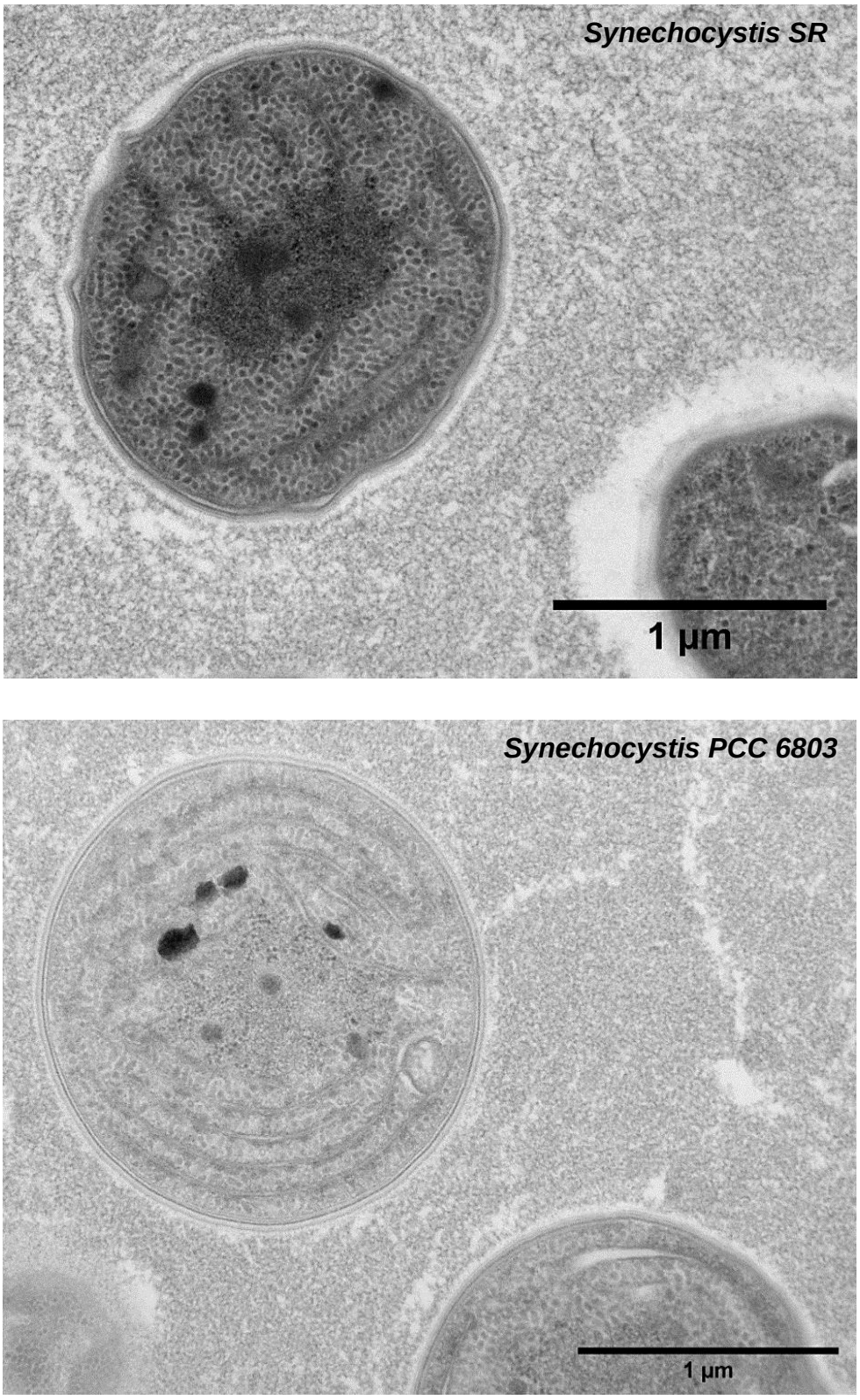

Figure 3.4 Electron micrographs of cyanobacterial cells.
The panels show transmission electron micrographs of cells from cultures of *Synechocystis SR* or *Synechocystis PCC 6803* that had been grown for 5 days under high light intensity followed by 2 days in low light.

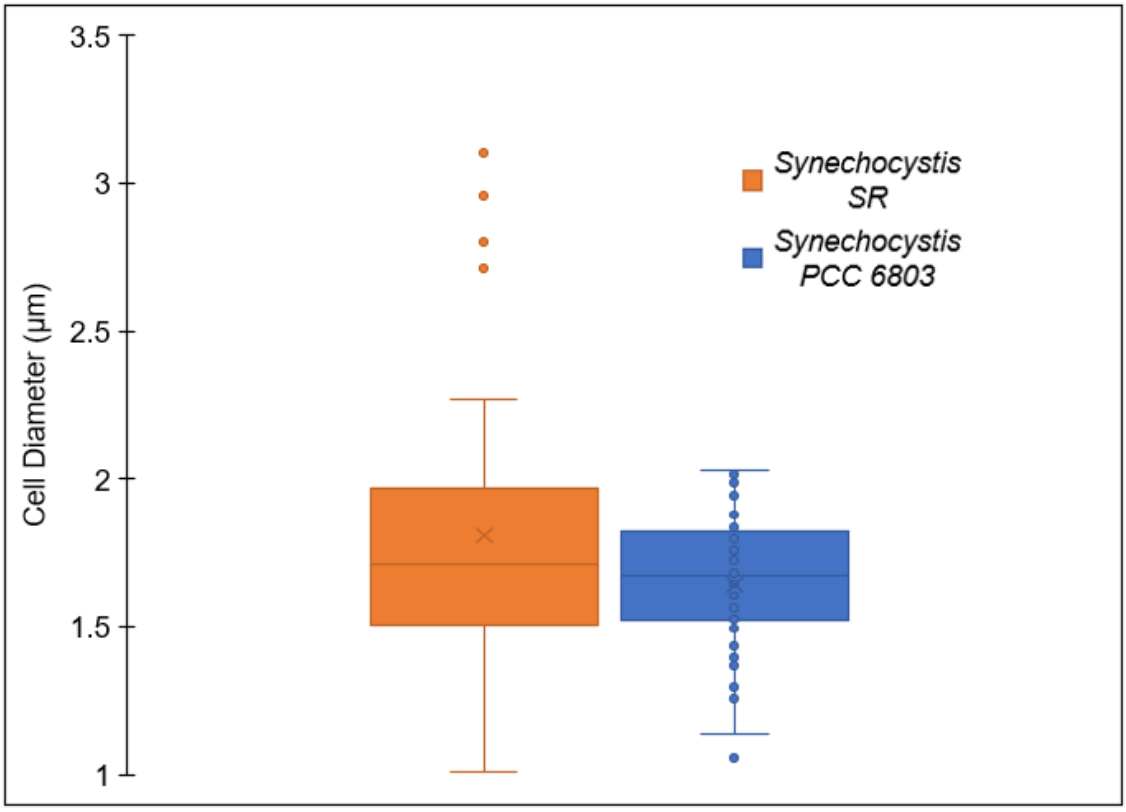

Figure 3.5 Box and whisker plot of cyanobacterial cell diameter data.
Cell diameter was measured on transmission electron micrograph images. Data was obtained from 35 cells each for both cyanobacterial strains.

3.2 Treatments with Fumonisin B1

Once cyanobacterial growth was optimized, the next objective was to identify a biotic or abiotic stress that could be applied to trigger enhanced lipid production in *Synechocystis SR.* Fumonisin B1 (FB1), a mycotoxin previously used in our research group to activate stress in Arabidopsis cell cultures (Smith et al., 2015) was evaluated. In the first instance, the ability of FB1 to activate cell death was investigated in the cyanobacteria (*Synechocystis SR, Synechocystis PCC 6803*) and the microalga *Chlamydomonas reinhardtii*, using *Arabidopsis thaliana* cell suspension cultures as a positive control. Cell cultures of these 4 organisms were treated with a final concentration of 10 µm FB1 and monitored over a period of 5 days. Both cyanobacterial strains and *C. reinhardtii* were not greatly affected by the toxin on the basis of visual appearance of the cultures (Figure 3.6). Within the same time-frame, Arabidopsis cells exposed to the mycotoxin died and were completely bleached revealing that *Synechocystis SR, Synechocystis PCC 6803* and *Chlamydomonas reinhardtii* were not negatively impacted by FB1 even, boosted the growth by showing a slightly more intense colour and density in day 2, 5 and 5, respectively. Oppositely, the culture of *Arabidopsis thaliana* presented clumps stuck to the wall of the flask since the inoculation, by day 2, an intense discolouration appeared remaining a minor shade of yellow tone representing that only few cells had survived while for day 5, the content of the flask was totally bleached meaning that no cell was alive. Overall, the surprising visual results indicated that *Synechocystis,* which are photosynthetic prokaryotes and *Chlamydomonas reinhardtii,* a unicellular eukaryotic organism, improved its proliferation as a response mechanism and survived to 10 µm FB1 however, the same dose was lethal for *Arabidopsis thaliana*, a multicellular eukaryote.

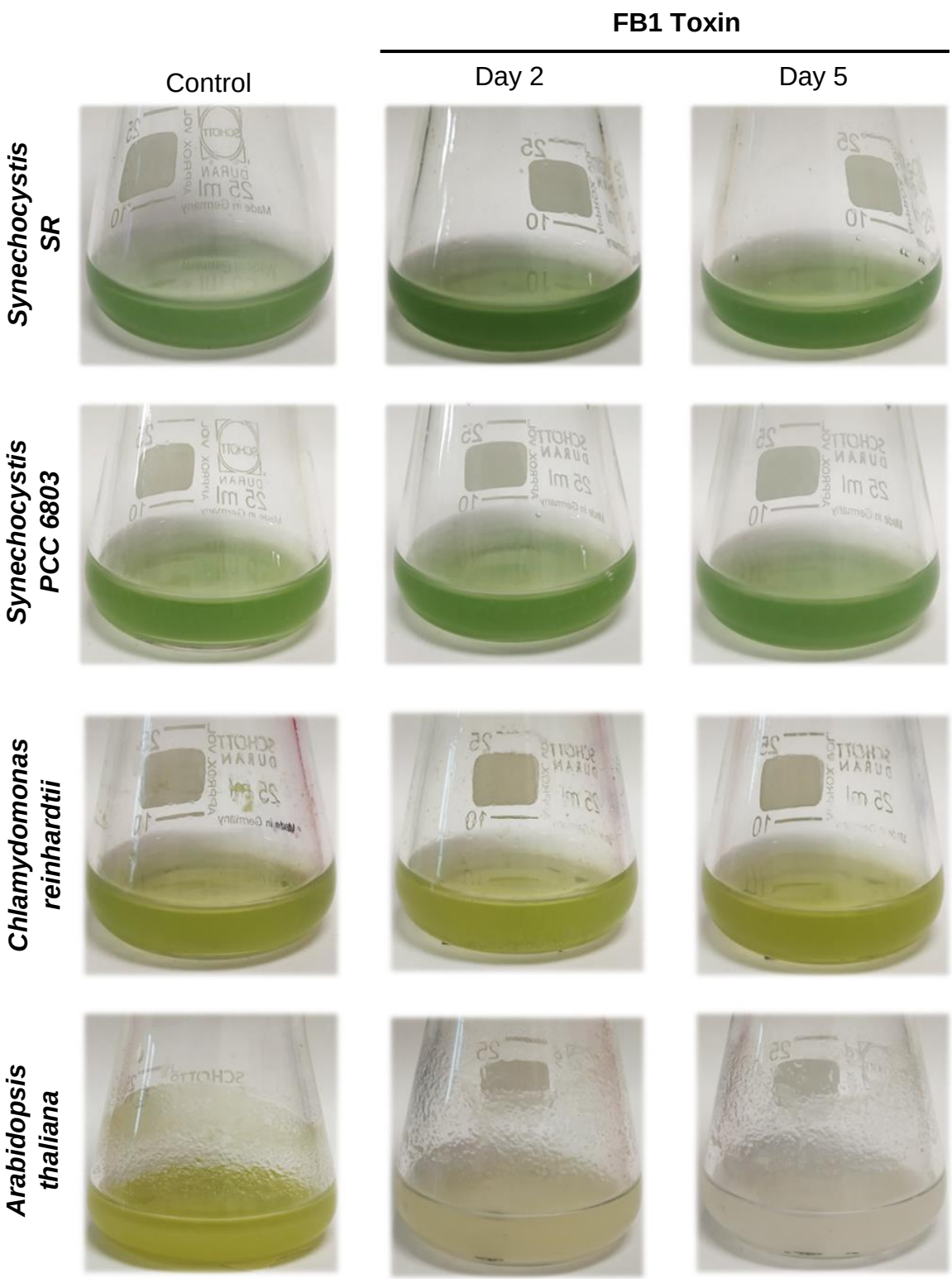

Figure 3.6 Response of cyanobacterial, microalgal, and plant cells to FB1. Triplicate cell cultures were treated with 10 µM FB1 and photographs of a representative culture taken at the indicated time-points. Cell death is apparent only in Arabidopsis cell cultures.

Next, a more detailed analysis of *Synechocystis SR* and *Synechocystis PCC 6803* was conducted to investigate if FB1 had any effects on the cyanobacteria. The cultures were exposed to a range of FB1 doses for a 2-week period. As observed in the previous experiment, there were no changes in visual appearance of the cultures (data not shown). In *Synechocystis SR*, there was an increase in the average cell density in response to FB1 treatment, though this was not statistically significant (Figure 3.7). Such an increase in cell density was not seen in *Synechocystis PCC 6803* similarly treated with FB1 (Figure 3.7). Taken together, these results show that FB1 does not affect the growth and multiplication of cyanobacterial cultures.

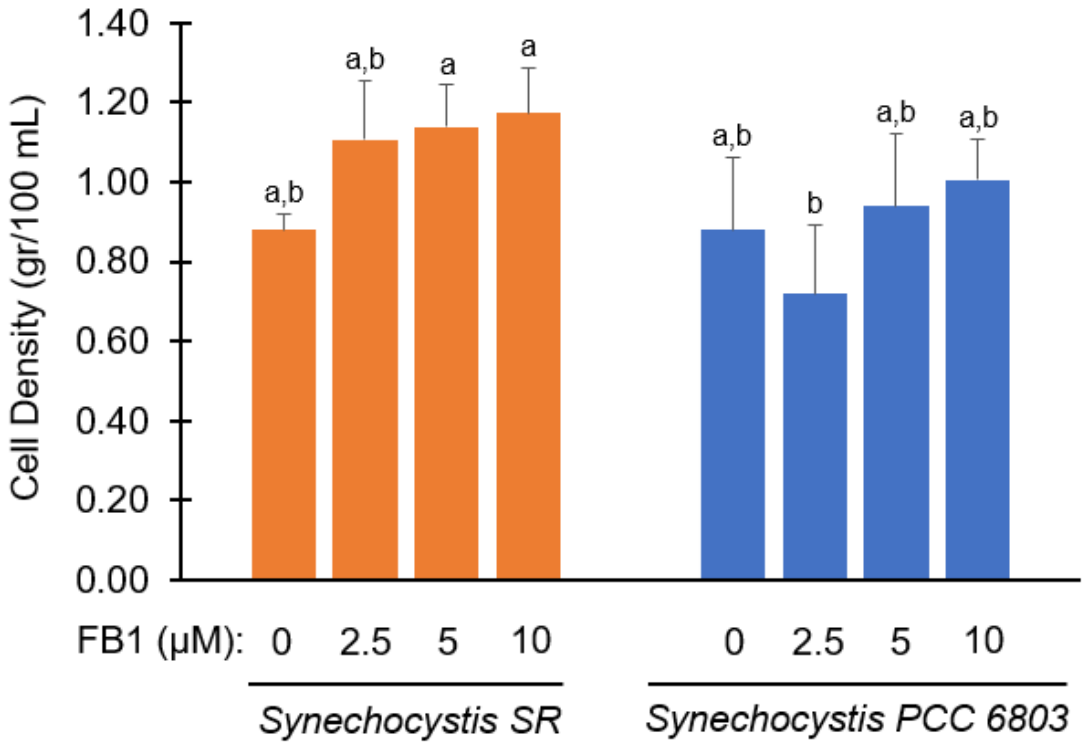

Figure 3.7 Dose-response of cyanobacterial cell density to FB1 treatment
Synechocystis SR or *Synechocystis PCC 6803* cultures were treated with the indicated FB1 concentrations and cell density analysed 2 weeks later. Bars represent mean±SD (n = 3). Bars with the same letter are not statistically different ($p \leq 0.05$).

The same FB1-treated cell cultures were analysed using the MTT assay, which relies on the conversion of the yellow MTT solution to a purple formazan product that is then quantified by spectrophotometric measurements. Conversion of the

MTT solution is dependent upon the activity of cellular dehydrogenase enzymes, making the assay a good indicator of cell metabolism. Figure 3.8 shows that cellular metabolism was very different between the two cyanobacterial strains, even in untreated cultures. Concentrations of 2.5 and 10 µM FB1 caused a significant increase in metabolic activity of *Synechocystis SR* cultures, while only the highest concentration of 10 µM FB1 triggered a significant rise in metabolic activity in *Synechocystis PCC 6803*. Overall, the level of metabolic activity as measured via the MTT assay was far lower in *Synechocystis PCC 6803* than *Synechocystis SR*. This demonstrates that, though these strains appear similar in size (Figure 3.5), they have very distinct metabolic profiles. Taken together, these results confirm that a biotic stress can activate increases in cyanobacterial metabolic activity. Furthermore, the MTT assay can be used to biochemically distinguish between *Synechocystis SR* and *Synechocystis PCC 6803*.

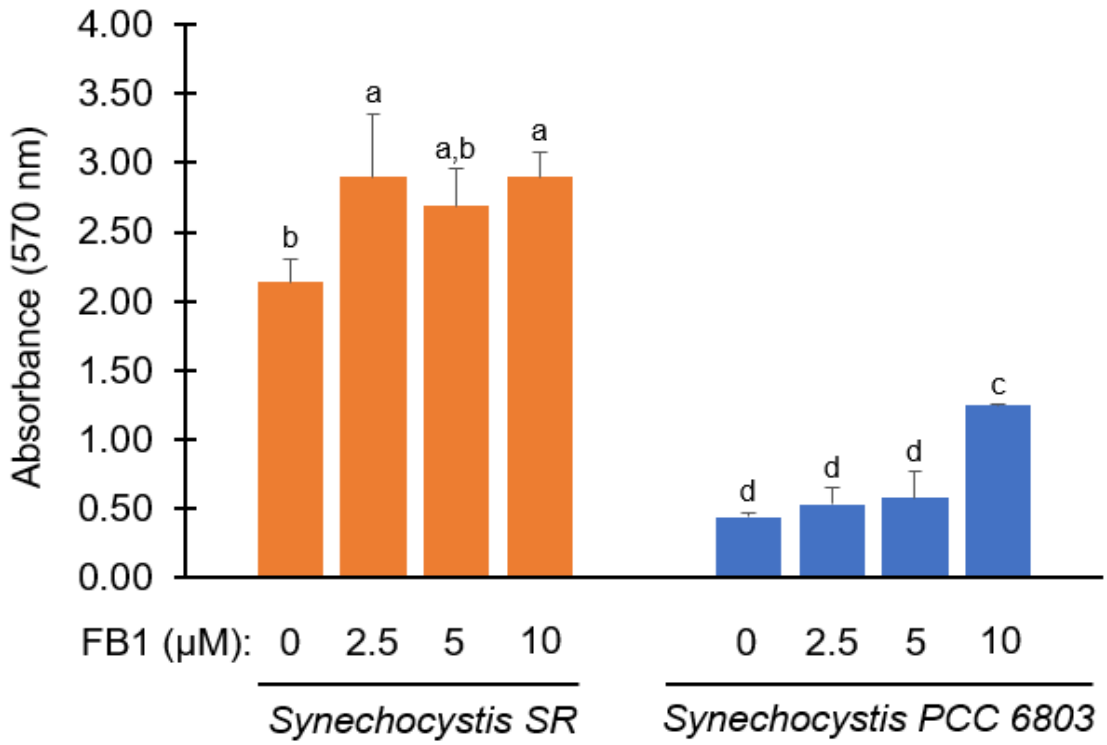

Figure 3.8 Effects of FB1 on cellular metabolism
Cells were treated with the indicated FB1 concentrations and aliquots taken for quantitative analysis with the MTT assay 2 weeks later. Bars represent mean±SD (n = 3). Bars with the same letter are not statistically different ($p \leq 0.05$).

3.3 Treatments with NaCl

3.3.1 Cyanobacterial growth in high salinity under high light

After evaluating the effects of a mycotoxin on the growth and metabolic activity of cyanobacterial strains, results indicated no adverse effects of FB1 on cell growth. It was speculated that lack of real growth repression by the toxin could be an indication that the cyanobacteria are not under any stress and so would probably not activate the lipid biosynthetic pathway. Thus, salinity and ionic stress were selected as an alternative inexpensive abiotic stress that could be applied on cyanobacterial cultures to manipulate lipid biosynthesis. Sodium chloride is a major component of seawater, an abundant resource which could be used as a low-cost treatment for activation of lipid production in *Synechocystis SR.* If it works, this would represent a commercially attractive option that is scalable for industrial production of algal lipids to be used in a number of different applications.

In a preliminary experiment, the effects of salinity stress on growth of cyanobacterial strains were studied. Fresh BG-11 medium was inoculated with *Synechocystis SR* or *Synechocystis PCC 6803* culture and NaCl added to a final concentration of 0, 50, 100, 200, 400 or 600 mM NaCl. The tubes were incubated under continuous high light intensity (150 $\mu mol.m^{-2}.s^{-1}$) for 5 days. Photographs taken at the end of the incubation period showed very poor growth for both strains, with no discernible trend in growth or appearance of culture across the NaCl dose range (Figure 3.9). *Synechocystis SR* seemed to have reasonable growth and the typical blue-green appearance at 100 mM NaCl than in control or other NaCl treatments. Equally, *Synechocystis PCC 6803* displayed slightly better growth and culture appearance at 400 mM NaCl. The random tubes showing better growth under NaCl stress were later confirmed to be attributable to a diminished rate of compressed air bubbling into individual tubes, a problem corrected in subsequent experiments. Overall, these results are in agreement with earlier observations that cyanobacteria under no stress have poor growth in continuous high light incubation (Figure 3.1). Importantly, the current results show that salt stress severely curbs cyanobacterial growth under these light conditions.

However, because this was a preliminary experiment associated with technical problems of unequal compressed air bubbling rates, the results should be treated with caution and no firm conclusions can be drawn.

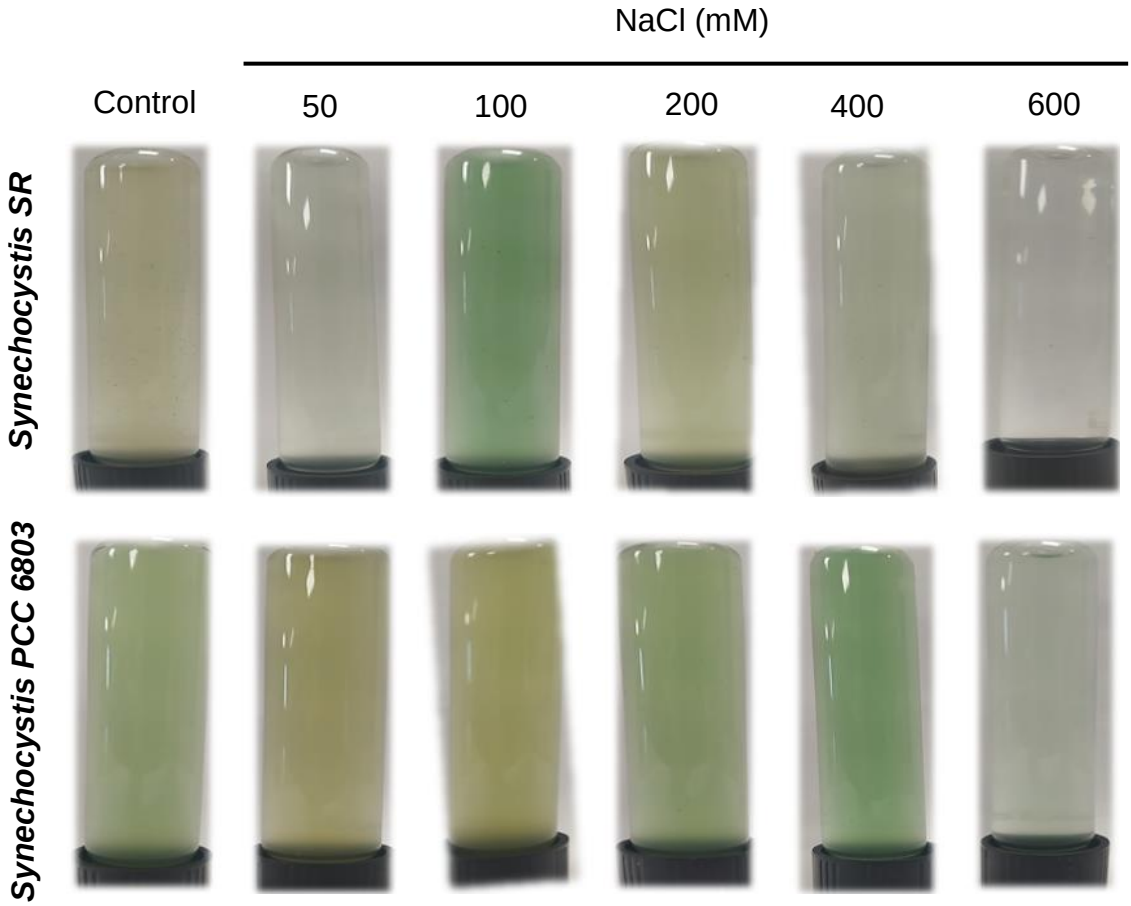

Figure 3.9 Effects of NaCl on cyanobacterial growth under high light intensity.
Synechocystis SR or *Synechocystis PCC 6803* inoculum was added to BG-11 medium containing the indicated amounts of NaCl. The cultures were incubated under continuous high light (150 µmol.m^{-2}.s^{-1}) and photographs of representative cultures taken after 5 days of growth.

In order to diminish the impact of salt stress on cyanobacterial growth, an experiment was designed to allow the inoculum to acclimate to salt under low light incubation prior to raising the light intensity to permit the cultures to enter the logarithmic growth phase. The hypothesis was that this would provide rapidly growing biomass with a metabolic status adjusted for growth under salt. Therefore, BG-11 was inoculated with *Synechocystis SR* or *Synechocystis PCC 6803* inoculum in a final concentration of 600 mM NaCl. The cultures were

incubated at low light intensity (75 µmol.m^{-2}.s^{-1}) to enable the cells to acclimate, and then ramped up to 150 µmol.m^{-2}.s^{-1}.

In contrast to the poor growth seen when the cultures were incubated continuously under high light intensity (Figure 3.9), a period of acclimation at low light prior to high light incubation under the highest salt concentration led to improved multiplication of blue-green cyanobacterial cultures (Figure 3.10).

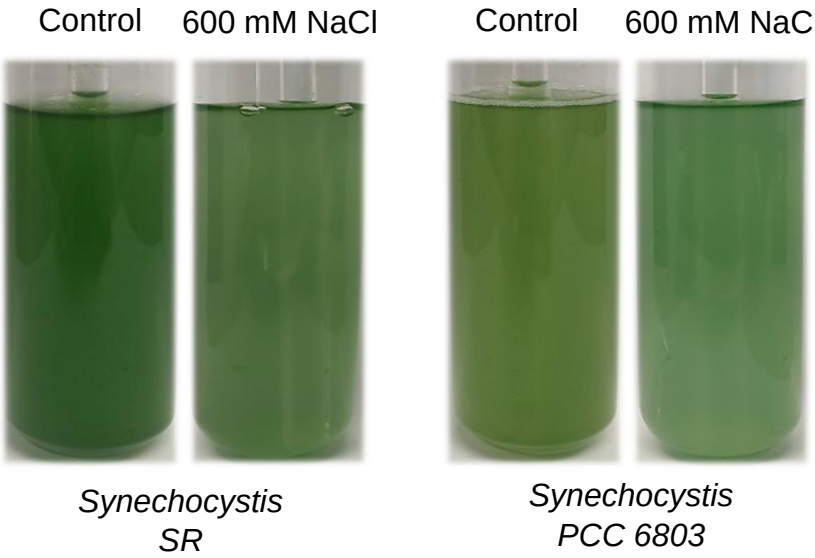

Figure 3.10 Effects NaCl on cyanobacteria under a step-up light intensity program.
Inoculum of *Synechocystis SR* or *Synechocystis PCC 6803* was added to plain BG-11 medium (control) or medium spiked with water or 600 mM NaCl and grown for a week under a step-up light regime - 4 days in low light (75 µmol.m^{-2}.s^{-1}) followed by 3 days in high light (150 µmol.m^{-2}.s^{-1}). Photographs were taken 7 days after inoculation.

Growth of these cultures was kinetically monitored by quantitative measurements of optical density. During the first 5 days of low light intensity (75 µmol.m^{-2}.s^{-1}), the cultures remained in lag phase for both cyanobacterial strains, with notably increased exponential growth when the light intensity was stepped up to 150 µmol.m^{-2}.s^{-1} (Figure 3.10). *Synechocystis SR* had an extended exponential growth phase lasting until day 11, with transition to the stationary phase happening on day 12 in the untreated control cultures. The exponential phase of untreated *Synechocystis PCC 6803* lasted until day 9, the cultures entered the stationary phase sooner and started to decline by day 11. In both strains, growth

under salt stress was lower than control cultures, but salt impacted *Synechocystis PCC 6803* more than it did *Synechocystis SR* as seen by the optical density differences prior to start of the stationary phase (Figure 3.9). Overall, these results demonstrate that light is strong regulator of the effects of salt on cyanobacteria.

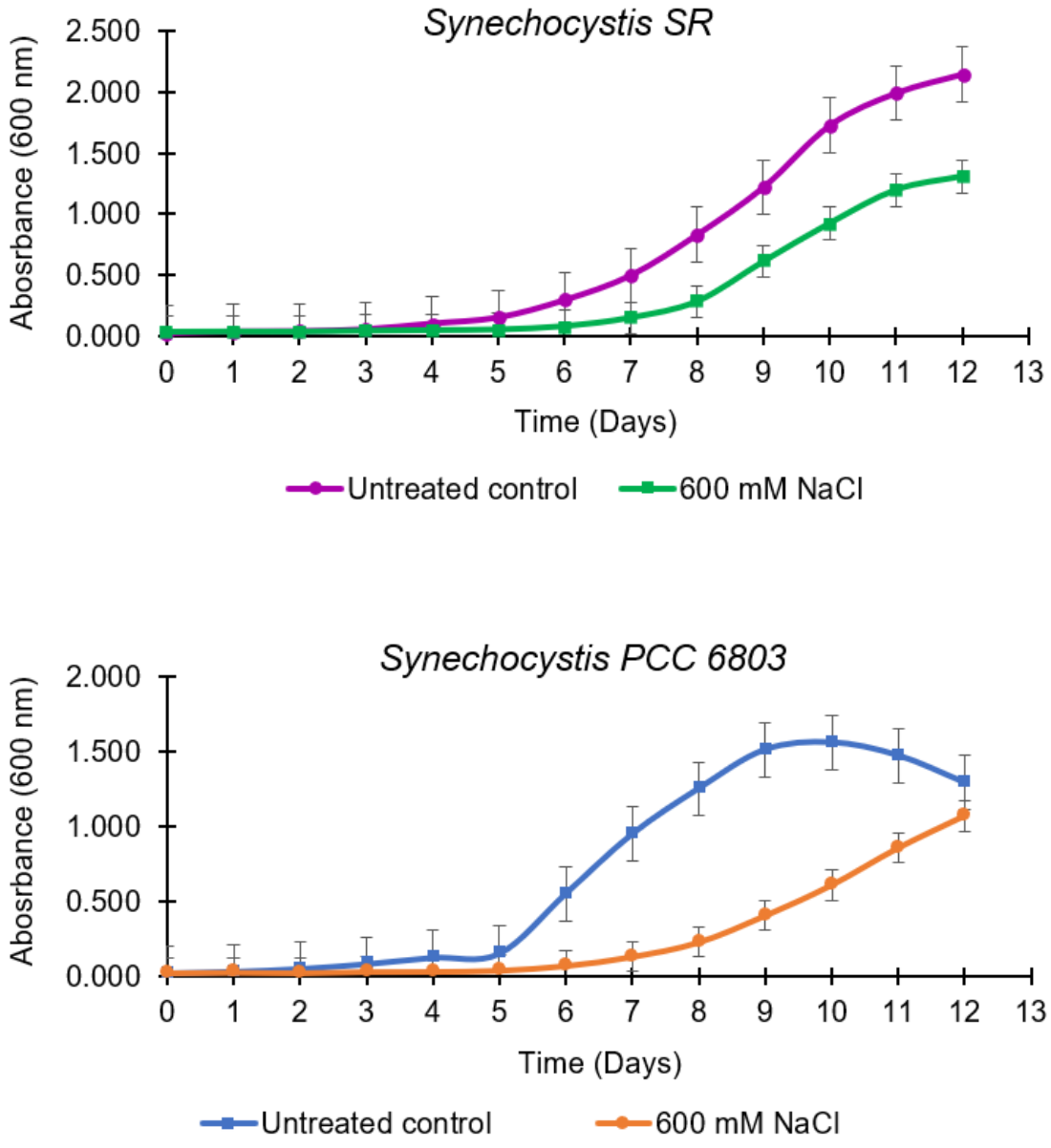

Figure 3.11 Kinetic growth profile of cyanobacteria exposed to NaCl in a step-up light regime.
Synechocystis SR and *Synechocystis PCC 6803* inoculum was added to BG-11 medium containing 0 or 600 mM NaCl and incubated in a step-up light regime - 5 days at low light (75 µmol.m^{-2}.s^{-1}) followed by high light (150 µmol.m^{-2}.s^{-1}) for 7 days. Optical density was measured at the indicated time-points. Error bars represent standard error of mean (*n* = 3).

3.3.2 Salt-induced changes in cell ultrastructure

Next, the ultrastructure of cyanobacterial cells in control or high salinity (600 mM NaCl) conditions was examined by transmission electron microscopy. Control *Synechocystis SR* cells had clearly visible ellipsoidal membranes presumably bearing the photosynthetic machinery (equivalent to chloroplast thylakoids), which increased in abundance in NaCl-treated cells (Figure 3.12). However, cells in high salinity developed numerous membrane-bound vesicles, whose contents remain to be determined. In *Synechocystis PCC 6803* control cells, densely packed thylakoids were visible, but their appearance somewhat became less distinct in high salinity (Figure 3.13). In contrast to *Synechocystis SR*, the membrane-bound vesicles appearing in NaCl-treated cells were much fewer in *Synechocystis PCC 6803* (Figure 3.13).

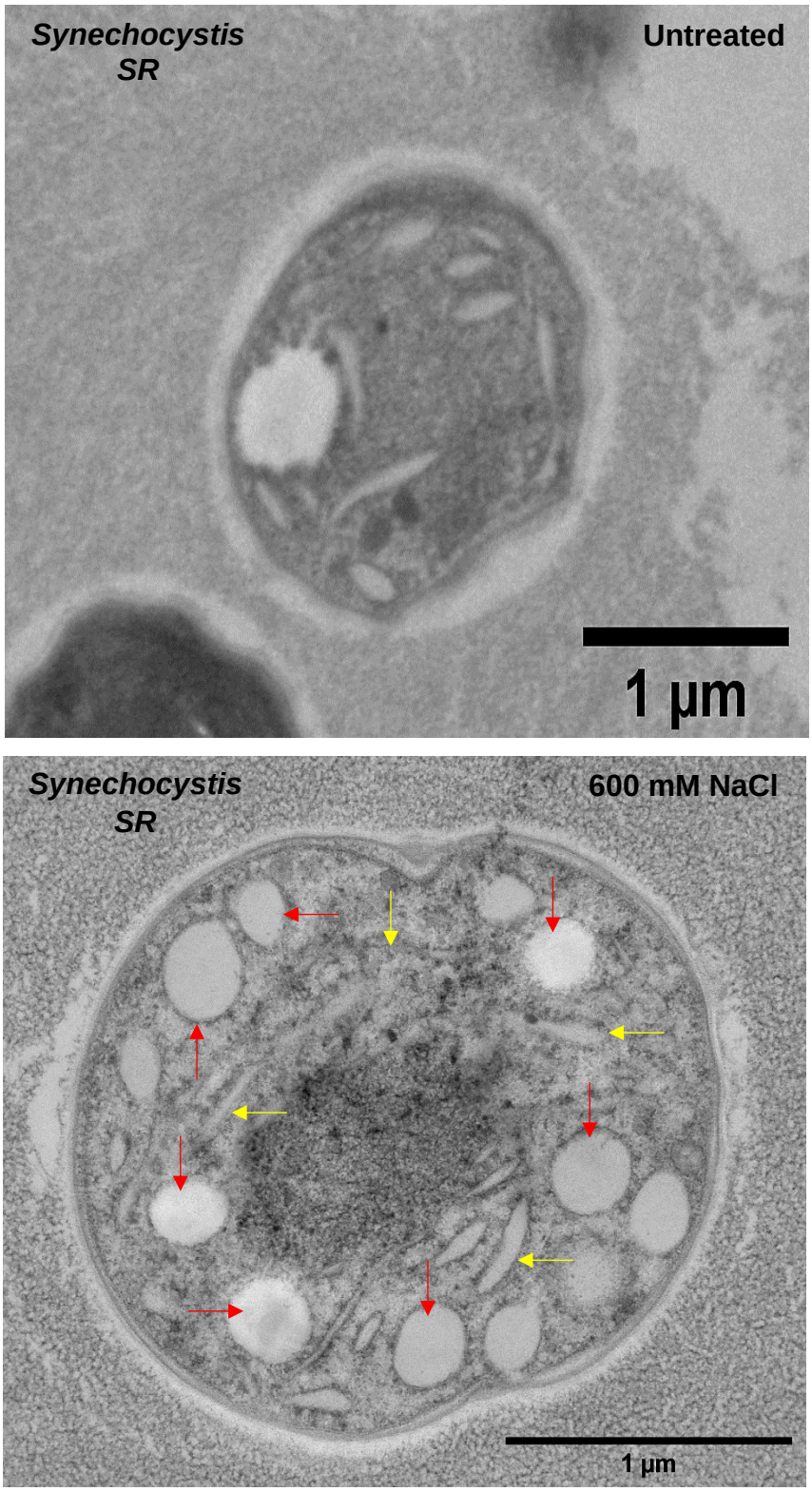

Figure 3.12 Electro micrograph of control and NaCl-treated *Synechocystis SR* cells.
Cyanobacterial cells were exposed to 0 or 600 mM NaCl for 5 days at low light (75 µmol.m^{-2}.s^{-1}) followed by and 7 days at high light (150 µmol.m^{-2}.s^{-1}). Red arrows indicate membrane-bound vesicles and yellow arrows "thylakoid" membranes.

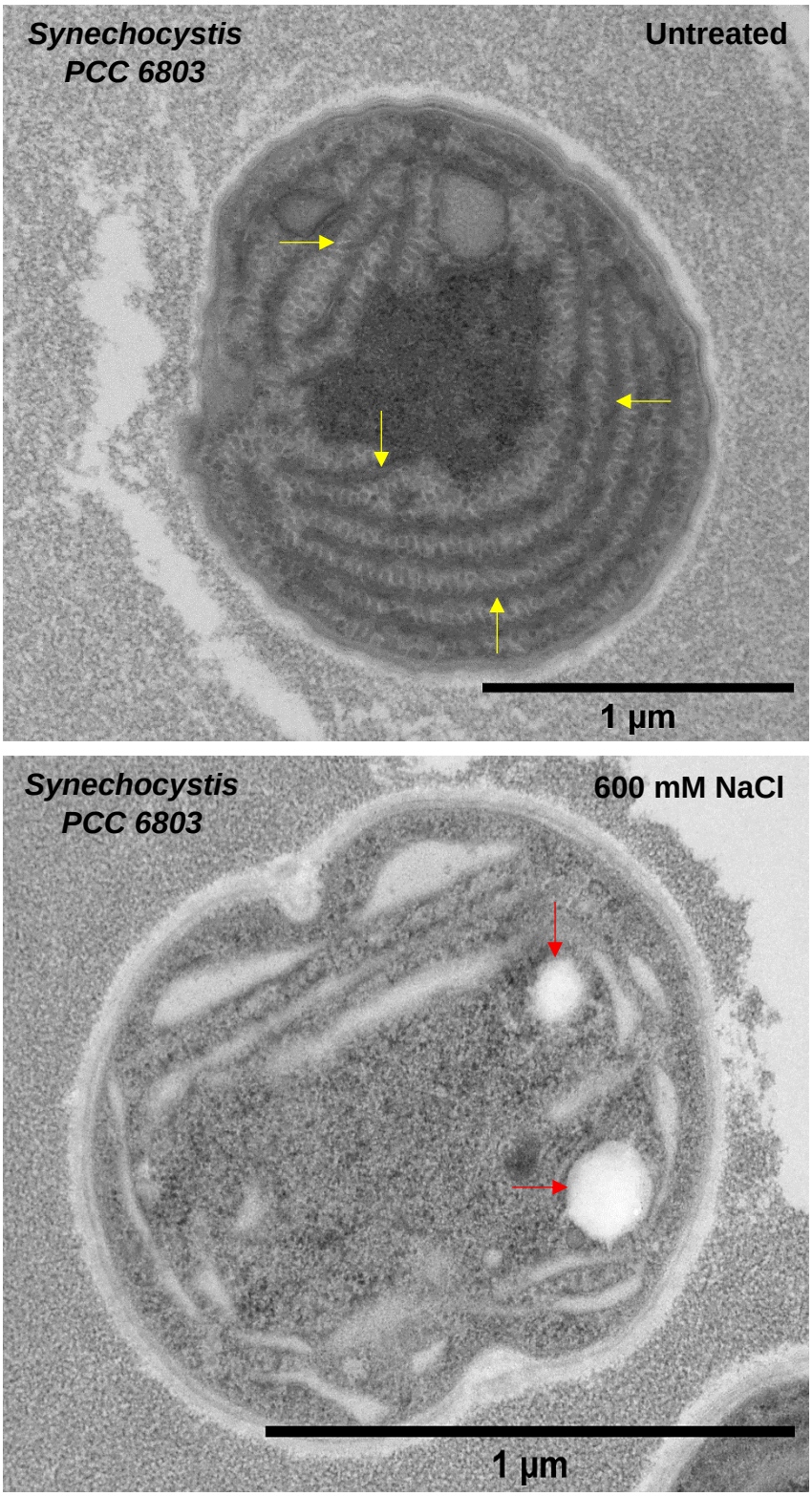

Figure 3.13 Electro micrograph of control and NaCl-treated *Synechocystis PCC 6803* cells.
Cyanobacterial cells were exposed to 0 or 600 mM NaCl for 5 days at low light (75 µmol.m^{-2}.s^{-1}) followed by and 7 days at high light (150 µmol.m^{-2}.s^{-1}). Red arrows indicate membrane-bound vesicles and yellow arrows "thylakoid" membranes.

As explained in section 3.1, there was no significant difference in cell diameter between untreated *Synechocystis SR* and *Synechocystis PCC 6803* (Figure 3.4). Untreated *Synechocystis SR* cells had an average cell diameter of ~1.81 ± 0.48 µm (*n* = 35), which is not statistically different from ~1.79 ± 0.39 µm (*n* = 35) the diameter of cells under high salinity (600 mM NaCl). Likewise, *Synechocystis PCC 6803* control cell diameter averaged at 1.64 ± 0.24 µm (*n* = 35), which is not significantly different from the high salinity cell average diameter of ~1.44 ± 0.41 µm (*n* = 35). Figure 3.13 shows a box plot of the cell diameters before and after application of salt stress in both cyanobacterial strains. Overall, these results show that the adaptive response to salinity stress in these two organisms differs at the subcellular level, though cell size remains unaffected.

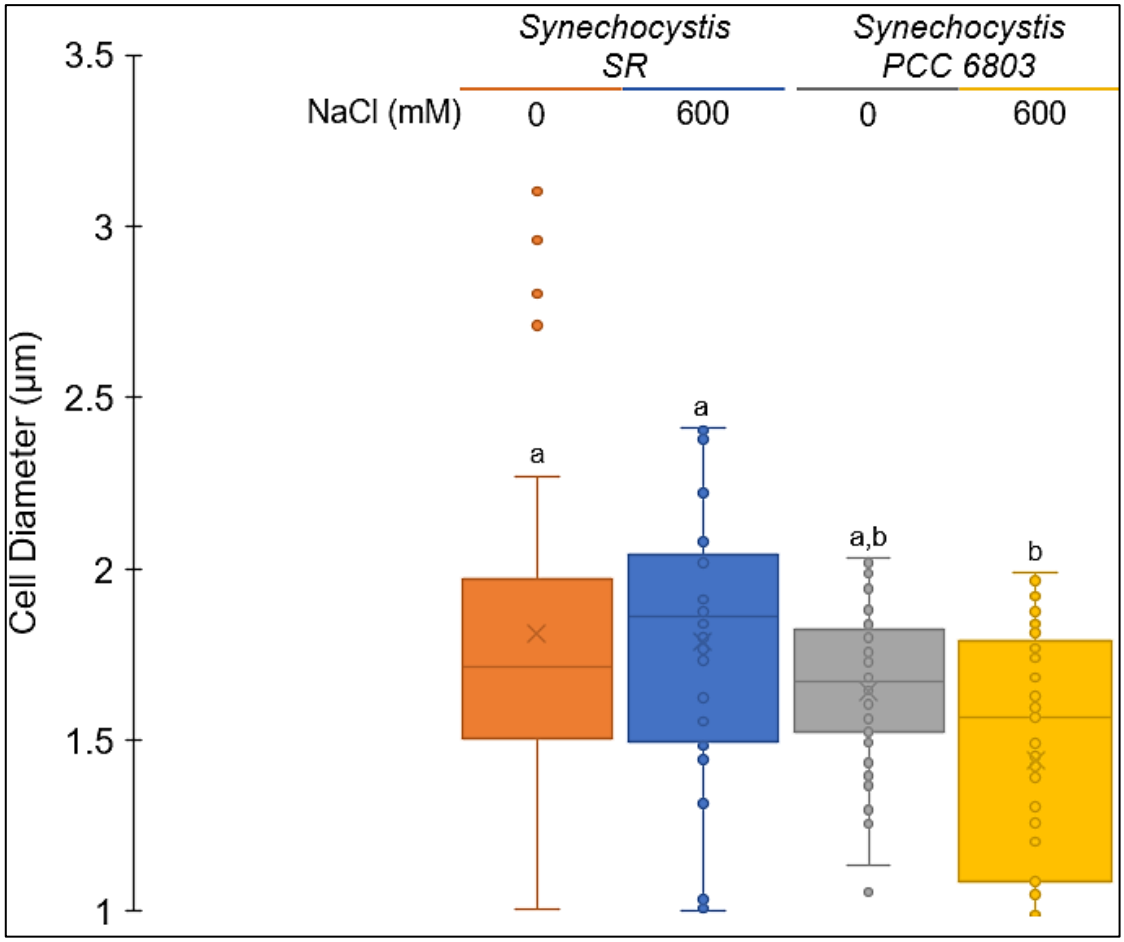

Figure 3.14 Box and whisker plot of untreated cyanobacterial and under 600 mM NaCl cell diameter data.
Cell diameter was measured on transmission electron micrograph images. Data was obtained from 35 cells each for each cyanobacterial strain.

3.3.3 Effect of high salinity on cyanobacteria under low light conditions

Considering that light intensity and salinity stress play an important role in cyanobacterial growth, the impact of NaCl on cells under low light was considered. In these experiments, biomass was first bulked up in absence of stress by inoculating BG-11 medium and growing the cultures under a step-down light regime of 5 days high light (150 $\mu mol.m^{-2}.s^{-1}$) followed by 2 days low light (75 $\mu mol.m^{-2}.s^{-1}$). Cyanobacterial cultures grown for a week under a step-down light regime were treated with a final concentration of 0, 200, 400 or 600 mM NaCl and immediately incubated at low light intensity (75 $\mu mol.m^{-2}.s^{-1}$). On the basis of visual appearance of the cultures, it was clear that the impact of salt stress on *Synechocystis SR* was minimal, with an equally blue-green hue across all the treatments (Figure 3.15). Even the highest concentration of salt (600 mM NaCl) appeared quite similar to the control culture. In contrast to this, *Synechocystis PCC 6803* had a lighter hue of colouration and there was a noticeable reduction in the cell density of the culture treated with 600 mM NaCl (Figure 3.15). Therefore, on the basis of visual appearance, salinity stress impacted *Synechocystis PCC 6803* growth more than it did *Synechocystis SR*.

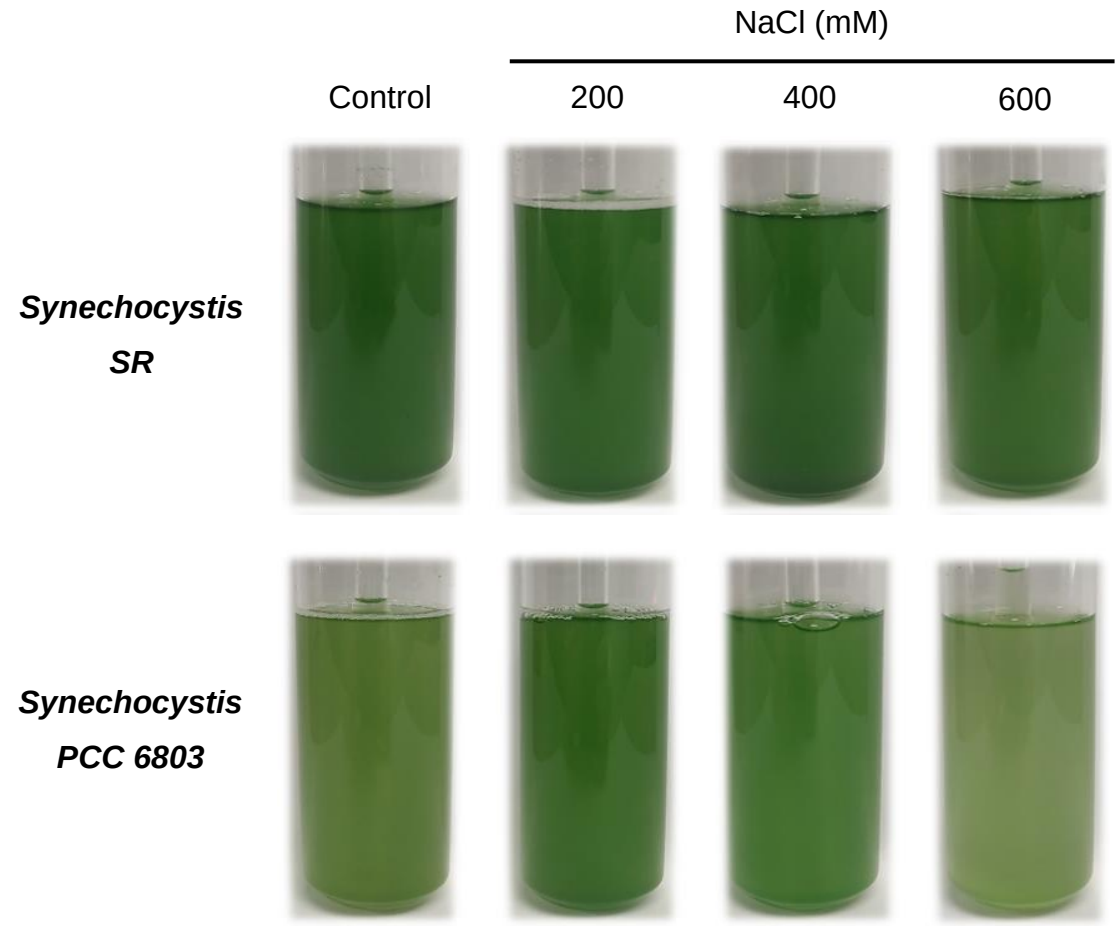

Figure 3.15 Effects of NaCl on cyanobacterial growth under low light. *Synechocystis SR* and *Synechocystis PCC 6803* cultures grown for a week under a step-down light regime (5 days high light followed by 2 days low light) were exposed to the indicated NaCl treatments for 7 days under continuous low light. Photographs were taken after 7 days exposure to salt stress. Low light, 75 $\mu mol.m^{-2}.s^{-1}$; high light, 150 $\mu mol.m^{-2}.s^{-1}$.

The kinetic growth profile of these cultures from the moment of addition of NaCl was monitored using optical density measurements. Direct comparison of the untreated controls showed that *Synechocystis PCC 6803* did not grow in the 7 days incubation period under low light (Figure 3.16). Untreated *Synechocystis SR* cultures grew significantly (Figure 3.16) suggesting that this strain was capable of harvesting significant light energy to drive photosynthesis under the diminished light intensity. This might indicate fundamental differences in the light-harvesting complexes of these two cyanobacterial strains. The nature of these differences might require metabolomics analysis to compare photosynthetic pigments or proteomic analysis to compare the protein components of these complexes.

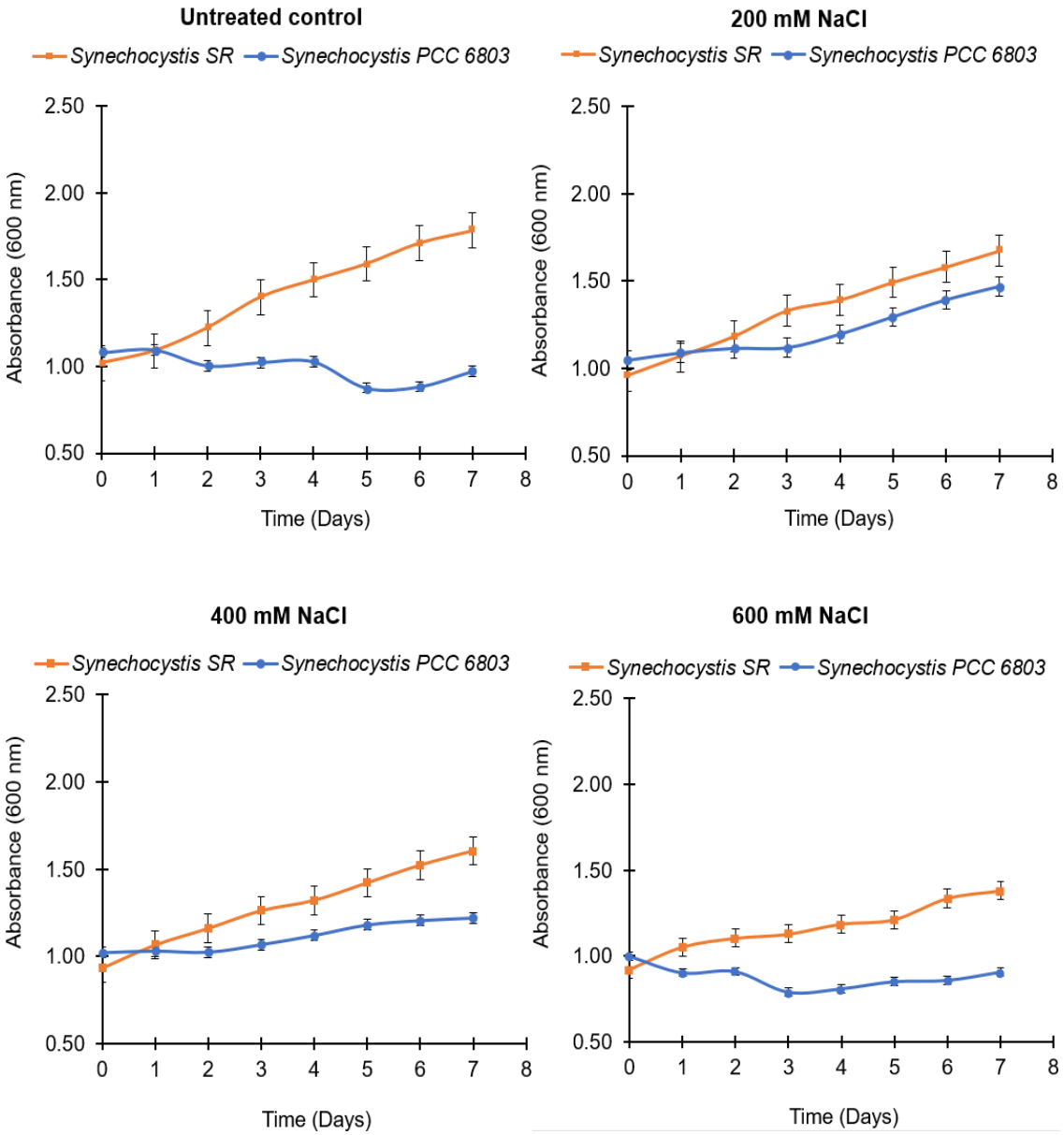

Figure 3.16 Kinetic profiles of cyanobacterial growth in response to NaCl stress under low light.
Synechocystis SR and *Synechocystis PCC 6803* cultures grown for a week under a step-down light regime (5 days high light followed by 2 days low light) were exposed to the indicated NaCl treatments for 7 days under continuous low light. Optical density was measured immediately after treatment and every 24 h subsequently for 7 days. Error bars represent standard error of mean (n = 3). Low light, 75 µmol.m^{-2}.s^{-1}; high light, 150 µmol.m^{-2}.s^{-1}.

While control *Synechocystis PCC 6803* cultures did not grow at low light in the 7-day period under investigation, an interesting observation is that there was some growth at the low levels of salt stress, with the most growth registered at 200 mM NaCl (Figure 3.16). However, when salinity was increased to 600 mM NaCl, there was a cessation of growth. These results indicate that mild stress stimulates growth in *Synechocystis PCC 6803*, while extreme stress stops growth. However, across the entire dose range of NaCl, *Synechocystis SR* registered positive growth (Figure 3.16), indicating that this strain is more resilient to NaCl stress. Therefore, any of these salt concentrations can be used to investigate if adaptation to stress is underpinned by activation of lipid biosynthesis.

3.4 Fatty acid synthesis gene expression

3.4.1 Identification of fatty acid synthesis genes

An objective of this research was to use stress to stimulate biosynthesis of fatty acids in cyanobacteria. The fatty acid biosynthesis pathway is well characterised in the model organism *Escherichia coli*, in which all the fatty acid synthesis (FAS) genes have been identified. In order to identify *Synechocystis* orthologues of FAS genes, the protein sequences of the 8 *E. coli* FAS enzymes were used to interrogate the *Synechocystis PCC 6803*-limited cyanobacterial genomic database (CyanoBase) using the Basic Local Alignment Search Tool (BLAST). The *Synechocystis PCC 6803* orthologous genes identified using this method are given in Table 3.1. A total of 10 *Synechocystis PCC 6803* FAS genes were identified, with redundancy seen between the targets identified using *FabA* and *FabZ* or *FabB* and *FabF* (Table 3.1). Additionally, 4 of the *E. coli* proteins had more than one orthologue in cyanobacteria, resulting in more putative FAS genes identified in the *Synechocystis PCC 6803* genome.

Table 3.1 Homologous *Escherichia coli* and *Synechocystis PCC 6803* FAS genes.

Escherichia coli		***Synechocystis PCC 6803***	
Gene ID	Protein name	Gene ID	Abbreviation
FabA	3-hydroxyacyl-ACP dehydrase	*sll1605*	*DH*
FabZ	3-hydroxyacyl-ACP dehydrase	*sll1605*	*DH*
FabI	enoyl-ACP reductase	*slr1051*	*ENR1*
		slr0886	*ENR2*
		slr1994	*ENR3*
FabB	3-ketoacyl-ACP synthase I	*sll1069*	*KS1*
		slr1332	*KS2*
FabF	3-ketoacyl-ACP synthase II	*sll1069*	*KS1*
		slr1332	*KS2*
FabH	3-ketoacyl-ACP synthase III	*slr1511*	*KS3*
FabG	3-ketoacyl-ACP reductase	*slr2124*	*KR1*
		sll1709	*KR2*
AccABCD	Acetyl-CoA carboxylase	*slr0435*	*ACCase*

Reverse-transcription polymerase chain reaction (RT-PCR) using gene-specific primers (Appendix I) indicated that all the FAS genes are expressed in both *Synechocystis PCC 6803* and *Synechocystis SR* growing under normal growth conditions (Figure 3.17). The 16S and 5S rRNA were used as constitutive reference controls (Figure 3.17). The same amplicon size expected from the specific primers were obtained in the two cyanobacterial strains, strongly suggesting that the FAS gene sequences are not different between these strains.

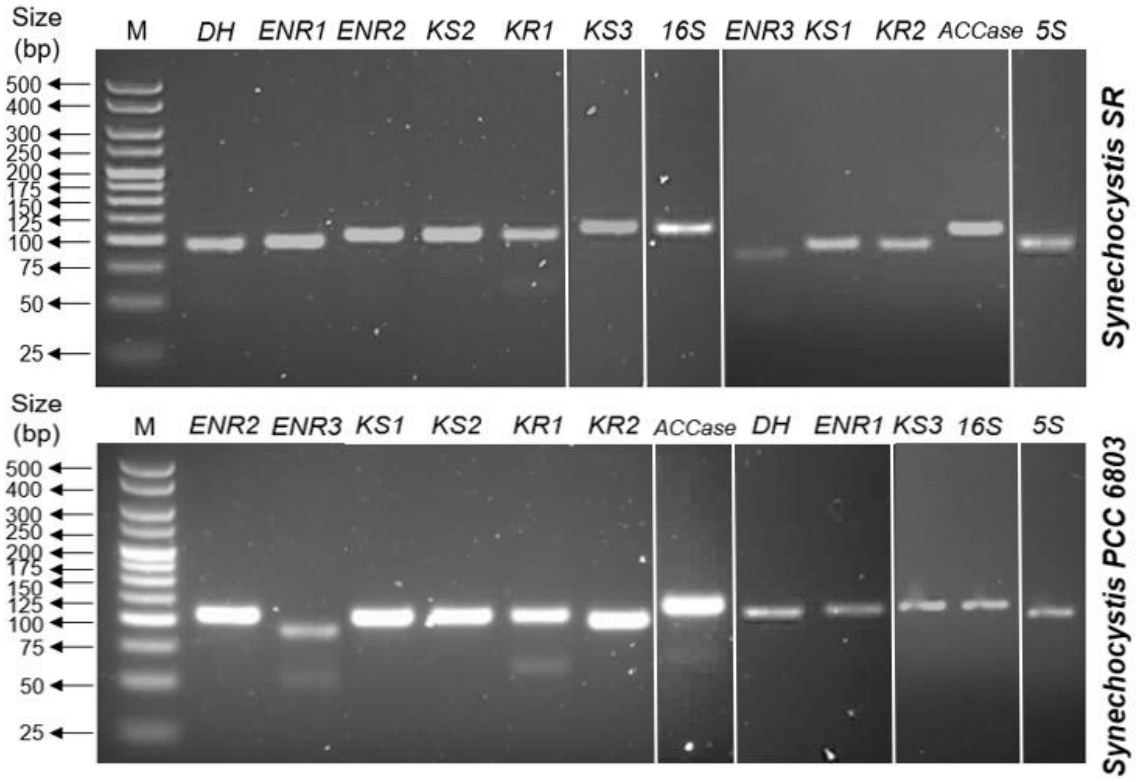

Figure 3.17 Agarose gel electrophoresis of RT-PCR products amplified from selected cyanobacterial genes.
Gene specific primers were used to PCR-amplify cDNA derived from *Synechocystis PCC 6803* or *Synechocystis SR* RNA extracted from normally growing cells. Constitutive reference control genes 5S and 16S rRNA were included amongst the FAS genes (Table 3.1).

3.4.2 Response of FAS genes to salinity stress under step-up light regime

Inoculum of S*ynechocystis SR* or *Synechocystis PCC 6803* cells was added to BG11 medium containing a final concentration of 0, 200, 400, or 600 mM NaCl and allowed to grow under a step-up light regime (3 days at 75 µmol.m^{-2}.s^{-1}

followed by 2 days at 150 µmol.m^{-2}.s^{-1}). At the end of the 5 days growth period, cells were harvested for RNA extraction. The integrity of the RNA samples was confirmed by gel electrophoresis and visualisation of the major RNA species (see Appendix II for representative gels).

FAS gene expression in response to salinity stress was conducted by quantitative RT-PCR analysis using 5S and 16S rRNA as constitutive reference controls. All the 10 FAS genes were activated on exposure to NaCl in both *Synechocystis SR* and *Synechocystis PCC 6803* (Figures 3.18 and 3.19). Transcript accumulation increased at low salt concentrations, peaked, and then declined at the highest levels of NaCl. Although the gene expression profile was similar between the two strains, gene activation peaked at 200 mM NaCl in *Synechocystis PCC 6803*, while the peak in *Synechocystis SR* occurred at 400 mM NaCl. The expression profile was very similar across all the 10 genes within each strain. This indicates that salinity stress activates the entire pathway by targeting every metabolic step. Why certain genes are activated to a much higher level than others might be a reflection of different protein turnover rates. Remarkably, even enzymes with more than one gene, such as enoyl-ACP reductase (ENR), had all the genes activates, though the peak differed somewhat. Perhaps genes, within a multi-gene family encoding the same enzyme, showing the highest peak expression contribute more to the protein products. However, the existence of multiple genes for the same enzyme to create redundancy is possibly an insurance against deleterious mutations.

Across all the genes, expression was higher in *Synechocystis SR* than in *Synechocystis PCC 6803*. This suggests that the FAS pathway of *Synechocystis SR* is much more responsive to salinity. If this translates to the protein products, then this strain is expected to make more fatty acids under salinity stress than in *Synechocystis PCC 6803*. Increased FAS gene expression in *Synechocystis SR* than *Synechocystis PCC 6803*, reflects the increased metabolic activity under stress as previously described in section 3.2. This is also reflected in the better growth performance of *Synechocystis SR* than *Synechocystis PCC 6803* under salt stress (section 3.3). Overall, these results confirmed the hypothesis that sub-lethal salinity stress activates FAS gene expression in cyanobacterial cells.

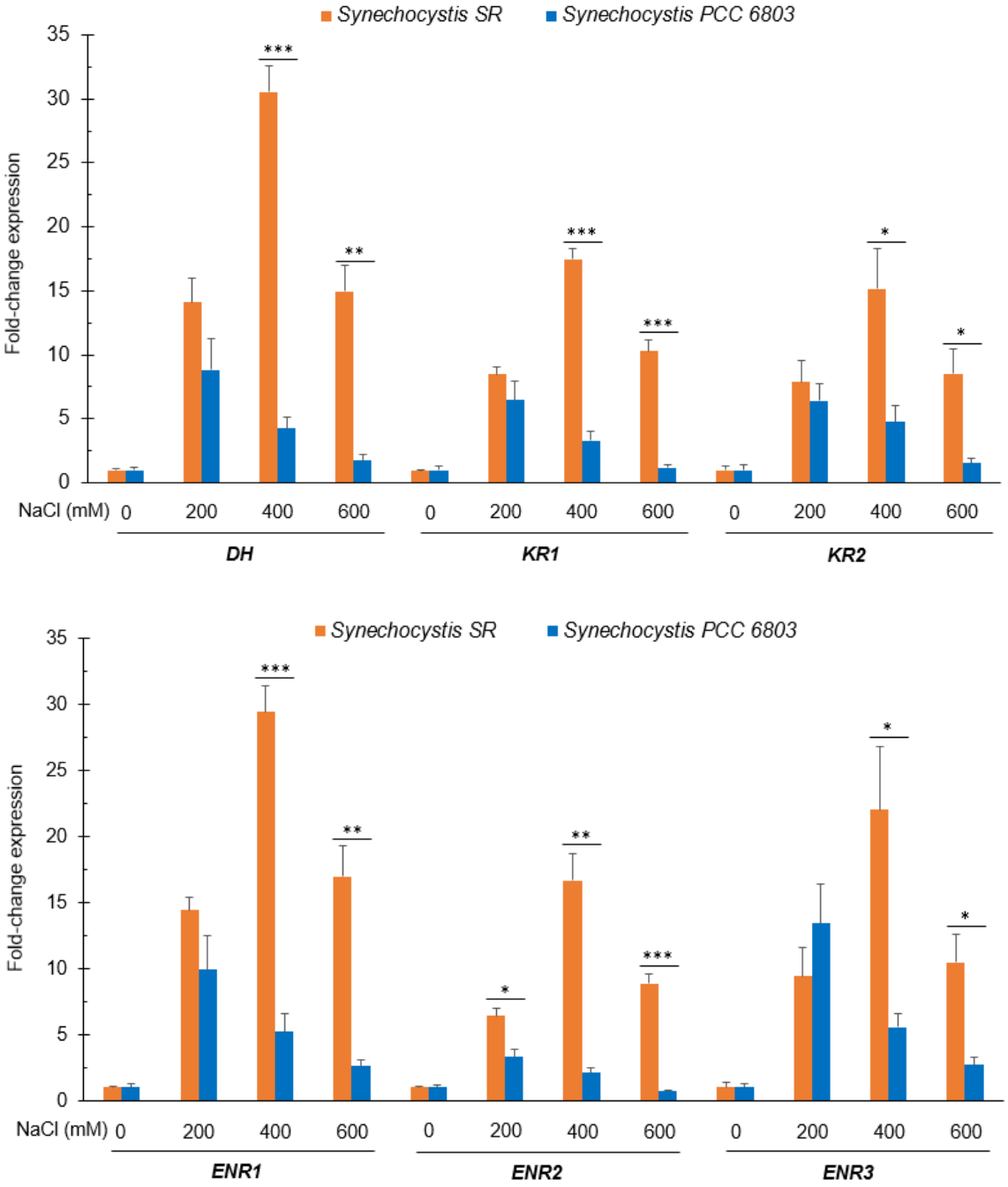

Figure 3.18 Activation of 6 cyanobacterial FAS gene expression by salinity stress under a step-up light regime.
Quantitative RT-PCR was performed with cDNA synthesised from RNA samples extracted from cyanobacterial cultures treated for 5 days with the indicated amounts of NaCl under a step-up light regime (3 days at 75 µmol.m^{-2}.s^{-1} followed by 2 days at 150 µmol.m^{-2}.s^{-1}). Bars represent mean ± SD (n = 3). Significant differences between *Synechocystis SR* and *Synechocystis PCC 6803* at each concentration are indicated by one ($p \leq 0.05$), two ($p \leq 0.01$) or three asterisks ($p \leq 0.001$).

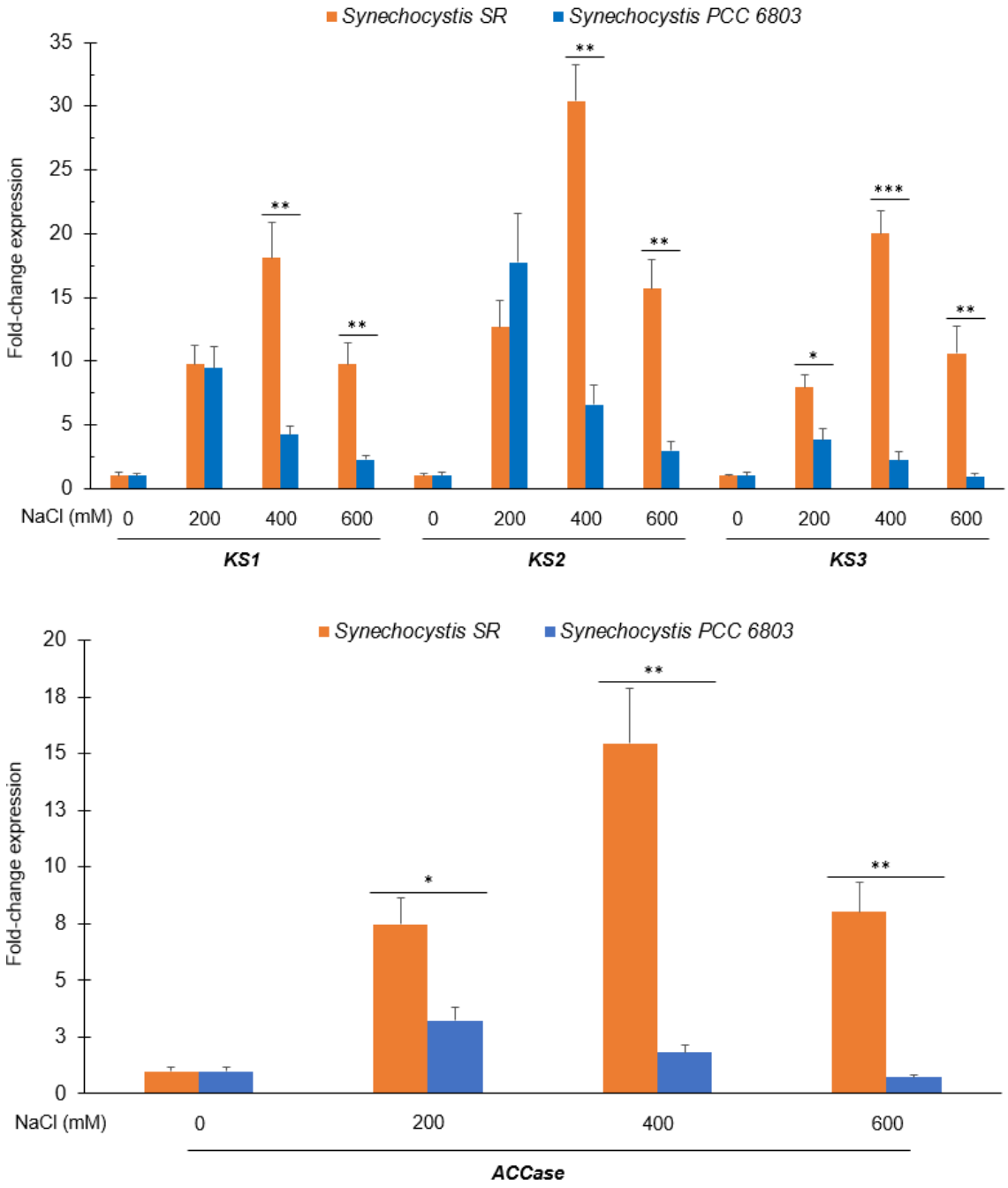

Figure 3.19 Activation of 4 cyanobacterial FAS gene expression by salinity stress under a step-up light regime.
Quantitative RT-PCR was performed with cDNA synthesised from RNA samples extracted from cyanobacterial cultures treated for 5 days with the indicated amounts of NaCl under a step-up light regime (3 days at 75 µmol.m^{-2}.s^{-1} followed by 2 days at 150 µmol.m^{-2}.s^{-1}). Bars represent mean ± SD (n = 3). Significant differences between *Synechocystis SR* and *Synechocystis PCC 6803* at each concentration are indicated by one ($p \leq 0.05$), two ($p \leq 0.01$) or three asterisks ($p \leq 0.001$).

3.4.3 Response of FAS genes to salinity stress under step-down light regime

Having demonstrated the superior performance of *Synechocystis SR* in salinity stress-activated FAS gene expression, a more detailed time-course study on this strain was conducted. Considering the NaCl concentration and light intensity conditions providing for the highest growth under salt treatment (Figure 3.16), a concentration of 200 mM NaCl was chosen for this experiment. Therefore, cultures of *Synechocystis SR* generated in step-down growth conditions were exposed to 200 mM NaCl and then incubated under continuous low light (75 $\mu mol.m^{-2}.s^{-1}$). Triplicate samples were harvested at 0, 1, 2, or 4 days after treatment for RNA extraction. Integrity of RNA samples was verified by gel electrophoresis (see Appendix II for representative gel). FAS gene expression was analysed by quantitative RT-PCR using cDNA template and 5S rRNA as a constitutive reference gene.

Expression profiling shows that gene activation soared at 4 days, with very little or no increase in the first two days (Figures 3.20 and 3.21). In fact, for some genes there was a significant suppression of transcripts in the first two days of exposure to salt. Under these experimental conditions, there was bigger sample variance, which resulted in some of the fold-change increases in gene expression at 4 days not being statistically significant. Furthermore, the fold-increase in some of the genes was comparatively lower than the fold-change induced by 200 mM NaCl in experiments reported in the preceding section (3.4.2). For example, *DH* was activated 15-fold by 200 mM NaCl in section 3.4.2 experiments (Figure 3.18), while in Figure 3.19 *DH* was activate 5-fold. This discrepancy relates to two factors. Firstly, section 3.4.2 experiments samples were exposed to NaCl for longer (5 days) than the experiments described here (4 days). It is possible that the extra day could account for the further increase in gene expression and better statistical significance across all genes. Secondly, in the former experiments, the cells were inoculated for growth in salt in a step-up light regime, while in the latter biomass was generated in a step-down regime, after which the cells were exposed to salt under constant low light (75 $\mu mol.m^{-2}.s^{-1}$). The level of stress appears higher under step-up conditions as evidenced by relatively reduced grow

when compared to cultures treated at constant low light (Figure 3.22). Overall, these results show that NaCl stress activates FAS gene expression.

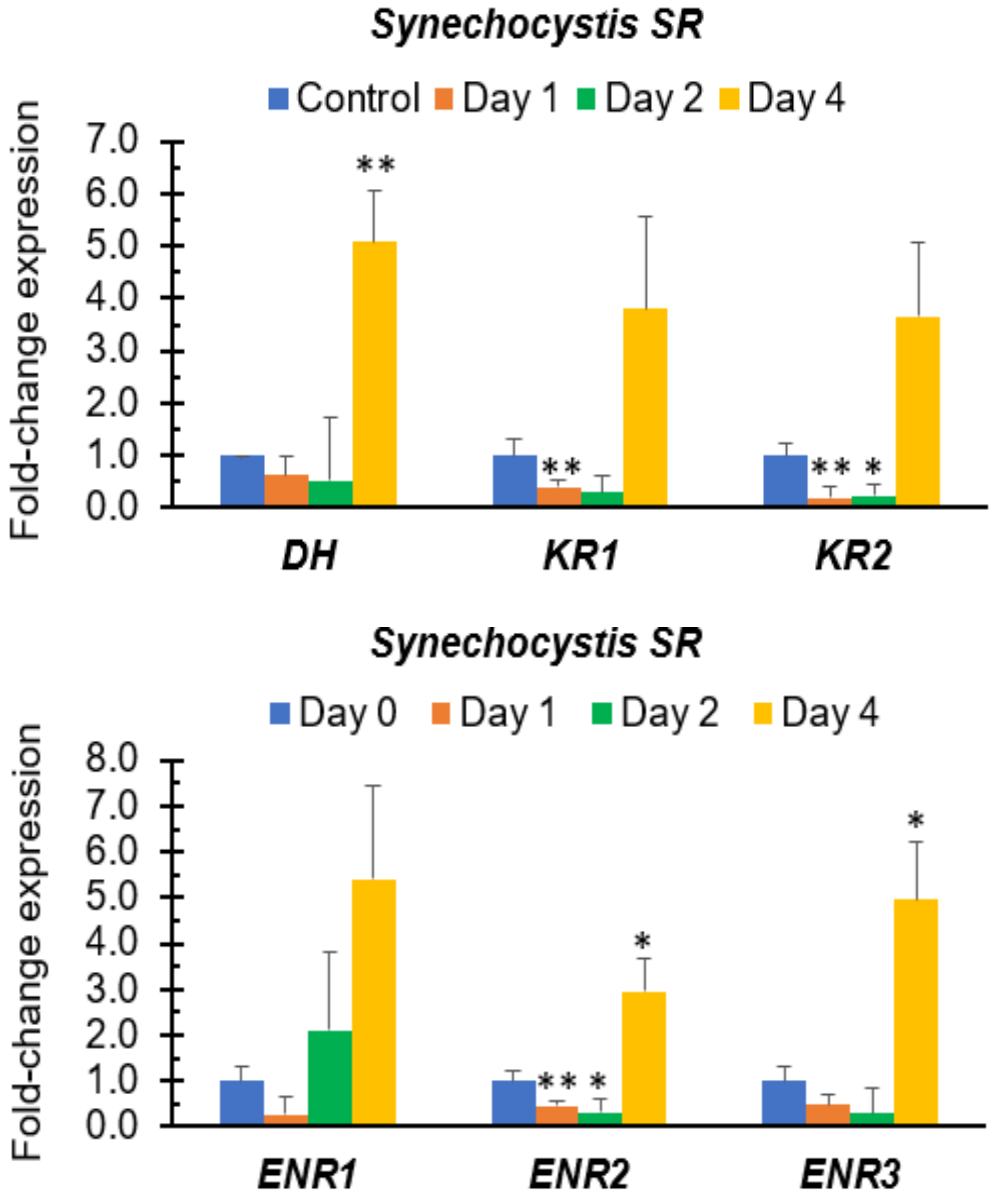

Figure 3.20 Time-course of 6 FAS genes' response to NaCl
Cyanobacterial cultures were treated with 200 mM NaCl under continuous low light (75 µmol.m^{-2}.s^{-1}) and samples harvested at the indicated time-points for RNA extraction. Bars represent mean ± SD (n = 3). Statistically significant differences between control and NaCl-treated cultures are indicated by one ($p \leq 0.05$) or two ($p \leq 0.01$) asterisks.

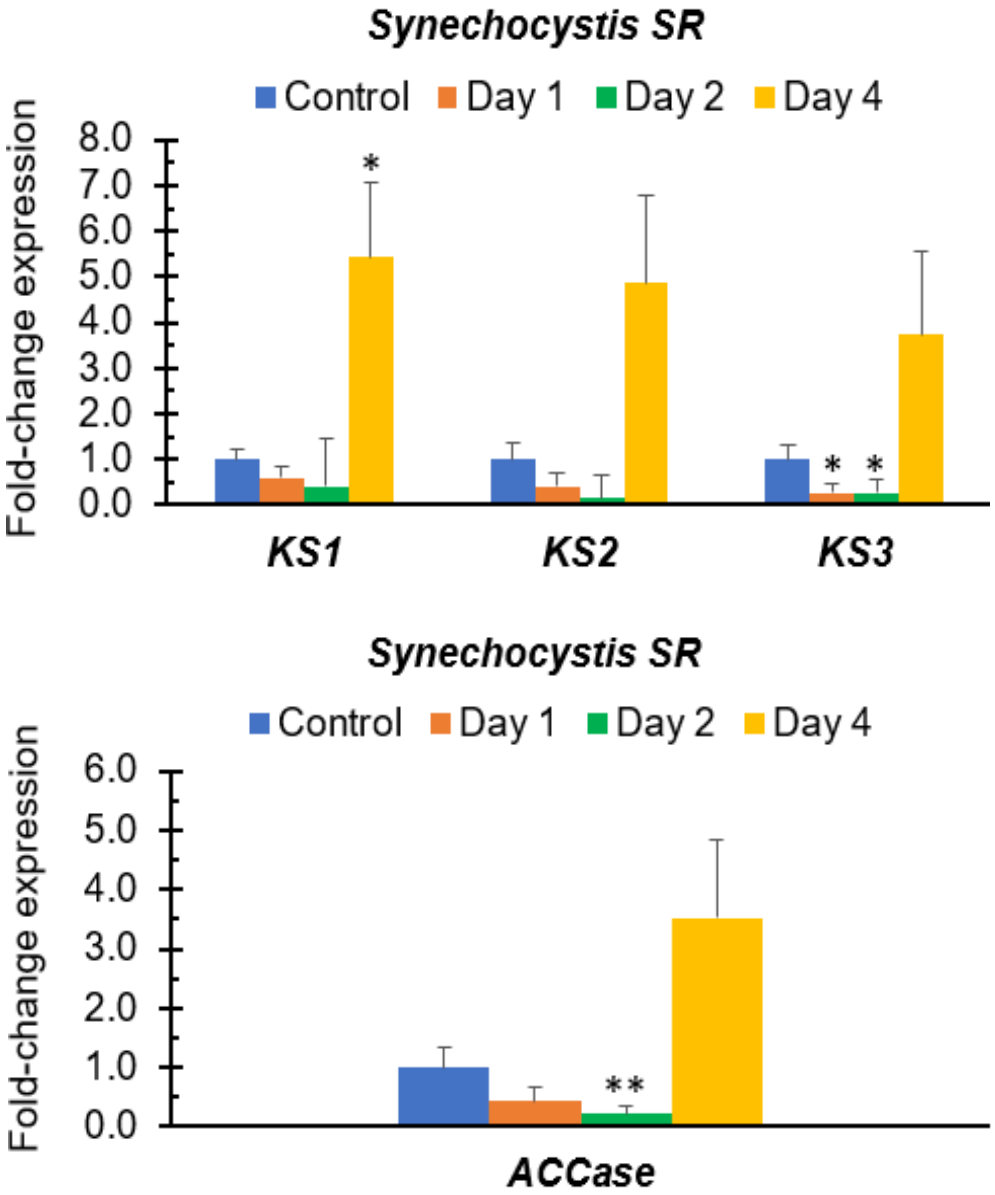

Figure 3.21 Time-course of 4 FAS genes' response to NaCl.
Cyanobacterial cultures were treated with 200 mM NaCl under continuous low light (75 µmol.m^{-2}.s^{-1}) and samples harvested at the indicated time-points for RNA extraction. Bars represent mean ± SD (n = 3). Statistically significant differences between control and NaCl-treated cultures are indicated by one ($p \leq 0.05$) or two ($p \leq 0.01$) asterisks.

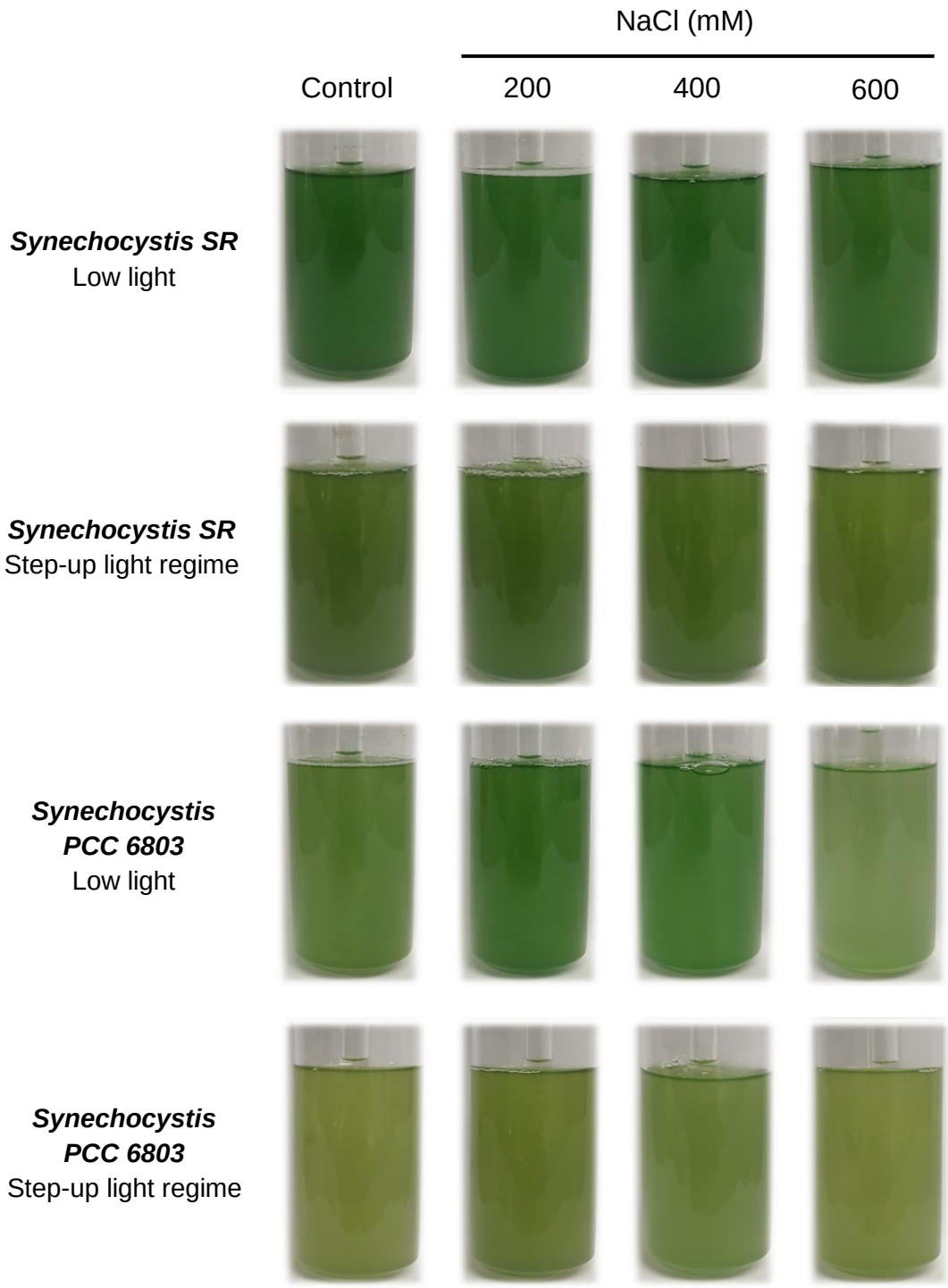

Figure 3.22 Growth of NaCl-treated cyanobacteria under different light regimes.
Cyanobacterial cultures, previously generated by step-down growth, were treated with the indicated amounts of NaCl and incubated for 10 days under either continuous low light (75 µmol.m^{-2}.s^{-1}) or step-up light conditions (7 days at 75 µmol.m^{-2}.s^{-1} followed by 3 days at 150 µmol.m^{-2}.s^{-1}).

3.5 Lipid analyses and quantification

Because NaCl treatment activated FAS gene expression, this prompted an investigation of the effects of salinity stress on fatty acid accumulation. The light conditions that showed the best growth under salinity (Figure 3.16) were adopted for these experiments. *Synechocystis SR* cultures were grown under step-down light conditions to generate sufficient biomass. The cultures were then treated in triplicates with 0, 200, 400, or 600 mM NaCl for 5 days under continuous low light (75 µmol.m^{-2}.s^{-1}). After harvesting the cultures, the fatty acids were derivatised to methyl esters and the Fatty Acid Methyl Esters (FAMEs) analysed by Gas Chromatography–Mass Spectrometry (GC-MS), with C17:00 spiked in all samples as an internal standard. The typical chromatogram obtained from the GC-MS runs is shown in Figure 3.23.

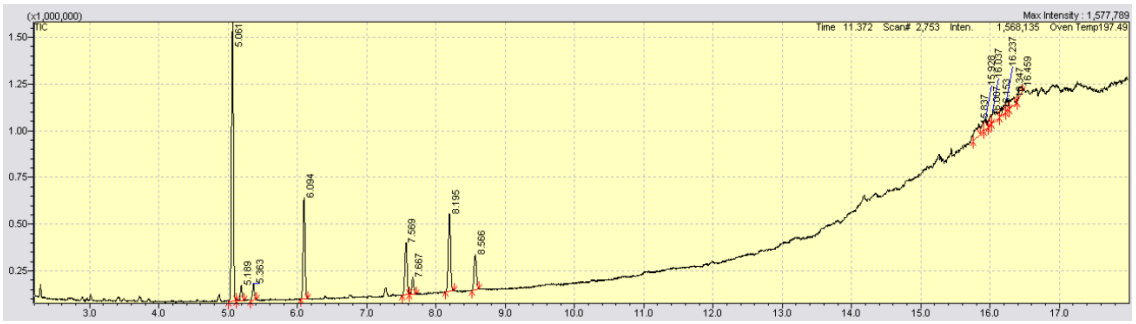

Figure 3.23 A typical chromatogram of cyanobacterial fatty acid methyl esters.
Fatty acid methyl esters were extracted from *Synechocystis SR* cultures and analysed by GC-MS.

The total lipid content of all samples was calculated as a percentage of the cell dry weight. There was a remarkable greater than 2-fold increase in total lipid content in response to salinity stress (Figure 3.24). An interesting observation is that no further statistically significant change in total lipid content existed when NaCl was increases from 200 mM through to 600 mM. In growth assays, it was clear that biomass declined with increasing NaCl concentration (Figure 3.16). The current results show that low levels of NaCl that do not suppress growth can be used to effectively ramp up lipid production to the same levels as extremely high salinity levels. The significance of these results is that use of mild salinity stress

are desirable for increased lipid yields due to activation of the FAS machinery within individual cells as well as enabling heightened biomass production, which allows for very high lipid production.

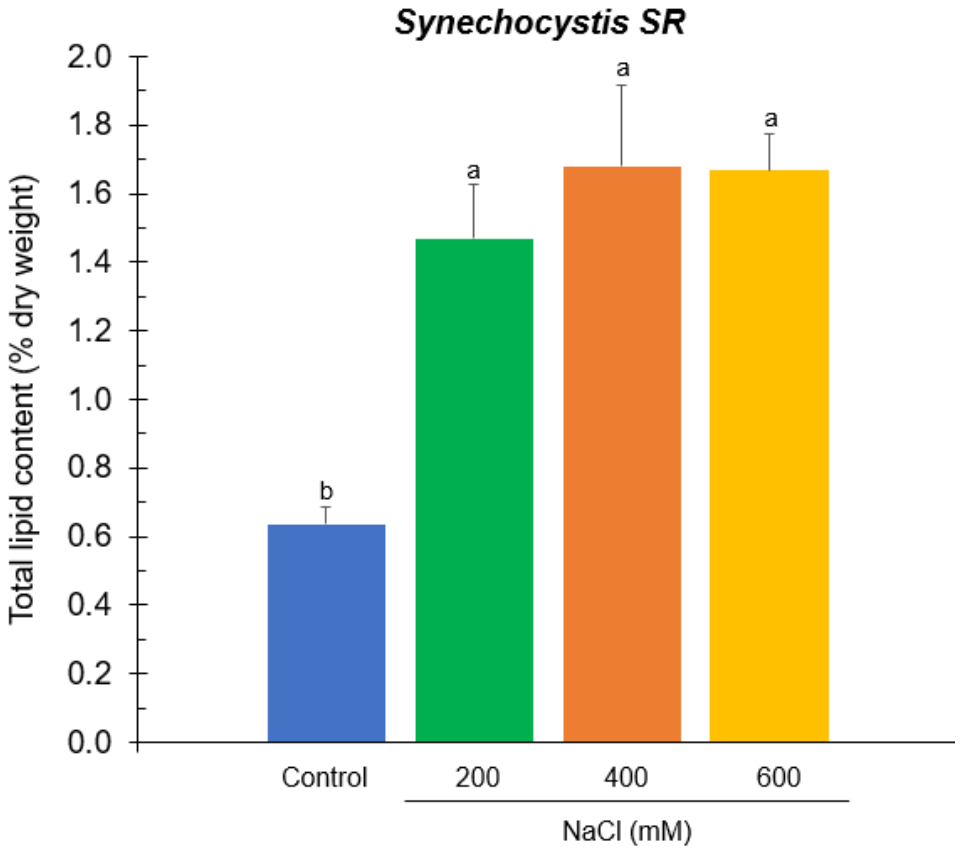

Figure 3.24 Total lipid content of NaCl-treated *Synechocystis SR*.
Cyanobacterial cells were exposed to the indicated levels of NaCl for 5 days under continuous low light (75 µmol.m^{-2}.s^{-1}). Bars represent mean ± SD (n = 3). Bars that share the same letter are not significantly (p > 0.05) different.

The FAME composition of the lipids was determined (Figure 3.25). Table 3.2 provides a list of the major FAMEs putatively detected and considered in the analysis. There were two key observations made from these data. Firstly, although salinity at all NaCl concentrations had increased the total amount of lipid (Figure 3.24), salinity did not change the lipid profile as is evident from Figure 3.25. The profile was exactly the same between the controls and NaCl treatments. Secondly, there were no quantitative differences in the level of

individual FAMEs between the control and NaCl treatments (Figure 3.25). Thus, salinity increases the amount of total lipids, but does not change the proportion of individual FAMEs within the total lipid. This suggests that stress activates a master regulator of the entire FAS pathway and enables higher accumulation of fatty acids within the cells.

Table 3.2 FAMEs detected in *Synechocystis SR* lipids.

FAME	Common name
C16:0	Palmitic acid
C16:1	Palmitoleic acid
C18:0	Stearic acid
C18:1a	Oleic acid
C18:1b	Elaidic acid
C18:2	Linoleic acid
C18:3	Linolenic acid

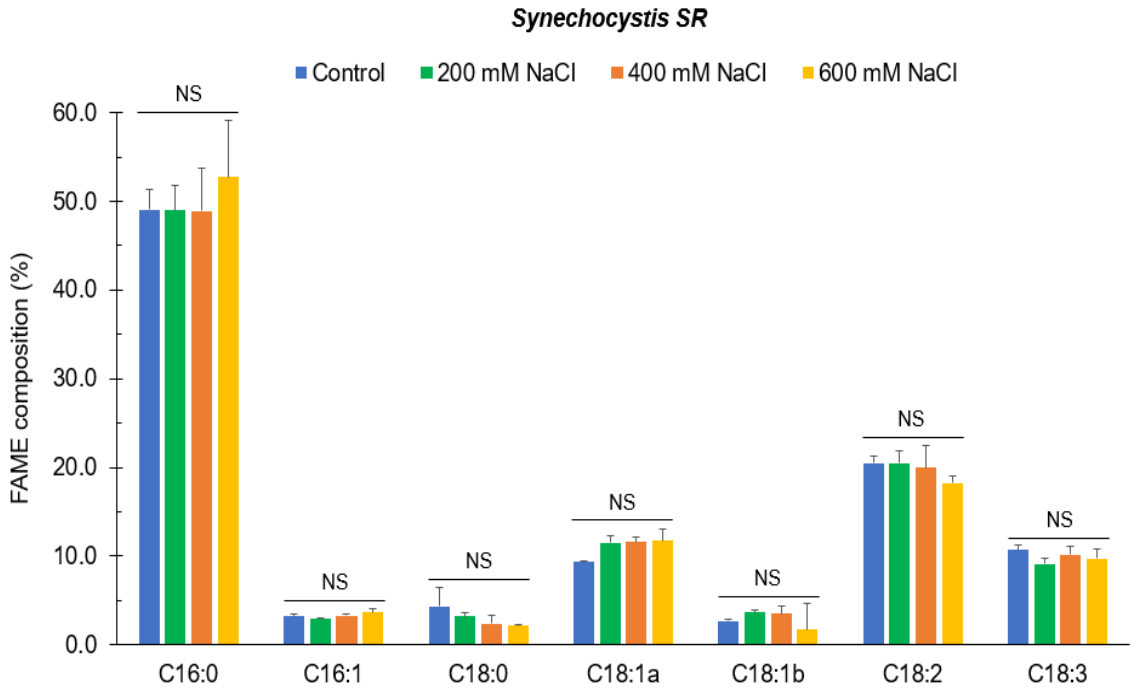

Figure 3.25 FAME content of Synechocystis SR lipids under salinity stress. Cyanobacterial cells were exposed to the indicated levels of NaCl under continuous low light (75 µmol.m-2.s-1). Individual FAME comparisons across different NaCl treatments. Error bars represent mean ± SD (n = 3). NS, represent no significant difference across the indicated averages ($p > 0.05$)

3.6 Protein analyses

Protein samples from control or NaCl-treated *Synechocystis SR* and *Synechocystis PCC 6803* cultures were labelled with iTRAQ tags for quantification of the global proteome response to salinity. The samples were submitted for analysis to the Durham University's Bioscience Proteomics Facility. However, the analysis was not completed in time for inclusion in this thesis. The delay was a result of events beyond anyone's control[1].

[1] An outbreak of COVID-19 impacted millions of people during 2020. Pandemic control measures included total lockdown of the country, which restricted work, study and leisure activities.

4 General Discussion

Cyanobacteria and microalgae are very attractive systems for cheap conversion of waste to valuable industrial products. This derives from their ability to grow in wastewater and rapid solar-powered conversion of atmospheric carbon to biomass. The overall goal of this project was to explore the exploitation of a recently isolated cyanobacterial strain as a source of lipids, which are an important feedstock for the production of renewable energy and manufacturing of diverse industrial products. This required a 2-stage system entailing (i) the growth phase for generation of biomass and (ii) the lipid production phase where cells switch from normal growth metabolism to maximal lipid biosynthesis. For phase 1, different light regimes were considered, while phase 2 focused in biotic and abiotic stress factors to ramp up lipid production.

4.1 Impact of light on cyanobacterial growth

Light intensity is a physical environmental factor that plays an important role in the growth of photosynthetic organisms. Attempts to cultivate both *Synechocystis SR* and *Synechocystis PCC 6803* under continuous high light (150 $\mu mol.m^{-2}.s^{-1}$) for a week or longer led to poor growth, with the resultant cultures characterised by a very low cell density and pale yellow colour indicative of low chlorophyll content. However, better growth was achieved when cells were exposed to combinations of low (75 $\mu mol.m^{-2}.s^{-1}$) and high (150 $\mu mol.m^{-2}.s^{-1}$) light intensity in tandem sequence of low-to-high (named step-up light regime) or high-to-low (named step-down light regime). The highest growth was observed in the step-down light regime.

Light energy is captured by photosynthetic pigment molecules and channelled to photosystem I (PSI) and photosystem II (PSII) reaction centres to initiate electron transfer that drives complex biochemical reactions to produce organic compounds required for growth processes and biomass production. The ATP and NADPH derived from the light-dependent reactions of photosynthesis is then used in the Calvin-Benson cycle to fix CO_2, with key organic molecules from the cycle siphoned by diverse metabolic pathways for synthesis of sugars, lipids, amino acids, and many other building blocks for anabolic processes.

However, the phycobilisomes (the cyanobacterial light-harvesting peripheral-antenna system) usually intercept excess light energy, which exceeds the capacity of the electron transfer system and the rate at which the Calvin-Benson cycle consumes ATP and NADPH. Because the excess energy is not harnessed into generation of ATP and NADPH via the electron transfer system, the excited singlet chlorophyll molecules in the reaction centre are further excited to the triplet state, which can transfer energy to oxygen to produce the damaging singlet oxygen. The highly reactive singlet oxygen causes photo-oxidative damage leading to cell death via peroxidation of membrane lipids and damage to proteins. To prevent photo-oxidative damage, the excess energy can be safely dissipated via non-photochemical quenching (NPQ) processes releasing the excess energy as heat (El Bissati et al., 2000) or diverting the harvested energy away from PSII via the relocation of phycobilisomes from PSII to PSI in a process known as state transition (Bald et al., 1996; Joshua & Mullineaux, 2004). The latter process reduces the quantum yield of photosynthesis.

Therefore, a combination of photo-oxidative damage and state transition reducing the quantum yield of photosynthesis might account for the diminished cyanobacterial growth seen under continuous high light. Cultures grown under step-up light conditions had better growth than cultures in continuous high light. This difference can be explained by the amount of photosynthetic machinery (light-harvesting complexes) produced under these two growth conditions. In Arabidopsis, high light-grown plants possess fewer light-harvesting complexes (and photosystems) than low light-grown plants (Walters & Horton, 1994). Thus, adaptation to the first (low light) phase of a step-up regime possibly enables the cells to accumulate more phycobilisomes and photosystems, which boost photosynthetic yields after transfer to higher light. However, the best growth under step-down conditions was very surprising. In Arabidopsis, plants grown under high light rapidly changed their ratio of chlorophyll *a*/*b* when transferred to low light (Walters & Horton, 1994), suggesting that the high light phase of step-down prepares cells for rapid changes in their photosynthetic machinery to enable them to grow rapidly when high light stress is relieved.

Other researchers using cyanobacteria have reported similar results. For example, Cordara et al. (2018) demonstrated that growth of *Synechocystis* in a photobioreactor increases with increasing light intensity, but plateaus at very high light intensity due to photoinhibition. A study conducted by Bellan et al. (2020) showed optimal growth of the microalga *Nannochloropsis gaditana* at 150 $\mu mol.m^{-2}.s^{-1}$, with reduced proliferation at saturating (1000 $\mu mol.m^{-2}.s^{-1}$) or limiting (10 $\mu mol.m^{-2}.s^{-1}$) light intensities. The same study also reported that NPQ was activated considerably when these cultures were exposed to high light. Dechatiwongse et al. (2014) reported cessation of growth of the cyanobacterium *Cyanothece* sp. ATCC 51142 when light intensity was lowered to 23 $\mu mol.m^{-2}.s^{-1}$. Conversely, photoinhibition curbed cyanobacterial growth at a light intensity of 320 $\mu mol.m^{-2}.s^{-1}$ (Dechatiwongse et al., 2014). In contrast to our findings in this project, Kopečná et al. (2012) reported considerable growth of *Synechocystis* sp. *PCC 6803* at 300 $\mu mol.m^{-2}.s^{-1}$, with inhibition of cell proliferation occurring at 600 $\mu mol.m^{-2}.s^{-1}$. The differences are likely attributable to differences in aeration strategy - Kopečná et al. (2012) used orbital shaking for aeration, while in my project compressed air was bubbled into the cultures.

Previous experiments have been conducted using a series of independent cultures set at specific light intensities over a broad range of values. However, our approach was to combine more than one light intensity sequentially on the same culture vessel. More elaborate versions of our approach have been adopted and termed the photonfluxostat strategy (Du et al., 2016). In this strategy, a dynamic adjustment of the incident light intensity is applied, being sequentially increased with increases in cell density to maintain a nearly constant irradiance in the culture. This avoids reaching levels that could trigger photoinhibition, thus maintaining a steady-state exponential growth with no light limitation. Appropriate control software (Kroon et al., 1992) and photobioreactors (Melnicki et al., 2013) software (Kroon et al., 1992) to implement the photonfluxostat strategy have been developed. However, though the step-down light regime used in this project is counterintuitive, it resulted in the best growth rates and differs from what has been used by others in the reported literature.

4.2 Impact of biotic and abiotic stress on cyanobacterial growth

After biomass production had been optimised, the next stage of the project was to develop an operational switch to turn on lipid production. The focus was on identifying stress factors that could trigger activation of the cyanobacterial lipid biosynthetic pathway. The first biotic stress examined was application of the mycotoxin fumonisin B1 (FB1), which has been extensively used by our research group to activate stress responses in Arabidopsis cell suspension cultures (Chivasa et al., 2005; Chivasa et al., 2013; Smith et al., 2015). While FB1 treatment killed Arabidopsis cells as previously reported (Chivasa et al., 2005), the mycotoxin killed neither algal (*Chlamydomonas reinhardtii*) nor the photosynthetic prokaryotic (*Synechocystis SR, Synechocystis PCC 6803*) cells, even when applied at very high concentrations. This indicated that FB1 treatment is incapable of stressing these organisms and, therefore, unlikely to trigger stress-induced lipid production. While FB1 was not useful for this project, these FB1-insensitive photosynthetic organisms might be useful research tools in understanding why photosynthetic land plants are susceptible to the mycotoxin.

FB1 is a mycotoxin mainly produced by the fungus *Fusarium verticillioides* and it activates cell death in several plant and animal species, including Arabidopsis (Stone et al., 2000) tomato (*Solanum lycopersicum*) (Abbas et al., 2000), corn (*Zea mays*), horse (*Equus caballus*), mouse (*Mus musculus*) and rat (*Rattus norvegicus)* (Soriano et al., 2005; Riley & Merrill Jr, 2019). One known mechanism of cell death activation is inhibition of ceramide synthase, which disrupts sphingolipid biosynthesis. Concurrent treatment of cells with FB1 and addition of ceramide prevents cell death (Bostock et al., 2001), confirming that ceramide depletion is the trigger for cell death.

Although the reason for the lack of response to FB1 in *C. reinhardtii* and the cyanobacterial strains is unclear, an important clue lies in the putative ceramide synthase sequences. Alignments of ceramide synthase protein sequences of Arabidopsis, tomato, horse, mouse, and shows a high sequence identity between 97-100%, accounting for their binding to FB1. In contrast, attempts to identify homologues of Arabidopsis ceramide synthase in the cyanobacterial strains and *C. reinhardtii* using homology searches did not yield any candidates. This could

be an indication of sequence divergence or the absence of the sphingolipid pathway in these organisms. If it is the former, then sequence divergence could be the reason for failure of FB1 to bind to the homologues and activate cell death.

Attention was then turned to salinity stress using NaCl. There were 3 key observations made on the impact of the interaction of salinity stress and light on cyanobacteria. First, growth was completely inhibited when cyanobacterial inoculum was added to BG-11 medium spiked with NaCl and incubated under continuous high light. Second, if the inoculated NaCl-treated BG-11 medium was incubated under a step-up light regime (4 days low light followed by 3 days high light) the cyanobacteria survived and the cultures multiplied under high salinity. Third, growing the cultures under normal step-down conditions first, followed by exposing the cells to salinity stress under continuous low light were the best conditions to obtain the maximum amount of biomass metabolically activated by NaCl.

These results are accounted for by the altered behaviour of major components of the photosynthetic machinery under salinity stress. Phycobilisomes are light-harvesting mobile structures located in thylakoids. Their mobility in response to changing levels of illumination enables them to safely dissipate excess energy through the state transition mechanism. Conversely, photosystem complexes are stationary and their union with phycobilisomes is transitory. Under optimal growth conditions in cyanobacteria, association of phycobilisomes with PSII and PSI is required for energy exchange and photosynthetic productivity. Under excess light, the phycobilisome complexes with mostly PSII (as well as PSI) is broken to allow for dissipation of excess energy through state transition. However, in cyanobacteria exposed to osmotic stress, these phycobilisome-photosystem complexes are rigidly fixed due to reduced mobility of phycobilisomes, inherently limiting the reaction of state transition processes (Joshua & Mullineaux, 2004). In fact, attachment of phycobilisomes to reaction centres of photosystems is strengthened by increasing salt concentration (Joshua & Mullineaux, 2004). The mechanism of phycobilisome immobilisation is not fully understood, but it has been postulated that salt molecules “capture” available water molecules, thereby limiting the aqueous environment in which phycobilisomes can easily translocate

(Joshua & Mullineaux, 2004). Because of this effect of salinity on phycobilisomes' physical interactions with photosystem reaction centres, cyanobacteria under salinity stress become vulnerable to photodamage under high light.

Thus, the failure of S*ynechocystis SR* or *Synechocystis PCC 6803* inoculum to grow under salinity stress when incubated in continuous strong illumination can be accounted for by photodamage arising from inhibition of the protective state transition mechanism. On the contrary, when similar inoculated BG-11 medium containing salt was incubated under step-up conditions (4 days low light followed by 3 days high light), the cultures grew. During the initial phase of low light, the cells did not contend with excess light and so had no requirement for state transition, resulting in growth. When the cells were moved to the high light phase, they kept on growing even though they were exposed to strong illumination. The question arising from this is why did the cells continue to grow under prohibitive high light and high salinity conditions? Two possible explanations may account for this observation. First, it is possible that during the low light growth phase, adaptive molecular responses are switched on to maintain ion homeostasis, such as activation of membrane transporter proteins conferring resistance to salt stress. A second possibility is that the culture cell density attained under low light growth is sufficient to decrease the amount of light harvested by a single cell to below a threshold causing photodamage. A combination of the two is also possible.

In terms of acclimation to salinity stress, a role for cyanobacterial Na^+/H^+ antiporter (Tsunekawa et al., 2009), Na^+-pumping ATPase (Soontharapirakkul et al., 2011), and Mrp-system (Blanco-Rivero et al., 2005) has been proposed. These membrane pumps are thought to efflux damaging sodium ions from the cells to protect from salt stress. Other mechanisms include synthesis of compatible solutes such as glycine betaine, sucrose, trehalose, and glucosylglycerol. For example, *Synechocystis PCC 6803* has been reported to accumulate glucosylglycerol to survive under salt stress (Klähn & Hagemann, 2011). Thus, exposure to salinity stress under low light likely enabled activation of these and more adaptive responses, which managed to maintain ion

homeostasis to an extent that high light ceased to be damaging when the cultures were eventually transferred to these conditions.

Finally, the conditions least affecting S*ynechocystis SR* and *Synechocystis PCC 6803* were initial growth under step-down light regime in the absence of salt followed by salinity treatment at continuous low light. These conditions generated the highest treated biomass used for subsequent experiments. Under these conditions, S*ynechocystis SR* performed much better than *Synechocystis PCC 6803*, consistent with previous reports that the former has superior stress resilience than other cyanobacterial species (Abedi et al., 2019b). The reason for better biomass yield performance under these conditions is the absence of excess light and the most likely activation of molecular and biochemical stress-adaptive responses as discussed above.

4.3 Salinity-induced transcriptional activation of fatty acid biosynthesis

One of the central objectives of this research project was to boost the lipid biosynthetic pathway in *Synechocystis SR* after applying NaCl stress treatments. The nucleotide sequences of putative genes in the pathway were initially acquired by database searches of the model organism *E. coli*, with the cyanobacterial homologues identified by BLAST-searching the reference database of *Synechocystis PCC 6803*. A total of 10 putative cyanobacterial fatty acid synthesis (FAS) genes were thus identified, viz. *DH, KR1, KR2, ENR1, ENR2, ENR3, KS1, KS2, KS3* and *ACCase*. Results showed that all the FAS genes were up-regulated when the cells were exposed to salinity stress, with the response consistently stronger in *Synechocystis SR* than *Synechocystis PCC 6803*. In accordance with the gene expression data, GC-MS analysis of fatty acid methyl esters (FAMEs) revealed a 2-fold increase in cyanobacteria cultures exposed to salinity stress. The increase in total lipid was not associated with any change of the FAME profile, in agreement with the gene expression data showing that the entirety of the FAS pathway was activated by NaCl.

In addition to increased membrane pump activity for ion homeostasis, and compatible solutes for protection of macromolecules, cyanobacterial cells

exposed to salinity stress are known to activate central metabolic pathways, such as glycolysis, oxidative pentose phosphate pathway, the Calvin-Benson cycle and the tricarboxylic acid cycle (reviewed by Cui et al., 2020). Salinity also increases lipid biosynthesis and accumulation in cyanobacteria. For example, salt treatments activate fatty acid production in the microalgae *Scenedesmus vacuolatus* (Anand et al. (2019) and *Chlorella vulgaris* (Church et al. (2017). Atikij et al. (2019) showed that the unicellular alga *Chlamydomonas reinhardtii* (137C) increased lipid production in response to different salts. They found that activation of lipid production peaked after 5 days' growth in 200 mM KCl or after 7 days of growth in 250 mM NaCl. The highest lipid accumulation across all salt treatments evaluated was seen in cells grown in 120 mM LiCl.

In *Synechocystis 7942* total lipid production is activated by salt stress, with the increase registered for mono-unsaturated fatty acids despite the decrease on saturated fatty acids (Verma et al., 2019). Unsaturated fatty acids have a lower melting point and might increase membrane fluidity under salt stress, perhaps being a mitigating response to alleviate mobility of crucial proteins (e.g., phycobilisomes during state transition) and passage of key solutes across membranes.

These results raise two important questions that have not yet been addressed in this field. First, why and how does stress (including high salinity) activate lipid production? A plausible hypothesis relates to the metabolic connection between photosynthesis and the major primary metabolic pathways, such as carbohydrate, amino acid, and nucleic acid synthesis. Abiotic stresses, such as salinity and low/high temperature, appear not to have a single specific cellular target, but rather affect numerous primary pathways. As a result, there is often a general slowdown in cellular metabolism associated with abiotic stresses. A particular problem for photosynthetic organisms is that light-harvesting continues under stress, creating the problem of photodamage (as explained in section 4.1). The primary metabolic pathways responsible for synthesis of building blocks withdraw molecules from the Calvin-Benson cycle. If stress reduces flow of metabolites from the Calvin-Benson cycle, then the products of the photosynthetic light reactions (ATP, NADPH) will accumulate. This will lead to

over reduction of reaction centre chlorophylls and generation of the undesirable superoxide radicals and other cell-damaging reactive oxygen species. We speculate that to avert reactive oxygen species-dependent cell damage, lipid production is activated as a metabolic sink of (solar) energy. A corollary to this is that the fatty acid metabolic pathway has relatively low sensitivity to salinity stress.

While the reason for cyanobacterial activation of lipid production under stress can be explained by the hypotheses above, the mechanism by which this occurs is unclear. Our results revealed direct transcriptional activation of all genes in the fatty acid synthesis pathway. Similarly, a study by Kumar et al. (2017) revealed that nutrient (N and P) limitation stress activates *ACCase* expression, the gene for the commitment step in the fatty acid biosynthesis pathway. Stress-induced *ACCase* expression was attended by increased lipid accumulation (Kumar et al., 2017). Recent studies have implicated the transcription regulator LexA as playing a key role in transcriptional regulation of *Synechocystis PCC 6803* fatty acid synthesis genes. LexA is a transcriptional repressor that binds to the promoter/enhancer sequences of fatty acid synthesis genes (Kizawa et al., 2017). Loss-of-function mutants lacking a functional LexA gene express higher levels of fatty acid synthesis genes and accumulate more fatty acids under normal conditions and nutrient-limitation (N, P) stress in comparison with wildtype cells (Kizawa et al., 2017). De-repression of salt-inducible genes in *PCC 6803* appears to be controlled via dephosphorylation of LexA at serine-173 within an hour of NaCl treatment (Takashima et al., 2020). The identity of the responsible phosphatase and how salt activates this dephosphorylation remains unclear.

However, in bacteria such as *Escherichia coli*, LexA is an important regulator of the so-called SOS response to DNA damage. Under normal growth conditions (in the absence of stress), *E. coli* LexA binds the SOS regulon promoter and to promoter sequences of genes encoding proteins that drive DNA repair and replication, and cell division genes (Fernández de Henestrosa et al., 2000; Courcelle et al., 2001; Wade et al., 2005). When cellular DNA is damaged, the SOS response is activated to abolish this LexA-mediated suppression of target gene expression. This starts when RecA binds to single-stranded DNA stretches

at the damage sites. RecA binds to LexA and changes its conformation, which triggers self-cleavage between Ala^{84}-Gly^{85} by the catalytic duo Ser^{119} and Lys^{156}, thus abolishing repression of the SOS regulon (Horii et al., 1981; Slilaty & Little, 1987; Luo et al., 2001).

The second question arising from our results is – what is the physiological significance of stress-induced lipid production to cyanobacteria? Why do the cells choose lipid as an energy sink instead of carbohydrates or amino acids/protein as a mechanism for avoiding photodamage under salt stress? Again, this question has not been addressed through research. A possible hypothesis is that it is quite possible that a progressive increase in stress could end up shutting down photosynthesis when the stress reaches its maximal level. Thus, switching to lipid accumulation during the sub-lethal stress levels could help the organism store much needed energy-dense lipids for use in keeping alive during the extreme stress or on exit from the stress. Protein and carbohydrates have relatively less energy per unit mass, hence lipid is the preferred storage molecule. This hypothesis could be tested by comparative study of stress survival between high and low oil-accumulating species.

4.4 *Synechocystis SR* and *Synechocystis PCC 6803* are different strains

Synechocystis SR and *Synechocystis PCC 6803* were indistinguishable when examined under the microscope. Although the genome of *Synechocystis SR* has not yet been sequenced, amplicons of housekeeping and FAS genes PCR-amplified from cDNA of this strain with primers designed for *Synechocystis PCC 6803* gave the expected size, suggesting no major sequence divergence between the strains. However, the two strains were distinguishable when examined at the metabolic level or in their response to external stimulation (FB1 and NaCl).

First, an assay of cell metabolic activity using the MTT reagent revealed very different cellular metabolic responses between *Synechocystis SR* and *Synechocystis PCC 6803* before and after treatment with the FB1 mycotoxin. Second, differences between the ultrastructure of *Synechocystis SR* and

Synechocystis PCC 6803 after NaCl treatment were observed by transmission electron microscopy. Third, the growth response profile of *Synechocystis SR* and *Synechocystis PCC 6803* was different when both strains were exposed to salinity stress. *Synechocystis SR* was more tolerant to salt stress than *Synechocystis PCC 6803*. Fourth, the gene expression kinetic profile of all FAS genes across the NaCl concentrations was different between these two cyanobacteria. *Synechocystis SR* showed higher gene expression than *Synechocystis PCC 6803*. Overall, these properties reveal that *Synechocystis SR* and *Synechocystis PCC 6803* are distinct strains.

4.5 Conclusions and proposed industrial exploitation of *Synechocystis SR*

The potential for using algae and blue-green algae as bio-factories for the production of important industrial products requires an understanding of the underpinning biology. Lipid is a very important bio-product that can be converted to valuable industrial chemicals, renewable energy, beauty products, etc. It has been known that stress-adaptive responses of algae and blue-green algae includes heightened production of lipids. With the discovery of a stress-resilient strain of *Synechocystis SR* (Abedi et al., 2019b), we wanted to explore the possibility of using this organism in lipid production for industrial applications. Our study has identified salinity stress as an elicitor of transcriptional activation of the entire fatty acid synthesis pathway in *Synechocystis SR*, triggering a 2-fold accumulation of lipid. Light was identified as a critical factor that determines how the growth and yield performance in the presence of salinity stress. Implementation of the experimentally developed growing conditions will require adaptation for industrial-scale production using different systems, such as photobioreactors (PBRs), raceway ponds, or different versions of open ponds.

The remarkable ability of *Synechocystis SR* to withstand stress and grow in wastewaters where other cyanobacterial strains fail to grow combined with its stress-adaptive response to salinity that is characterised by improved lipid production provides a unique opportunity for industrial exploitation. Figure 4.1 represents a possible route we envisage as a lipid production workflow. The workflow has 3 separate phases:

1. Biomass Production (Phase 1) - To begin with, *Synechocystis SR* is inoculated into mineral-rich wastewater. Depending on the type of waste stream, the lighting will have to be carefully controlled to prevent constriction of growth due to excessive light-harvesting. Previous data has demonstrated that this strain is resilient and can withstand growth-inhibiting conditions. We also showed that toxins that would kill other organisms, such as FB1, may lead to better growth of the cyanobacterial cells. Cyanobacterial growth on waste effluent contributes to reduction of production costs and efforts to protect the environment and conservation of fresh water resources.

2. Lipid Production (Phase 2) - The biomass from Phase 1 is then transferred to another chamber/compartment with seawater to simulate the levels of experimentally verified NaCl required to activate lipid synthesis. Control of light during exposure to salts is critical. Lower levels are required, leading to energy savings if PBR systems are being used. Where direct solar energy is in use, shading the PBRs with cloth netting that partially blocks the light can be an option. This ensures that energy is not wasted via diversion of metabolites to photoprotection. Maximum lipid yield is achievable if light is tightly controlled. Seawater is a cheap and abundant resource, making this process cost-effective.

3. Biomass Harvesting & Lipid Extraction (Phase 3) – The biomass is then harvested and lipid extracted from either fresh or dried material. Depending on the final use, total lipid can be extracted without purification, or more sophisticated processes to isolate specific fatty acids can be deployed. For example, palmitic and linoleic acid can be enriched for to generate raw materials for the manufacture of diverse products, such as food additives, preservatives, cosmetics, and lubricants.

The cyanobacterial residue (biomass) can be used as feedstock in anaerobic digesters for methane production. The methane can be used at the factory to defray the costs of energy for the entire process. The final waste (anaerobic digestate) obtained from the biodigesters can be used as a nutrient-rich fertilizer (Dimambro, 2015).

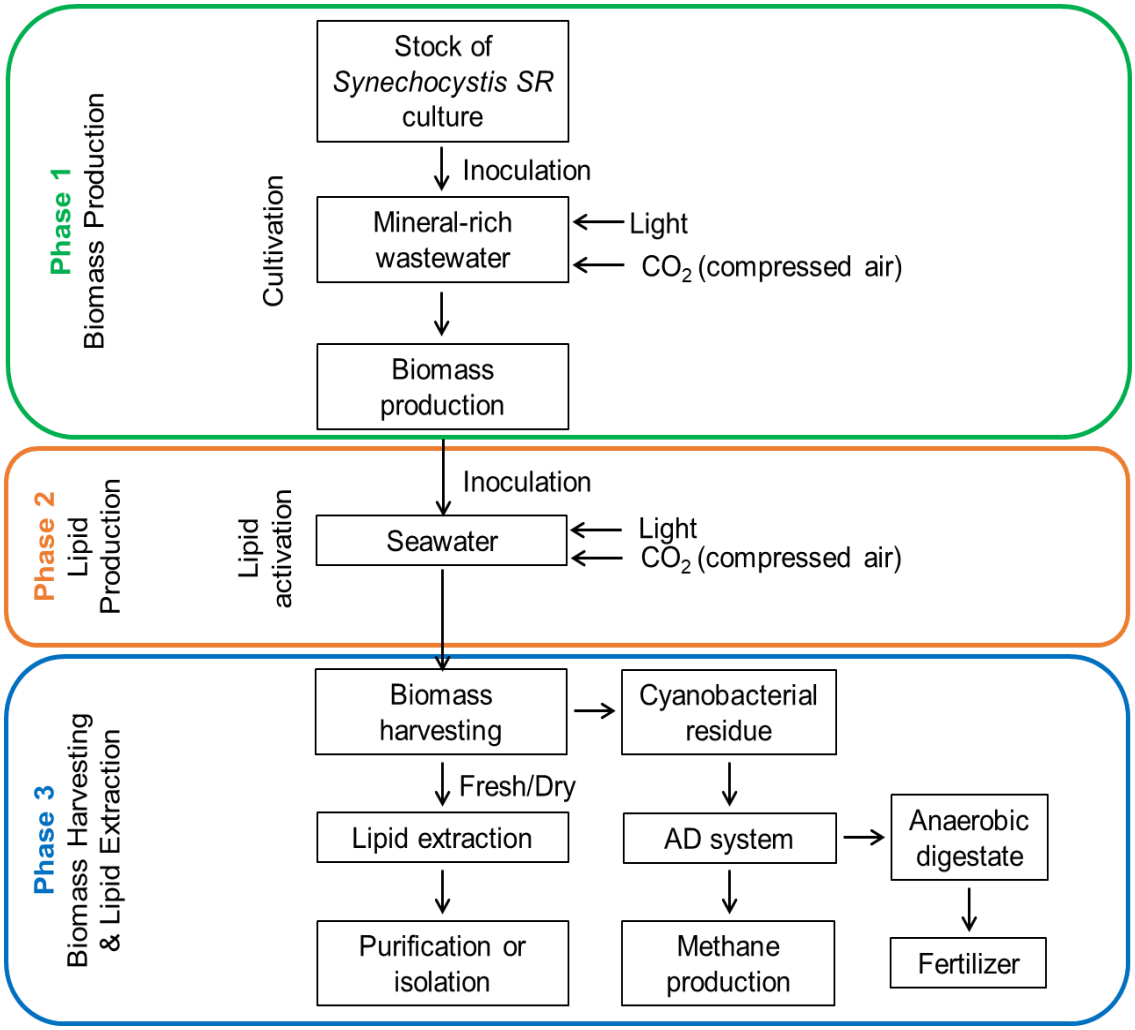

Figure 4.1 Proposed diagram for biomass and lipid production.

In phase 1, *Synechocystis SR* is inoculated in mineral-rich wastewater in order to generate biomass. This is transferred to seawater where lipids production is activated by salinity stress (phase 2). Finally in phase 3, lipids extracted are ready for purification or isolation, while cyanobacterial residue can be used as an additive to anaerobic digestion (AD) systems for boosting methane production. The digestate generated could be used as a bio-fertilizer.

4.6 Future research

Further work is needed to develop deeper and better understanding of *Synechocystis SR* and its potential utility in industrial applications. While the use of NaCl in activating lipid production has been demonstrated here, the response of the FAS pathway genes to seawater will be needed. This should be complemented by GC-MS analysis to measure the accumulation of fatty acids. Furthermore, the impact of salinity stress on the entire proteome was not completed in this study. Examining the global proteomic responses, beyond the FAS pathway, is likely to provide clearer understanding of the basis for stress resilience in *Synechocystis SR*.

5 References

Abbas, H., Smeda, R., Gerwick, B., & Shier, W. T. (2000). Fumonisin B1 from the fungus Fusarium moniliforme causes contact toxicity in plants: evidence from studies with biosynthetically labeled toxin. *Journal of natural toxins, 9*(1), 85-100.

Abedi, S., Astaraei, F. R., Ghobadian, B., Tavakoli, O., Jalili, H., Chivasa, S., & Greenwell, H. C. (2019). Bioenergy production using Trichormus variabilis–a review. *Biofuels, Bioproducts and Biorefining, 13*(5), 1365-1382.

Abedi, S., Astaraei, F. R., Ghobadian, B., Tavakoli, O., Jalili, H., Greenwell, H. C., Cummins, I., & Chivasa, S. (2019). Decoupling a novel Trichormus variabilis-Synechocystis sp. interaction to boost phycoremediation. *Scientific reports, 9*(1), 1-10.

Abomohra, A., Wagner, M., El-Sheekh, M., & Hanelt, D. (2013). Lipid and total fatty acid productivity in photoautotrophic fresh water microalgae: screening studies towards biodiesel production. *Journal of Applied Phycology, 25*(4), 931-936. https://doi.org/10.1007/s10811-012-9917-y

Amha, Y. M., Sinha, P., Lagman, J., Gregori, M., & Smith, A. L. (2017). Elucidating microbial community adaptation to anaerobic co-digestion of fats, oils, and grease and food waste. *Water research, 123*, 277-289.

Anand, V., Kashyap, M., Samadhiya, K., Ghosh, A., & Kiran, B. (2019). Salinity driven stress to enhance lipid production in Scenedesmus vacuolatus: A biodiesel trigger? *Biomass and Bioenergy, 127*, 105252.

Anto, S., Mukherjee, S. S., Muthappa, R., Mathimani, T., Deviram, G., Kumar, S. S., Verma, T. N., & Pugazhendhi, A. (2019). Algae as green energy reserve: Technological outlook on biofuel production. *Chemosphere, 242*, 125079.

Atikij, T., Syaputri, Y., Iwahashi, H., Praneenararat, T., Sirisattha, S., Kageyama, H., & Waditee-Sirisattha, R. (2019). Enhanced lipid production and molecular dynamics under salinity stress in green microalga Chlamydomonas reinhardtii (137C). *Marine drugs, 17*(8), 484.

Bald, D., Kruip, J., & Rögner, M. (1996). Supramolecular architecture of cyanobacterial thylakoid membranes: how is the phycobilisome connected with the photosystems? *Photosynthesis research, 49*(2), 103-118.

Batista, A. P., Ambrosano, L., Graça, S., Sousa, C., Marques, P. A. S. S., Ribeiro, B., Botrel, E. P., Castro Neto, P., & Gouveia, L. (2015). Combining urban wastewater treatment with biohydrogen production – An integrated

microalgae- based approach. *Bioresource Technology, 184*, 230-235. https://doi.org/10.1016/j.biortech.2014.10.064

Bellan, A., Bucci, F., Perin, G., Alboresi, A., & Morosinotto, T. (2020). Photosynthesis regulation in response to fluctuating light in the secondary endosymbiont alga Nannochloropsis gaditana. *Plant and Cell Physiology, 61*(1), 41-52.

Blacutt, A. A., Gold, S. E., Voss, K. A., Gao, M., & Glenn, A. E. (2018). Fusarium verticillioides: Advancements in understanding the toxicity, virulence, and niche adaptations of a model mycotoxigenic pathogen of maize. *Phytopathology, 108*(3), 312-326.

Blanco-Rivero, A., Leganes, F., Fernandez-Valiente, E., Calle, P., & Fernandez-Pinas, F. (2005). mrpA, a gene with roles in resistance to Na+ and adaptation to alkaline pH in the cyanobacterium Anabaena sp. PCC7120. *Microbiology, 151*(5), 1671-1682.

Blatti, J. L., Michaud, J., & Burkart, M. D. (2013). Engineering fatty acid biosynthesis in microalgae for sustainable biodiesel. *Current Opinion in Chemical Biology, 17*(3), 496-505. https://doi.org/10.1016/j.cbpa.2013.04.007

Bligh, E. G., & Dyer, W. J. (1959). A rapid method of total lipid extraction and purification. *Canadian journal of biochemistry and physiology, 37*(8), 911-917.

Bostock, R. M., Karban, R., Thaler, J. S., Weyman, P. D., & Gilchrist, D. (2001). Signal interactions in induced resistance to pathogens and insect herbivores. *European Journal of Plant Pathology, 107*(1), 103-111.

BP, B. P. (2018). *Statistical Review of World Energy*. https://www.bp.com/content/dam/bp/business-sites/en/global/corporate/pdfs/energy-economics/statistical-review/bp-stats-review-2018-full-report.pdf

Bradford, M. M. (1976). A rapid and sensitive method for the quantitation of microgram quantities of protein utilizing the principle of protein-dye binding. *Analytical biochemistry, 72*(1-2), 248-254.

Caporgno, M. P., Trobajo, R., Caiola, N., Ibáñez, C., Fabregat, A., & Bengoa, C. (2015). Biogas production from sewage sludge and microalgae co-digestion under mesophilic and thermophilic conditions. *Renewable Energy, 75*(C), 374-380. https://doi.org/10.1016/j.renene.2014.10.019

Chivasa, S., Ndimba, B. K., Simon, W. J., Lindsey, K., & Slabas, A. R. (2005). Extracellular ATP functions as an endogenous external metabolite regulating plant cell viability. *The Plant Cell, 17*(11), 3019-3034.

Chivasa, S., Tomé, D. F., & Slabas, A. R. (2013). UDP-glucose pyrophosphorylase is a novel plant cell death regulator. *Journal of proteome research, 12*(4), 1743-1753.

Church, J., Hwang, J.-H., Kim, K.-T., McLean, R., Oh, Y.-K., Nam, B., Joo, J. C., & Lee, W. H. (2017). Effect of salt type and concentration on the growth and lipid content of Chlorella vulgaris in synthetic saline wastewater for biofuel production. *Bioresource Technology, 243*, 147-153.

Cordara, A., Re, A., Pagliano, C., Van Alphen, P., Pirone, R., Saracco, G., dos Santos, F. B., Hellingwerf, K., & Vasile, N. (2018). Analysis of the light intensity dependence of the growth of Synechocystis and of the light distribution in a photobioreactor energized by 635 nm light. *PeerJ, 6*, e5256.

Courcelle, J., Khodursky, A., Peter, B., Brown, P. O., & Hanawalt, P. C. (2001). Comparative gene expression profiles following UV exposure in wild-type and SOS-deficient Escherichia coli. *Genetics, 158*(1), 41-64.

Crabtree, G. W., & Lewis, N. S. (2007). Solar energy conversion. *Physics Today, 60*(3), 37-42.

Cui, J., Sun, T., Chen, L., & Zhang, W. (2020). Engineering salt tolerance of photosynthetic cyanobacteria for seawater utilization. *Biotechnology advances*, 107578.

Dechatiwongse, P., Srisamai, S., Maitland, G., & Hellgardt, K. (2014). Effects of light and temperature on the photoautotrophic growth and photoinhibition of nitrogen-fixing cyanobacterium Cyanothece sp. ATCC 51142. *Algal Research, 5*, 103-111.

Dimambro, M. (2015). Novel uses for digestates: Protected horticulture. 20th European Biosolids & Organic Resources Conference & Exhibition. Manchester,

Du, W., Jongbloets, J. A., Hernández, H. P., Bruggeman, F. J., Hellingwerf, K. J., & dos Santos, F. B. (2016). Photonfluxostat: a method for light-limited batch cultivation of cyanobacteria at different, yet constant, growth rates. *Algal Research, 20*, 118-125.

Ehimen, E. A., Sun, Z. F., Carrington, C. G., Birch, E. J., & Eaton-Rye, J. J. (2011). Anaerobic digestion of microalgae residues resulting from the biodiesel production process. *Applied Energy, 88*(10), 3454-3463. https://doi.org/10.1016/j.apenergy.2010.10.020

El Bissati, K., Delphin, E., Murata, N., Etienne, A.-L., & Kirilovsky, D. (2000). Photosystem II fluorescence quenching in the cyanobacterium Synechocystis

PCC 6803: involvement of two different mechanisms. *Biochimica et Biophysica Acta (BBA)-Bioenergetics, 1457*(3), 229-242.

Fernández de Henestrosa, A. R., Ogi, T., Aoyagi, S., Chafin, D., Hayes, J. J., Ohmori, H., & Woodgate, R. (2000). Identification of additional genes belonging to the LexA regulon in Escherichia coli. *Molecular microbiology, 35*(6), 1560-1572.

Ferreira, A. F., Marques, A. C., Batista, A. P., Marques, P. A., Gouveia, L., & Silva, C. M. (2012). Biological hydrogen production by Anabaena sp.–yield, energy and CO2 analysis including fermentative biomass recovery. *International Journal of Hydrogen Energy, 37*(1), 179-190.

Fradique, M., Batista, A. P., Nunes, M. C., Gouveia, L., Bandarra, N. M., & Raymundo, A. (2010). Incorporation of Chlorella vulgaris and Spirulina maxima biomass in pasta products. Part 1: Preparation and evaluation. *Journal of the Science of Food and Agriculture, 90*(10), 1656-1664. https://doi.org/10.1002/jsfa.3999

González-Fernández, C., Sialve, B., & Molinuevo-Salces, B. (2015). Anaerobic digestion of microalgal biomass: challenges, opportunities and research needs. *Bioresource Technology, 198*, 896-906.

González-Fernández, M. C., Sialve, B., Bernet, N., & Steyer, J.-P. (2012). Impact of microalgae characteristics on their conversion to biofuel. Part II: Focus on biomethane production.

González-López, R., & Giampietro, M. (2018). Relational analysis of the oil and gas sector of Mexico: Implications for Mexico's energy reform. *Energy, 154*, 403-414. https://doi.org/10.1016/j.energy.2018.04.134

Ho, S.-H., Huang, S.-W., Chen, C.-Y., Hasunuma, T., Kondo, A., & Chang, J.-S. (2013). Bioethanol production using carbohydrate-rich microalgae biomass as feedstock. *Bioresource Technology, 135*, 191-198.

Horii, T., Ogawa, T., Nakatani, T., Hase, T., Matsubara, H., & Ogawa, H. (1981). Regulation of SOS functions: purification of E. coli LexA protein and determination of its specific site cleaved by the RecA protein. *Cell, 27*(3), 515-522.

Huang, Y., Chen, Y., Xie, J., Liu, H., Yin, X., & Wu, C. (2016). Bio-oil production from hydrothermal liquefaction of high-protein high-ash microalgae including wild Cyanobacteria sp. and cultivated Bacillariophyta sp. *Fuel, 183*, 9-19.

IEA, I. E. A. (2017). *Natural Gas Statics*.

IEA, I. E. A. (2018). *Gas 2019, Analysis and Forecasts to 2023.* https://www.iea.org/gas2018/

Ihsanullah, Shah, S., Ayaz, M., Ahmed, I., Ali, M., Ahmad, N., & Ahmad, I. (2015). Production of biodiesel from algae. *Journal of Pure and Applied Microbiology, 9*(1), 79-85.

Janssen, H. J., & Steinbuchel, A. (2014). Fatty acid synthesis in Escherichia coli and its applications towards the production of fatty acid based biofuels. *Biotechnology for Biofuels, 7*(1). https://doi.org/10.1186/1754-6834-7-7

Jinkerson, R. E., Radakovits, R., & Posewitz, M. C. (2013). Genomic insights from the oleaginous model alga Nannochloropsis gaditana. *Bioengineered, 4*(1), 37-43.

Johnson, M. B., & Wen, Z. (2009). Production of Biodiesel Fuel from the Microalga Schizochytrium limacinum by Direct Transesterification of Algal Biomass. *Energy & Fuels, 23*(10), 5179-5183. https://doi.org/10.1021/ef900704h

Joshi, S., Kumari, R., & Upasani, V. N. (2018). Applications of algae in cosmetics: An overview. *Int. J. Innov. Res. Sci. Eng. Technol, 7*, 1269-1278.

Joshua, S., & Mullineaux, C. W. (2004). Phycobilisome Diffusion Is Required for Light-State Transitions in Cyanobacteria. *Plant physiology, 135*(4), 2112-2119. https://doi.org/10.1104/pp.104.046110

Kim, K. H., Choi, I. S., Kim, H. M., Wi, S. G., & Bae, H.-J. (2014). Bioethanol production from the nutrient stress-induced microalga Chlorella vulgaris by enzymatic hydrolysis and immobilized yeast fermentation. *Bioresource Technology, 153*, 47-54.

Kizawa, A., Kawahara, A., Takashima, K., Takimura, Y., Nishiyama, Y., & Hihara, Y. (2017). The LexA transcription factor regulates fatty acid biosynthetic genes in the cyanobacterium Synechocystis sp. PCC 6803. *The Plant Journal, 92*(2), 189-198.

Klähn, S., & Hagemann, M. (2011). Compatible solute biosynthesis in cyanobacteria. *Environmental microbiology, 13*(3), 551-562.

Kopečná, J., Komenda, J., Bučinská, L., & Sobotka, R. (2012). Long-term acclimation of the cyanobacterium Synechocystis sp. PCC 6803 to high light is accompanied by an enhanced production of chlorophyll that is preferentially channeled to trimeric photosystem I. *Plant physiology, 160*(4), 2239-2250.

Kroon, B. M., van Hes, U. M., & Mur, L. R. (1992). An algal cyclostat with computer-controlled dynamic light regime. *Hydrobiologia, 238*(1), 63-70.

Kurade, M. B., Saha, S., Kim, J. R., Roh, H.-S., & Jeon, B.-H. (2020). Microbial community acclimatization for enhancement in the methane productivity of anaerobic co- digestion of fats, oil, and grease. *Bioresource Technology, 296*. https://doi.org/10.1016/j.biortech.2019.122294

Kurade, M. B., Saha, S., Salama, E.-S., Patil, S. M., Govindwar, S. P., & Jeon, B.-H. (2019). Acetoclastic methanogenesis led by Methanosarcina in anaerobic co-digestion of fats, oil and grease for enhanced production of methane. *Bioresource Technology, 272*, 351-359. https://doi.org/10.1016/j.biortech.2018.10.047

Lennen, R. M., Braden, D. J., West, R. M., Dumesic, J. A., & Pfleger, B. F. (2010). A process for microbial hydrocarbon synthesis: Overproduction of fatty acids in Escherichia coli and catalytic conversion to alkanes. *Biotechnology and Bioengineering, 106*(2), 193-202. https://doi.org/10.1002/bit.22660

Liu, C.-H., Chang, C.-Y., Liao, Q., Zhu, X., Liao, C.-F., & Chang, J.-S. (2013). Biohydrogen production by a novel integration of dark fermentation and mixotrophic microalgae cultivation. *International Journal of Hydrogen Energy, 38*(35), 15807-15814.

Liu, Z.-Y., Wang, G.-C., & Zhou, B.-C. (2008). Effect of iron on growth and lipid accumulation in Chlorella vulgaris. *Bioresource Technology, 99*(11), 4717-4722.

Luo, Y., Pfuetzner, R. A., Mosimann, S., Paetzel, M., Frey, E. A., Cherney, M., Kim, B., Little, J. W., & Strynadka, N. C. (2001). Crystal structure of LexA: a conformational switch for regulation of self-cleavage. *Cell, 106*(5), 585-594.

Ma, Y., Wang, Z., Yu, C., Yin, Y., & Zhou, G. (2014). Evaluation of the potential of 9 Nannochloropsis strains for biodiesel production. *Bioresource Technology, 167*, 503-509.

Manish, S., & Banerjee, R. (2008). Comparison of biohydrogen production processes. *International Journal of Hydrogen Energy, 33*(1), 279-286. https://doi.org/10.1016/j.ijhydene.2007.07.026

May, M. J., & Leaver, C. J. (1993). Oxidative stimulation of glutathione synthesis in Arabidopsis thaliana suspension cultures. *Plant physiology, 103*(2), 621-627.

McDonald, K. L., & Webb, R. I. (2011). Freeze substitution in 3 hours or less. *Journal of microscopy, 243*(3), 227-233.

Melnicki, M. R., Pinchuk, G. E., Hill, E. A., Kucek, L. A., Stolyar, S. M., Fredrickson, J. K., Konopka, A. E., & Beliaev, A. S. (2013). Feedback-controlled LED

photobioreactor for photophysiological studies of cyanobacteria. *Bioresource Technology, 134*, 127-133.

Mendez, L., Sialve, B., Tomás-Pejó, E., Ballesteros, M., Steyer, J., & González-Fernández, C. (2016). Comparison of Chlorella vulgaris and cyanobacterial biomass: cultivation in urban wastewater and methane production. *Bioprocess and Biosystems Engineering, 39*(5), 703-712. https://doi.org/10.1007/s00449-016-1551-7

Miranda, K., Attias, M., & Oliveira, M. (2002). Euglena gracilis as a model for the study of Cu2? and Zn2? toxicity and accumulation in eukaryotic cells. *Environ Pollut, 120*, 779786Ekelund.

Molino, A., Nanna, F., Ding, Y., Bikson, B., & Braccio, G. (2013). Biomethane production by anaerobic digestion of organic waste. *Fuel, 103*, 1003-1009. https://doi.org/10.1016/j.fuel.2012.07.070

Murashige, T., & Skoog, F. (1962). A revised medium for rapid growth and bio assays with tobacco tissue cultures. *Physiologia plantarum, 15*(3), 473-497.

Nagarajan, D., Lee, D.-J., Kondo, A., & Chang, J.-S. (2017). Recent insights into biohydrogen production by microalgae – From biophotolysis to dark fermentation. *Bioresource Technology, 227*, 373-387. https://doi.org/10.1016/j.biortech.2016.12.104

Nascimento, I., Marques, S., Cabanelas, I., Pereira, S., Druzian, J., Souza, C., Vich, D., Carvalho, G., & Nascimento, M. (2013). Screening Microalgae Strains for Biodiesel Production: Lipid Productivity and Estimation of Fuel Quality Based on Fatty Acids Profiles as Selective Criteria. *BioEnergy Research, 6*(1), 1-13. https://doi.org/10.1007/s12155-012-9222-2

Neag, E., Török, A. I., Cadar, O., Băbălău–Fuss, V., & Roman, C. (2019). Enhancing lipid production of Synechocystis PCC 6803 for biofuels production, through environmental stress exposure. *Renewable Energy, 143*, 243-251.

Oey, M., Sawyer, A. L., Ross, I. L., & Hankamer, B. (2016). Challenges and opportunities for hydrogen production from microalgae. *Plant biotechnology journal, 14*(7), 1487-1499.

Olivier, J. G. J., & Peters, J. A. H. W. (2018). *Trends in global CO2 and total greenhouse gas emissions: 2018 Report*.

Panwar, N. L., Kaushik, S. C., & Kothari, S. (2011). Role of renewable energy sources in environmental protection: A review. *Renewable and Sustainable Energy Reviews, 15*(3), 1513-1524. https://doi.org/10.1016/j.rser.2010.11.037

Paolini, F., & Paolini. (2010). *Renewable Energy." In Green Cities: An A-to-Z Guide*. https://search-credoreference-com.ezphost.dur.ac.uk/content/entry/greencities/renewable_energy/0?institutionId=1856

Patel, V. K., Sundaram, S., Patel, A. K., & Kalra, A. (2018). Characterization of seven species of cyanobacteria for high-quality biomass production. *Arabian Journal for Science and Engineering, 43*(1), 109-121.

Pawlita-Posmyk, M., Wzorek, M., & Płaczek, M. (2018). The influence of temperature on algal biomass growth for biogas production. *MATEC Web of Conferences, 240*. https://doi.org/10.1051/matecconf/201824004008

Pedersen, T. H., Grigoras, I. F., Hoffmann, J., Toor, S. S., Daraban, I. M., Jensen, C. U., Iversen, S. B., Madsen, R. B., Glasius, M., & Arturi, K. R. (2016). Continuous hydrothermal co-liquefaction of aspen wood and glycerol with water phase recirculation. *Applied Energy, 162*, 1034-1041.

Riley, R. T., & Merrill Jr, A. H. (2019). Ceramide synthase inhibition by fumonisins: a perfect storm of perturbed sphingolipid metabolism, signaling, and disease. *Journal of lipid research, 60*(7), 1183-1189.

Rittmann, B. E. (2008). Opportunities for renewable bioenergy using microorganisms. *Biotechnology and Bioengineering, 100*(2), 203-212. https://doi.org/10.1002/bit.21875

Schobert, H. (2013). *Composition, properties, and processing of natural gas*. Cambridge University Press. https://doi.org/10.1017/CBO9780511844188.011

Shah, S. H., Raja, I. A., Rizwan, M., Rashid, N., Mahmood, Q., Shah, F. A., & Pervez, A. (2018). Potential of microalgal biodiesel production and its sustainability perspectives in Pakistan. *Renewable and Sustainable Energy Reviews, 81*, 76-92.

Shuping, Z., Yulong, W., Mingde, Y., Kaleem, I., Chun, L., & Tong, J. (2010). Production and characterization of bio-oil from hydrothermal liquefaction of microalgae Dunaliella tertiolecta cake. *Energy, 35*(12), 5406-5411.

Silva-Neto, J. F., Nunes, A. J. P., Sabry-Neto, H., & Sá, M. V. C. (2012). Spirulina meal has acted as a strong feeding attractant for Litopenaeus vannamei at a very low dietary inclusion level. *Aquaculture Research, 43*(3), 430-437. https://doi.org/10.1111/j.1365-2109.2011.02846.x

Slilaty, S. N., & Little, J. W. (1987). Lysine-156 and serine-119 are required for LexA repressor cleavage: a possible mechanism. *Proceedings of the National Academy of Sciences, 84*(12), 3987-3991.

Smith, S. J., Kroon, J. T., Simon, W. J., Slabas, A. R., & Chivasa, S. (2015). A novel function for Arabidopsis CYCLASE1 in programmed cell death revealed by isobaric tags for relative and absolute quantitation (iTRAQ) analysis of extracellular matrix proteins. *Molecular & Cellular Proteomics, 14*(6), 1556-1568.

Soontharapirakkul, K., Promden, W., Yamada, N., Kageyama, H., Incharoensakdi, A., Iwamoto-Kihara, A., & Takabe, T. (2011). Halotolerant cyanobacterium Aphanothece halophytica contains an Na+-dependent F1F0-ATP synthase with a potential role in salt-stress tolerance. *Journal of Biological Chemistry, 286*(12), 10169-10176.

Soriano, J., Gonzalez, L., & Catala, A. (2005). Mechanism of action of sphingolipids and their metabolites in the toxicity of fumonisin B1. *Progress in lipid research, 44*(6), 345-356.

Soselisa, J. F., Suseno, S. H., & Setyaningsih, I. (2019). Characteristics of Combination Shark Liver Oil (Centrophorus sp.) And Spirulina Powder as Food Supplement. *Jurnal Pengolahan Hasil Perikanan Indonesia, 22*(2), 255-262.

Stanier, R., Kunisawa, R., Mandel, M., & Cohen-Bazire, G. (1971). Purification and properties of unicellular blue-green algae (order Chroococcales). *Bacteriological reviews, 35*(2), 171.

Stone, J. M., Heard, J. E., Asai, T., & Ausubel, F. M. (2000). Simulation of Fungal-Mediated Cell Death by Fumonisin B1 and Selection of Fumonisin B1–Resistant (fbr) Arabidopsis Mutants. *The Plant Cell, 12*(10), 1811-1822. https://doi.org/10.1105/tpc.12.10.1811

Sydney, E. B., Da Silva, T. E., Tokarski, A., Novak, A. C., de Carvalho, J. C., Woiciecohwski, A. L., Larroche, C., & Soccol, C. R. (2011). Screening of microalgae with potential for biodiesel production and nutrient removal from treated domestic sewage. *Applied Energy, 88*(10), 3291-3294. https://doi.org/10.1016/j.apenergy.2010.11.024

Takagi, M., & Yoshida, T. (2006). Effect of salt concentration on intracellular accumulation of lipids and triacylglyceride in marine microalgae Dunaliella cells. *Journal of bioscience and bioengineering, 101*(3), 223-226.

Takashima, K., Nagao, S., Kizawa, A., Suzuki, T., Dohmae, N., & Hihara, Y. (2020). The role of transcriptional repressor activity of LexA in salt-stress responses of the cyanobacterium Synechocystis sp. PCC 6803. *Scientific reports, 10*(1), 1-11.

Tan, I. S., & Lee, K. T. (2015). Solid acid catalysts pretreatment and enzymatic hydrolysis of macroalgae cellulosic residue for the production of bioethanol. *Carbohydrate polymers, 124*, 311-321.

Tao, H., Zhang, Y., Cao, X., Deng, Z., & Liu, T. (2016). Absolute quantification of proteins in the fatty acid biosynthetic pathway using protein standard absolute quantification. *Synthetic and systems biotechnology, 1*(3), 150-157.

Tsunekawa, K., Shijuku, T., Hayashimoto, M., Kojima, Y., Onai, K., Morishita, M., Ishiura, M., Kuroda, T., Nakamura, T., & Kobayashi, H. (2009). Identification and characterization of the Na+/H+ antiporter Nhas3 from the thylakoid membrane of Synechocystis sp. PCC 6803. *Journal of Biological Chemistry, 284*(24), 16513-16521.

Tsuzuki, M., Okada, K., Isoda, H., Hirano, M., Odaka, T., Saijo, H., Aruga, R., Miyauchi, H., & Fujiwara, S. (2019). Physiological Properties of Photoautotrophic Microalgae and Cyanobacteria Relevant to Industrial Biomass Production. *Marine Biotechnology, 21*(3), 406-415.

Uysal, O., Uysal, F. O., & Ekinci, K. (2015). Evaluation of microalgae as microbial fertilizer. *European Journal of Sustainable Development, 4*(2), 77-77.

Vardon, D. R., Sharma, B. K., Blazina, G. V., Rajagopalan, K., & Strathmann, T. J. (2012). Thermochemical conversion of raw and defatted algal biomass via hydrothermal liquefaction and slow pyrolysis. *Bioresource Technology, 109*, 178-187.

Vardon, D. R., Sharma, B. K., Scott, J., Yu, G., Wang, Z., Schideman, L., Zhang, Y., & Strathmann, T. J. (2011). Chemical properties of biocrude oil from the hydrothermal liquefaction of Spirulina algae, swine manure, and digested anaerobic sludge. *Bioresource Technology, 102*(17), 8295-8303.

Verma, E., Singh, S., & Mishra, A. (2019). Salinity-induced oxidative stress-mediated change in fatty acids composition of cyanobacterium Synechococcus sp. PCC7942. *International Journal of Environmental Science and Technology, 16*(2), 875-886.

Wade, J. T., Reppas, N. B., Church, G. M., & Struhl, K. (2005). Genomic analysis of LexA binding reveals the permissive nature of the Escherichia coli genome and identifies unconventional target sites. *Genes & development, 19*(21), 2619-2630.

Walters, R. G., & Horton, P. (1994). Acclimation of Arabidopsis thaliana to the light environment: changes in composition of the photosynthetic apparatus. *Planta, 195*(2), 248-256.

Wang, Y., He, B., Sun, Z., & Chen, Y.-F. (2016). Chemically enhanced lipid production from microalgae under low sub-optimal temperature. *Algal Research, 16*, 20-27.

World-Bank. (2019). *Mexico: Distribution of the gross domestic product (GDP) across economic sectors from 2008 to 2018.* Statista. https://www.statista.com/statistics/275420/distribution-of-gross-domestic-product-gdp-across-economic-sectors-in-mexico/

Yadav, G., Sekar, M., Kim, S.-H., Geo, V. E., Bhatia, S. K., Sabir, J. S., Chi, N. T. L., Brindhadevi, K., & Pugazhendhi, A. (2021). Lipid content, biomass density, fatty acid as selection markers for evaluating the suitability of four fast growing cyanobacterial strains for biodiesel production. *Bioresource Technology, 325*, 124654.

Yang, L., Nazari, L., Yuan, Z., Corscadden, K., & Xu, C. C. (2016). Hydrothermal liquefaction of spent coffee grounds in water medium for bio-oil production. *Biomass and Bioenergy, 86*, 191-198.

Zaidi, A. A., RuiZhe, F., Shi, Y., Khan, S. Z., & Mushtaq, K. (2018). Nanoparticles augmentation on biogas yield from microalgal biomass anaerobic digestion. *International Journal of Hydrogen Energy, 43*(31), 14202-14213.

Zeng, H.-Y., Li, C.-Y., & Yao, N. (2020). Fumonisin B1: A tool for exploring the multiple functions of sphingolipids in plants. *Frontiers in plant science, 11*.

Appendices

Appendix I. List of primers used to amplify target genes

Table S1. DNA primers used for PCR-amplification of target genes.

Gene abbreviation	DNA sequences	
	Forward primer (5' to 3')	**Reverse primer (5' to 3')**
DH	TTGTGGAATCCATGGCCCAG	CCCCATCAATGCCAGCAAAG
ENR1	TGGCGGTAGCATCATTACCC	TCATTTCCAGACCGGCCTTC
ENR2	ATGCCGTAGCTCCTGGTTTC	CTCCGGTTGACCATAGCGAG
ENR3	ACCAAGGAAATCCCCTTCCG	CTACTGGCTACGGGGGAAAG
KS1	CGCCGAAGATAAGGTACCCC	ATTAAAGCCCGACTCTGCCC
KS2	GGGAAAAACGGCCATCAAGC	ACCAATTGTCCCAGGGAACG
KS3	TGTACTTTCCCGTTGGGTGG	CAAATTGTCCTGGGCTTGGC
KR1	GGGTTAATTGCCTTGACCCG	AGCATGGGGGTATTTACGGC
KR2	ACCCGGAAGAGTTTATGCGG	TATAGGGCCGCATCAGTGAC
ACCase	AGCGGATCAAAAGTGGACGG	TGACTGCATCTCCCACTTCC
680316S	AGCTCGGGTGATCGACATTG	ATGGGTGGAATCCAACAGGG
68035S	TCATGGAACCACTCCGATCC	GGACTATTGTGCCGTGGGG

Appendix II. RNA gel electrophoresis used for simple quality control.

RNA was extracted from cyanobacterial cells and quantified using a NanoDrop. While the NanoDrop graphical output provides some indication of RNA quality, all samples were separated by gel electrophoresis. Presence of the major RNA bands confirmed that the samples were not degraded. Below is an example of such a gel.

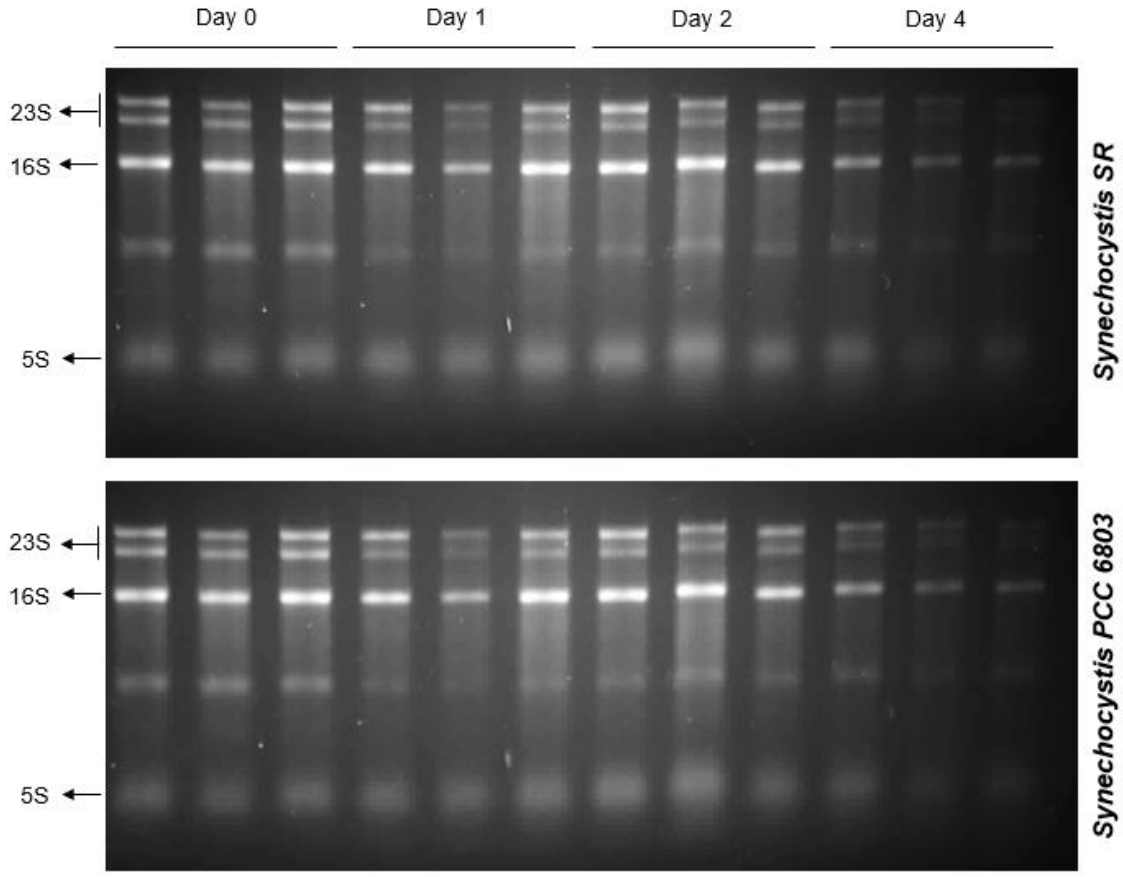

Figure S1. Gel electrophoresis used for quality control of RNA samples. Ethidium bromide-stained RNA samples of 200 mM NaCl-treated *Synechocystis SR* or *Synechocystis PCC 6803* harvested in triplicate at 0, 1, 2, and 4 days after treatment. Numbers on the right indicate the size of the RNA species in Svedberg units.